

**TP 14391E**

# **ICEBERG DETECTION PERFORMANCE ANALYSIS**

**Prepared for  
Transportation Development Centre  
of  
Transport Canada**

**by**

**Rutter Technologies Inc.**

**April 2005**



**TP 14391E**

# **ICEBERG DETECTION PERFORMANCE ANALYSIS**

**By**

**J. Ryan and C. Kirby  
Rutter Technologies Inc.**

**April 2005**

This report reflects the views of Rutter Technologies Inc. and not necessarily those of the Transportation Development Centre of Transport Canada.

The Transportation Development Centre does not endorse products or manufacturers. Trade or manufacturers' names appear in this report only because they are essential to its objectives.

### **Project Team**

Joe Ryan, Project Manager, Technical Advisor

Chris Kirby, Student Engineer

Steve Motty, Hardware Design Engineer

Andrew Menchions, Software Design Engineer

Max Johnson, Software Design Engineer

Un sommaire français se trouve avant la table des matières.

© 2005 Transport Canada



1. Transport Canada Publication No. <b>TP 14391E</b>		2. Project No. <b>5531</b>		3. Recipient's Catalogue No.	
4. Title and Subtitle <b>Iceberg Detection Performance Analysis</b>				5. Publication Date <b>April 2005</b>	
				6. Performing Organization Document No.	
7. Author(s) <b>J. Ryan and C. Kirby</b>				8. Transport Canada File No. <b>2450-C-404</b>	
9. Performing Organization Name and Address <b>Rutter Technologies 22 Pearl Place P.O. Box 427 St. John's, Newfoundland Canada A1C 5K4</b>				10. PWGSC File No. <b>MTB-4-00727</b>	
				11. PWGSC or Transport Canada Contract No. <b>T8200-044502/001/MTB</b>	
12. Sponsoring Agency Name and Address <b>Transportation Development Centre (TDC) 800 René Lévesque Blvd. West Suite 600 Montreal, Quebec H3B 1X9</b>				13. Type of Publication and Period Covered <b>Final</b>	
				14. Project Officer <b>C. Gautier</b>	
15. Supplementary Notes (Funding programs, titles of related publications, etc.) <b>Co-sponsored by the Program for Energy Research and Development (PERD) of Natural Resources Canada (NRCan)</b>					
16. Abstract <p>The Sigma S6 radar processor is a specialized computer-based system capable of enhancing the detection performance of marine radars. The processor is particularly suited to the challenging role of iceberg detection in sea and rain clutter.</p> <p>A two-phase Iceberg Analysis project was undertaken in 2003 to review radar data collected in 2002 and to characterize the system performance in terms of iceberg detection capability. This work included the analysis of specific iceberg targets that were representative of the most challenging situations encountered. In addition to this effort, an investigation of the effect of antenna speed on detection performance was conducted. The analysis included an assessment of the scan-to-scan processing and algorithms currently in use, and a comparison with the measured performance of new digital signal processing (DSP) filtering techniques. The DSP techniques included the implementation and analysis of performance of FIR (Finite Impulse Response) and IIR (Infinite Impulse Response) digital filters.</p> <p>The results show that the FIR filter is not practical in this application, as it requires a very large filter and very long associated processing time. However, significant success was achieved using the IIR filter, and it was demonstrated that detection performance could be improved using this type of filter coupled with a high-speed antenna.</p>					
17. Key Words <b>Iceberg detection, small target detection in clutter, radar signal processing, scan-to-scan processing, pulse filter, high-speed radar antenna, digital signal processing, DSP</b>				18. Distribution Statement <b>Limited number of copies available from the Transportation Development Centre</b>	
19. Security Classification (of this publication) <b>Unclassified</b>		20. Security Classification (of this page) <b>Unclassified</b>		21. Declassification (date) <b>—</b>	22. No. of Pages <b>xviii, 104</b>
				23. Price <b>Shipping/ Handling</b>	



1. N° de la publication de Transports Canada <b>TP 14391E</b>		2. N° de l'étude <b>5531</b>		3. N° de catalogue du destinataire	
4. Titre et sous-titre <b>Iceberg Detection Performance Analysis</b>				5. Date de la publication <b>Avril 2005</b>	
				6. N° de document de l'organisme exécutant	
7. Auteur(s) <b>J. Ryan et C. Kirby</b>				8. N° de dossier - Transports Canada <b>2450-C-404</b>	
9. Nom et adresse de l'organisme exécutant <b>Rutter Technologies 22 Pearl Place P.O. Box 427 St. John's, Newfoundland Canada A1C 5K4</b>				10. N° de dossier - TPSGC <b>MTB-4-00727</b>	
				11. N° de contrat - TPSGC ou Transports Canada <b>T8200-044502/001/MTB</b>	
12. Nom et adresse de l'organisme parrain <b>Centre de développement des transports (CDT) 800, boul. René-Lévesque Ouest Bureau 600 Montréal (Québec) H3B 1X9</b>				13. Genre de publication et période visée <b>Final</b>	
				14. Agent de projet <b>C. Gautier</b>	
15. Remarques additionnelles (programmes de financement, titres de publications connexes, etc.) <b>Coparrainé par le Programme de recherche et développement énergétiques (PRDE) de Ressources naturelles Canada (RNCan)</b>					
16. Résumé <p>Le processeur radar Sigma S6 est un système informatique spécialisé conçu pour améliorer la performance de détection des radars maritimes. Ce processeur est particulièrement bien adapté à la tâche exigeante que constitue la détection d'icebergs dans le clutter de mer et le clutter de pluie.</p> <p>En 2003, le projet <i>Analyse des icebergs</i> a été entrepris. Divisé en deux phases, il consistait à analyser les données radar recueillies en 2002 et à caractériser la performance du système, plus précisément sa capacité de détecter des icebergs. Ces travaux comprenaient l'analyse d'icebergs particuliers pris pour cibles lors de l'essai en mer et représentatifs des conditions de détection les plus défavorables. En parallèle, une étude a été menée sur l'effet de la vitesse de rotation de l'antenne sur la performance de détection. L'analyse comprenait une évaluation du traitement «d'un balayage à l'autre» et des algorithmes connexes actuellement utilisés, ainsi qu'une comparaison entre la performance obtenue et la performance mesurée de nouvelles techniques de filtrage par traitement numérique des signaux. À cette fin, des filtres numériques à réponse impulsionnelle finie (RIF) et à réponse impulsionnelle infinie (RII) ont été mis en oeuvre et leur performance a été analysée.</p> <p>Les résultats indiquent que le filtre RIF ne convient pas à cette application, car un tel filtre doit être très grand et qu'il s'ensuit un temps de traitement très long. Toutefois, le filtre RII s'est révélé satisfaisant, et il a été démontré que l'utilisation d'un tel filtre couplé à une antenne haute vitesse peut améliorer la performance de détection.</p>					
17. Mots clés <b>Détection d'icebergs, détection de petites cibles dans le clutter, traitement de signaux radar, traitement d'un balayage à l'autre, filtre à impulsion, antenne radar haute vitesse, traitement numérique de signaux</b>			18. Diffusion <b>Le Centre de développement des transports dispose d'un nombre limité d'exemplaires.</b>		
19. Classification de sécurité (de cette publication) <b>Non classifiée</b>		20. Classification de sécurité (de cette page) <b>Non classifiée</b>		21. Déclassification (date) <b>—</b>	22. Nombre de pages <b>xviii, 104</b>
					23. Prix <b>Port et manutention</b>

## **ACKNOWLEDGEMENTS**

The support and assistance of CCORE and OCEANS in providing the ground truthing and environmental monitoring during the field trials are greatly appreciated. The support from the Canadian Coast Guard (Ship's Electronic Workshop) in St. John's was very important to the success of the display comparison test. The assistance and significant technical support provided by Charles Gautier, Transportation Development Centre of Transport Canada, during the course of this project have also helped to make this project a success. The Program of Energy Research and Development (PERD) provided key funding for this project.

(Blank)



## **EXECUTIVE SUMMARY**

The Sigma S6 radar processor is a specialized computer-based system capable of enhancing the detection performance of marine radars. The processor is particularly suited to the challenging role of iceberg detection in sea and rain clutter. The processor was called the Modular Radar Interface (MRI) during its development and is currently marketed under the Sigma S6 name.

In the summer of 2002, a quantitative detection evaluation study was undertaken to assess the iceberg detection capability of the Sigma S6 radar processor system when used with a high-speed radar antenna. This work included a field trial at Twillingate, Newfoundland, and subsequent data analysis phases. The data collection program was quite successful in recording data on very small bergy bit and growler size iceberg targets in high sea states.

A two-phase Iceberg Analysis project was undertaken in 2003 to review the radar data collected in 2002 and to characterize the system performance in terms of iceberg detection capability. This work included the analysis of specific iceberg targets that were representative of the most challenging situations encountered. In addition to this effort, an investigation of the effect of antenna speed on detection performance was conducted. The analysis included an assessment of the scan-to-scan processing and algorithms currently in use, and a comparison with the measured performance of new digital signal processing (DSP) filtering techniques. The DSP techniques included the implementation and analysis of performance of FIR (Finite Impulse Response) and IIR (Infinite Impulse Response) digital filters.

The results show that the FIR filter is not practical in this application, as it requires a very large filter and very long associated processing time. However, significant success was achieved using the IIR filter, and it was demonstrated that detection performance could be improved using this type of filter coupled with a high-speed antenna.

(Blank)

## SOMMAIRE

Le processeur radar Sigma S6 est un système informatique spécialisé conçu pour améliorer la performance de détection des radars maritimes. Ce processeur est particulièrement bien adapté à la tâche exigeante que constitue la détection d'icebergs dans le clutter de mer et le clutter de pluie. D'abord désigné *interface modulaire radar* (IMR) au cours de son développement, le processeur est maintenant commercialisé sous le nom de Sigma S6.

À l'été 2002, une évaluation de détection quantitative a eu lieu, afin de déterminer la capacité du processeur radar Sigma S6 de détecter des icebergs, lorsque jumelé à une antenne radar haute vitesse. L'étude comprenait un essai en mer à Twillingate, Terre-Neuve, suivi de l'analyse des données recueillies. Le programme de collecte de données s'est avéré un succès, des bergy bits et des bourguignons ayant été détectés dans des conditions de grosse mer.

En 2003, le projet *Analyse des icebergs* a été entrepris. Divisé en deux phases, il consistait à analyser les données radar recueillies en 2002 et à caractériser la performance du système, plus précisément sa capacité de détecter des icebergs. Ces travaux comprenaient l'analyse d'icebergs particuliers pris pour cibles lors de l'essai en mer et représentatifs des conditions de détection les plus défavorables. En parallèle, une étude a été menée sur l'effet de la vitesse de rotation de l'antenne sur la performance de détection. L'analyse comprenait une évaluation du traitement «d'un balayage à l'autre» et des algorithmes connexes actuellement utilisés, ainsi qu'une comparaison entre la performance obtenue et la performance mesurée de nouvelles techniques de filtrage par traitement numérique des signaux. À cette fin, des filtres numériques à réponse impulsionnelle finie (RIF) et à réponse impulsionnelle infinie (RII) ont été mis en oeuvre et leur performance a été analysée.

Les résultats indiquent que le filtre RIF ne convient pas à cette application, car un tel filtre doit être très grand et qu'il s'ensuit un temps de traitement très long. Toutefois,

le filtre RII s'est révélé satisfaisant, et il a été démontré que l'utilisation d'un tel filtre couplé à une antenne haute vitesse peut améliorer la performance de détection.

# TABLE OF CONTENTS

1	BACKGROUND.....	1
2	PHASE 1 – TWILLINGATE FIELD TRIAL AND ANALYSIS.....	3
	2.1 ENVIRONMENTAL CONDITIONS.....	6
3	DATA SUMMARY.....	7
	3.1 ICEBERG DATA.....	12
4	DETECTION PERFORMANCE.....	16
	4.1 ANALYSIS METHODOLOGY.....	21
	4.2 ANALYSIS RESULTS.....	23
	4.2.1 <i>Wave Rider Detection</i> .....	23
	4.2.2 <i>Wave Rider Analysis with 256 Scans Processed, 120 rpm</i> .....	25
	4.2.3 <i>Wave Rider Analysis with 64 Scans Processed, 120 rpm</i> .....	26
	4.2.4 <i>Bergy Bit Detection</i> .....	27
	4.2.5 <i>Bergy Bit Analysis with 256 Scans Processed, 120 rpm</i> .....	30
	4.2.6 <i>Bergy Bit Analysis with 64 Scans Processed, 120 rpm</i> .....	31
	4.2.7 <i>Examination of the Effect of Antenna Speed</i> .....	32
	4.2.8 <i>Analysis of Close Range Bergy Bits and Growlers</i> .....	39
	4.2.9 <i>Close-Range Target #1</i> .....	39
	4.2.10 <i>Close-Range Targets #2 and #3</i> .....	42
	4.2.11 <i>Verification of Close-Range Targets using S6 Image Processor</i> .....	44
	4.2.12 <i>Close-Range Detection Conclusions</i> .....	46
5	PHASE 2 – DSP ENHANCED PROCESSING.....	47
	5.1 DIGITAL FILTER REVIEW.....	47
	5.2 FIR (NON-RECURSIVE FILTERS).....	49
	5.3 IIR (RECURSIVE FILTERS).....	50
	5.3.1 <i>Butterworth</i> .....	50
	5.3.2 <i>Bessel</i> .....	51
	5.3.3 <i>Comparison of FIR and IIR Filtering Characteristics</i> .....	52
	5.4 FILTER DESIGN AND IMPLEMENTATION.....	57
	5.5 PRELIMINARY ANALYSIS.....	58
	5.6 IIR FILTER ANALYSIS.....	60
6	DSP DETECTION PERFORMANCE.....	63
	6.1 FILTER BANDWIDTH ANALYSIS.....	63
	6.2 FILTER ORDER ANALYSIS.....	66
	6.3 FILTER ATTENUATION ANALYSIS.....	74

6.4	STATIONARY TARGET CONSIDERATIONS AND CONCLUSIONS .....	78
6.5	MOVING TARGET CONSIDERATIONS AND CONCLUSIONS .....	82
7	COMPARISON OF DSP PROCESSING TO CONVENTIONAL RADAR.....	86
7.1	TEST SETUP.....	86
7.2	COMPARATIVE TEST.....	88
8	CONCLUSIONS.....	100
8.1	DETECTION .....	100
	8.1.1 <i>Iceberg Detection</i> .....	100
	8.1.2 <i>Antenna Speed Effects</i> .....	101
8.2	DIGITAL FILTER PROCESSING .....	101
	8.2.1 <i>Target Motion</i> .....	102
8.3	DISPLAY COMPARISONS .....	102
9	RECOMMENDATIONS.....	103

## LIST OF FIGURES

Figure 1	Mobile Radar Unit at Twillingate, Newfoundland.....	4
Figure 2	Interior View of Mobile Radar Unit.....	5
Figure 3	Wind Direction for June 14 to 16.....	9
Figure 4	Wind Speed for June 14 to 16.....	10
Figure 5	Wave Height for June 14 to 16.....	10
Figure 6	Iceberg Position Plot, June 14.....	12
Figure 7	Iceberg to the North of the Radar Site.....	14
Figure 8	Iceberg to the West of the Radar Site.....	15
Figure 9	Icebergs in Sea Clutter on June 15 (Raw Data).....	17
Figure 10	Raw Data with STC Applied.....	18
Figure 11	Scan Averaging and STC Applied.....	19
Figure 12	Full Processing Applied.....	20
Figure 13	Probability of Detection of Wave Rider Buoy, 256 scans, 120 rpm.....	25
Figure 14	Probability of Detection of Wave Rider Buoy, 64 scans, 120 rpm.....	27
Figure 15	Growler and Bergy Bit Targets, 15:45 NDT.....	28
Figure 16	Growler and Bergy Bit Targets, 15:46 NDT.....	28
Figure 17	Radar Image Before (Left) and After (Right) Bergy Bit Split.....	29
Figure 18	Probability of Detection of a Bergy Bit, 256 scans, 120 rpm.....	30
Figure 19	Probability of Detection of a Bergy Bit, 64 Scans, 120 rpm.....	31
Figure 20	Detection vs. Antenna Speed - Constant Average Time, 12:00 NDT.....	35
Figure 21	Detection vs. Antenna Speed - 256 Scans Averaged, 12:00 NDT.....	37
Figure 22	Detection vs. Antenna Speed - Constant Average Time, 16:10 NDT.....	38
Figure 23	Field Photographs of Close-Range Target #1 at 20:13 NDT (0.8 nmi).....	40
Figure 24	Field Photographs of Close-Range Target #1 at 17:58 NDT (1.6 nmi).....	40
Figure 25	Detection Performance for Target #1 at 1.4 nmi.....	41
Figure 26	Detection Performance for Target #1 at 0.8 nmi.....	41
Figure 27	Photograph of Target #2 at 20:18 NDT (1 nmi).....	42
Figure 28	Detection Performance for Target #2 at 0.9 nmi.....	43
Figure 29	Photograph of Target #3 at 20:18 NDT (1.2 nmi).....	43

Figure 30	Detection Performance for Target #3 at 1.1 nmi .....	44
Figure 31	Close-Range Targets at 20:16 NDT, Viewed with 256 Scans Averaged.....	45
Figure 32	Physical Representation of General FIR Filter .....	49
Figure 33	Block Representation of Multi-Stage Biquadratic IIR Filter.....	51
Figure 34	Digital Filter Frequency Response for Various Filters .....	52
Figure 35	Step Response for Various Digital Filters.....	53
Figure 36	Impulse Response for Various Digital Filters.....	54
Figure 37	IIR Digital Filter Frequency Response for Increasing Order .....	55
Figure 38	IIR Digital Filter Step Response for Increasing Order .....	56
Figure 39	Detection Performance for Fixed Processing Time (128 scans) .....	58
Figure 40	Detection Performance for Fixed Processing Time (256 scans) .....	59
Figure 41	Performance of Filters with Bandwidth = 0.0068 Hz .....	63
Figure 42	Performance of Filters with Bandwidth = 0.0045 Hz .....	64
Figure 43	Performance of Filters with Bandwidth = 0.0034 Hz .....	64
Figure 44	Performance of Filters with Bandwidth = 0.0025 Hz .....	65
Figure 45	Performance of Filters with Bandwidth = 0.0017 Hz .....	65
Figure 46	Pfa Performance of Second Order Butterworth Filters .....	67
Figure 47	Pd Performance of Second Order Butterworth Filters .....	68
Figure 48	Pfa Performance of Third Order Butterworth Filters .....	69
Figure 49	Pd Performance of Third Order Butterworth Filters .....	70
Figure 50	Pfa Performance of Fourth Order Butterworth Filters .....	71
Figure 51	Pd Performance of Fourth Order Butterworth Filters .....	72
Figure 52	Pfa Performance of Filters with Matched 50 dB Attenuation .....	74
Figure 53	Pd Performance of Filters with Matched 50 dB Attenuation .....	75
Figure 54	Pfa Performance of Filters with Matched 75 dB Attenuation .....	76
Figure 55	Pd Performance of Filters with Matched 75 dB Attenuation .....	77
Figure 56	Pd versus Pfa for the Wave Rider in High Sea Clutter (IIR Filter) .....	79
Figure 57	Pfa versus Threshold for the Wave Rider in High Sea Clutter (IIR Filter).....	80
Figure 58	Pd vs. Threshold for the Wave Rider in High Sea Clutter (IIR Filter).....	81
Figure 59	Scan Average Processing on Moving Targets .....	83
Figure 60	Filter Bandwidth Effect on Moving Target Detection .....	84



Figure 61 Marine Radar Display Video - Gain 2, SEA 3.....	88
Figure 62 Marine Radar Display Video - Gain 2, SEA 5.....	89
Figure 63 Marine Radar Display Video - Gain 2, SEA 6.....	90
Figure 64 Marine Radar Display Video - Gain 3, SEA 7.....	91
Figure 65 Marine Radar Display Video - Gain 3, SEA 7, ENHANCE .....	92
Figure 66 Marine Radar Display Video - AUTO Clutter, Gain 6 .....	93
Figure 67 Sigma S6 Display - RAW Video .....	94
Figure 68 Sigma S6 Display - STC Applied.....	95
Figure 69 Sigma S6 Display - STC and 256 Scan Average .....	96
Figure 70 Sigma S6 Display - STC, CFAR and 256 Scan Average .....	97
Figure 71 Sigma S6 Display - STC and 48 Scan Average .....	98
Figure 72 Sigma S6 Display - STC, CFAR and 48 Scan Average .....	99

## LIST OF TABLES

Table 1 Radar Site Characteristics.....	3
Table 2 Iceberg Position and Identification.....	13
Table 3 Iceberg Measurements from Photographs .....	29
Table 4 Target Size Summary.....	44
Table 5 Close-Range Target Detection Summary.....	45
Table 6 Summary of Order - Bandwidth Combinations of Butterworth Filters .....	61
Table 7 Summary of Scan Averaging Filters .....	62

## GLOSSARY OF ACRONYMS

ADC	Analog-to-Digital Converter
ACP	Azimuth Count Pulse
ARP	Azimuth Reset Pulse
CVD	Composite Video Decoder
CFAR	Constant False Alarm Rate
CPLD	Complex PLD
CMOS	Complementary Metal Oxide Semiconductor
dBFS	Decibels Full Scale
DLL	Dynamic Link Library
DMA	Direct Memory Access
ENOB	Effective Number of Bits
GPS	Global Positioning System
I/O	Input/Output
LAN	Local Area Network
Mbps	Megabits per Second
MB/s	MegaBytes per Second
MHT	Multiple Hypothesis Tracker
MRI	Modular Radar Interface
MSPS	Million Samples Per Second
NDT	Newfoundland Daylight Time
PC	Personal Computer
PCB	Printed Circuit Board
PCI	Peripheral Component Interconnect - bus type
Pd	Probability of Detection
Pfa	Probability of False Alarm
PLCC	Plastic Leaded Chip Carrier
PLD	Programmable Logic Device
PRF	Pulse Repetition Frequency
PROM	Programmable Read-only Memory
RAM	Random Access Memory
RMS	Root Mean Square
RPM	Rotations Per Minute
RSi4000	Radar Interface Card
SINAD	Signal to Noise and Distortion
SNR	Signal-to-Noise Ratio
STC	Sensitivity Time Control

(Blank)

# 1 BACKGROUND

In the summer of 2002 a quantitative detection evaluation study was undertaken to assess the iceberg detection capability of the Sigma S6 radar processor system when used with a high-speed radar antenna.

The Transportation Development Centre (TDC) of Transport Canada sponsored a field trial at Twillingate, Newfoundland, using a mobile radar unit owned by TDC. The mobile radar unit is a self-contained unit with a Raytheon Pathfinder MK2 mounted on its roof. This radar has been specifically modified for radar research activities to operate at 120 rpm, almost five times the speed of the standard antenna. The main purpose of the high-speed antenna is to provide increased opportunities to detect growlers and other small targets in high sea states. The objectives of the research were to investigate whether the increase in opportunities translates into an increase in detection performance, and to assess the overall performance of the modified radar with advanced signal processor in the iceberg detection application.

In order to facilitate evaluation of the Sigma S6 system, it was equipped with recording capability for the trial. This would permit both in-field evaluation and post-field trial evaluation of the system. This was possible as the data recording capability provides full bandwidth raw radar data. This capability enables the re-creation of the exact situation as it occurred in the field and the application of different processing and tracking parameters. In addition, the raw recorded data may be used to develop new processing techniques and algorithms.

The main focus of the trial was to determine system detection performance on growlers and bergy bits in high sea states. In order to facilitate this and to maximize the probability of getting the desired data, an extended field trial was designed. Once the equipment was deployed at Long Point, Twillingate, conditions were monitored and field personnel mobilized when conditions were suitable for data collection. This mode of operation permitted leaving the equipment in the field for a six-week period. Overall

data was collected on numerous growler and bergy bit targets in sea states up to 3.5 m significant wave height (5.9 m maximum wave height) and wind speeds to 35 kn. Iceberg aerial ground truth data was collected by C-CORE, and surface-based ground truthing of iceberg targets was conducted by Sigma Engineering Limited and Oceans Limited. Oceans Limited also provided weather forecasting for the site and in-situ measurements of wind and wave data.

A two-phase Iceberg Analysis project was undertaken in 2003 to review data collected in 2002 and to characterize the system performance in terms of iceberg detection capability. This work included the analysis of specific iceberg targets that were representative of the most challenging situations encountered. In addition to this effort, an investigation of the effect of antenna speed on detection performance was conducted. During the analysis, discussions with the project authority on the use of digital signal processing (DSP) techniques for improved scan-to-scan processing resulted in a change in focus of the project. It was decided that it was important to characterize the best filter in the iceberg detection role to ensure that optimum system performance is achieved. The remainder of the first phase focused on the use of DSP techniques and specifically on the use of an FIR (Finite Impulse Response) digital filter in place of the normal scan average processing. The results indicated that the FIR filter is not practical in this application as it requires very large filter and very long associated processing time. It was proposed that an IIR (Infinite Impulse Response) digital filter may provide the enhancement required in a practical implementation.

The second phase of the Iceberg Analysis project focused on the design, implementation and testing of the IIR filter. The objective of the filter design was to determine the important filter design parameters and their influence on performance. In parallel with this effort a comparison of the new filter with the capabilities of a standard marine radar display was conducted.

This report presents results from Phases 1 and 2 of the Iceberg Analysis project.

## 2 PHASE 1 – TWILLINGATE FIELD TRIAL AND ANALYSIS

During June 2002 a comprehensive field trial was undertaken to validate the performance of the new RSi4000 radar interface card and to collect a data set with the new card for assessment of the iceberg detection capability of the new system.

Twillingate, Newfoundland, was selected for the trial as it was expected to provide sufficient iceberg targets for an effective evaluation of the system. The Twillingate site had been used for a field trial in 1999 and so the logistics of using the site were well known. Table 1 provides the radar site characteristics. The site offered a very good field of view and long radar horizon.

**Table 1 Radar Site Characteristics**

Latitude	N49° 41.230'
Longitude	W54° 48.206'
Height	300 ft. (91 m)
Radar Horizon	21 nmi (39 km)

In 2002 TDC acquired and modified a cube van for use in the radar validation and future data acquisition trials. The van was outfitted as a self-contained unit capable of operating in a cold weather climate. The unit was fitted with a 5 kW generator and electric heat.

The objective of the field trial was to collect data on growlers and bergy bits in high sea states. As it was determined that there was little value in collecting data in low sea states, the field program was designed to maximize data collection opportunities during high sea state conditions. This was accomplished by deploying the field equipment at Long Point, Twillingate, and returning to St. John's to wait for weather opportunities. Oceans Limited provided daily forecasts for the Twillingate area and communication with the lighthouse keeper provided information on the ice situation. When the forecast

predicted sea states over 2 m, field personnel were mobilized to collect data. At the same time C-CORE mobilized to the area to conduct ground truthing overflights.

This method of data collection was used for the month of June 2002, and resulted in the collection of radar data on growlers and bergy bits for the highest sea conditions that occurred during this period.

Figure 1 shows the unit located at Twillingate, Newfoundland, overlooking the test site. The Raytheon Pathfinder MK2 is mounted on a prefabricated platform.



**Figure 1 Mobile Radar Unit at Twillingate, Newfoundland**



Figure 2 shows a view inside the van with the test setup. The radar processor is located in the rack unit at the far end of the table to the left of the display monitor. The equipment at the right of the picture is the logging equipment for the wave and wind data. In order to facilitate evaluation of the SeaScan system, it was equipped with recording capability for the trial. The tape unit used for the trial was an Exabyte M2 unit capable of close to 12 MB/s continuous recording. The unit is located on top of the rack unit in Figure 2.



**Figure 2 Interior View of Mobile Radar Unit**

## 2.1 ENVIRONMENTAL CONDITIONS

The main focus of the trial was to determine system detection performance on growlers and bergy bits in high sea states. In order to facilitate this and to maximize the probability of getting the desired data, an extended field trial was designed. Once the equipment was deployed at Long Point, Twillingate, conditions were monitored and field personnel mobilized when conditions were suitable for data collection. This mode of operation permitted leaving the equipment in the field for a six-week period.

Overall data was collected on numerous growler and bergy bit targets in sea states up to 3.5 m significant wave height (5.9 m maximum wave height) and wind speeds to 35 kn. Iceberg aerial ground truth data was collected by C-CORE and surface-based ground truthing of iceberg targets was conducted by Sigma Engineering Limited and Oceans Limited of St. John's. Oceans Limited also provided weather forecasting for the site and in-situ measurements of wind and wave data.

During the trial, radar data was collected on various sizes of icebergs ranging from growlers to very large icebergs. The data was collected during seven data collection days – June 5, 6, 14, 15, 16, 21, and 22, 2002. Oceans Limited was contracted to provide weather forecasting and ground truthing support for the trial. A comprehensive ground truth report was compiled by Oceans Limited and includes summaries of all environmental and iceberg data collected during the period. This report provides position information on icebergs that were observed visually from the surface and from aircraft.

Waves were measured using a non-directional Datawell wave rider buoy that was moored in position 49° 43.06'N; 54° 47.56'W (018° True at two miles from the radar site). Data was collected and archived through a Digital Wave Rider Receiver (DIWAR) and laptop interface. Wind speed and direction were measured in the vicinity of the radar site at a height of 2 m above the surface using a RM Young anemometer. Wind data was collected and archived through a Campbell Scientific Datalogger and laptop interface. A hand-held anemometer (Skywatch Elite) was used as a backup and this

unit also provided air temperature. Wind data from the Twillingate Lighthouse was also recorded on June 14, 15, 16, 21 and 22.

With the exception of June 16, icebergs were observed visually on each data collection day by Oceans Limited. On June 16 there was only one hour of radar data collection and during this period the visibility was only an 1/8 of a mile. Observations were typically taken every one to two hours. Visual observations were supported by photographs taken by Sigma Engineering Limited. These photographs were subsequently analyzed to confirm iceberg sizes. Additionally, three over flights were carried out by C-CORE. Information from these flights, which took place on June 5, 14 and 21, was also incorporated into the compilation of the iceberg data.

To support the project, five-day forecasts were issued daily by Oceans Limited. These forecasts were used for the planning of field trips and data collection events.

### **3 DATA SUMMARY**

The complete field data set includes environmental and iceberg ground truth data. Iceberg photographs are available in digital form and have been archived on CD for use in detailed analysis. For the trials the bulk of the iceberg ground truthing photographs were taken using a Canon S40 digital camera. This four-megapixel camera has a three times optical zoom and records focal length with each picture so that absolute target measurements may be made during the analysis task. The camera was calibrated using a target at a measured distance and tested for the range of focal lengths available. A spreadsheet was constructed so that iceberg target pixel dimensions could be entered along with range and focal length, and dimensions would be automatically calculated. The camera also permits audio annotation of each photograph for verbal identification of the object being photographed.

This section provides an example of the data available for analysis. The data selected was on the day with the highest sea state (June 15). Unfortunately, visibility during the day was very poor so ground truthing photographs could not be taken until later in the

day. This provided a very good opportunity to evaluate the operational capability of the system as field personnel were blind to the actual situation. Early in the morning a target was identified near a medium grounded iceberg at a range of 2.6 nmi. Visual confirmation of the target was not possible until later in the day but the target was tracked from 2.5 nmi into a range of about 0.8 nmi. At the near range the target entered into the shadow zone in front of the radar caused by terrain. The target was monitored intermittently as it moved through the shadow regions and at 0.6 nmi it was observed visually as a small bergy bit. A number of photographs were taken to document the target and to make size measurements.

A complete data summary is provided in the Oceans Limited ground truth report. Figure 3, Figure 4 and Figure 5 summarize the environmental conditions during the bergy bit data collection (June 15).

On June 15 a north-northwest to north wind prevailed during the first half of the radar data recording period. Then, about mid-period, the wind veered into the north-northeast. [**Note:** the R.M. Young anemometer located in the immediate vicinity of the radar site was observed to undergo erratic behaviour in turbulence eddies due to the influence of the local topography in the north-northeast winds. As a consequence, the quality of these data was very poor under these conditions.] Based on wind speeds recorded at the Twillingate Lighthouse weather station WDO combined with hand-held anemometer measurements, the wind speed over the water was estimated to be near 25 kn with gusts of 30 to possibly 35 kn early in the period. Winds of 15 to 20 kn prevailed in the north-northeast winds during the latter half of the recording period.

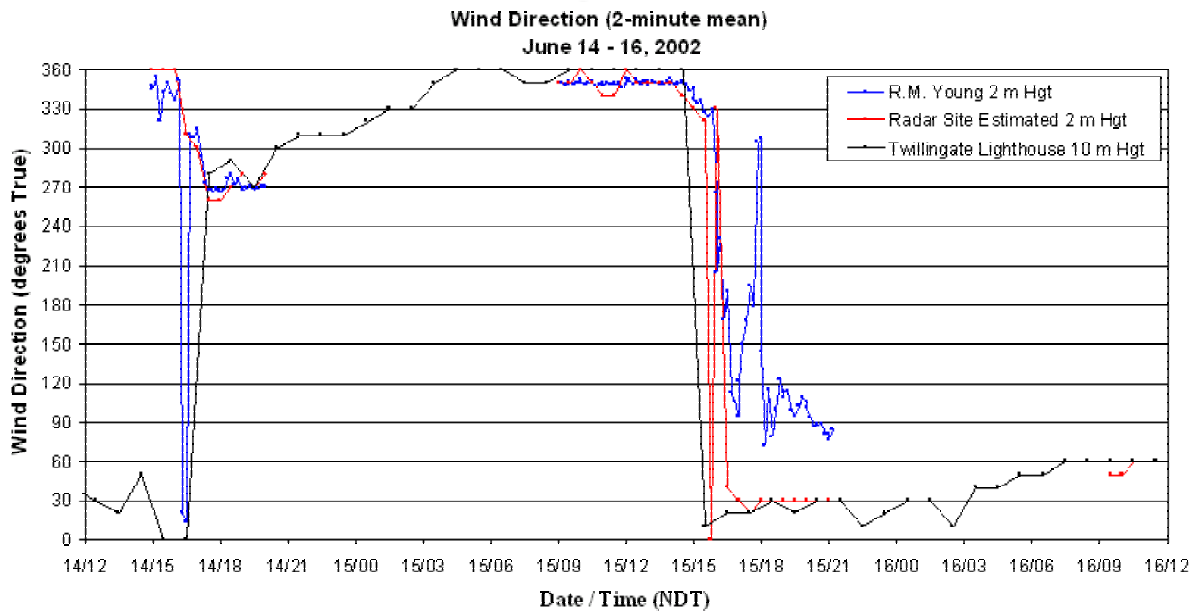


**Figure 3 Wind Direction for June 14 to 16**

The significant height of the combined seas ranged between about 2.9 m and 3.5 m during the data recording period, with an average zero-crossing period between 6 and 7 s. A maximum of wave height of 5.95 m was recorded during one 20-minute sampling period. Otherwise, the highest waves ranged between 4.2 m and 5.8 m during individual sampling periods.

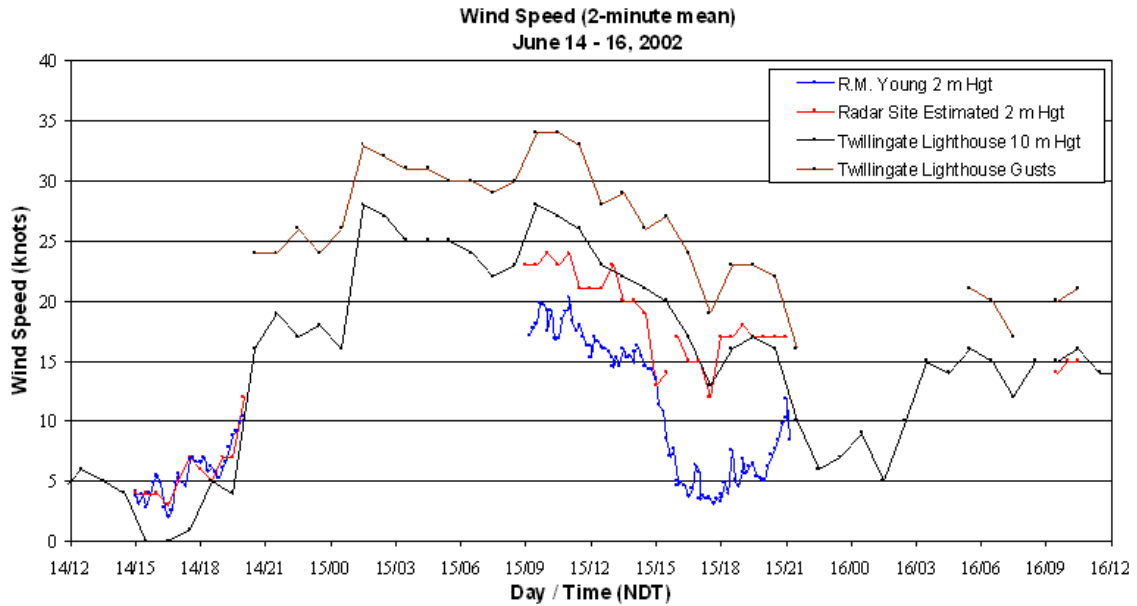


**Figure 4 Wind Speed for June 14 to 16**

Very poor visibility in fog prevailed early in the day, precluding visual observations of the water surface from the radar site and nearby locations. Consequently, it was not possible to partition the sea state into separate sea and swell components.

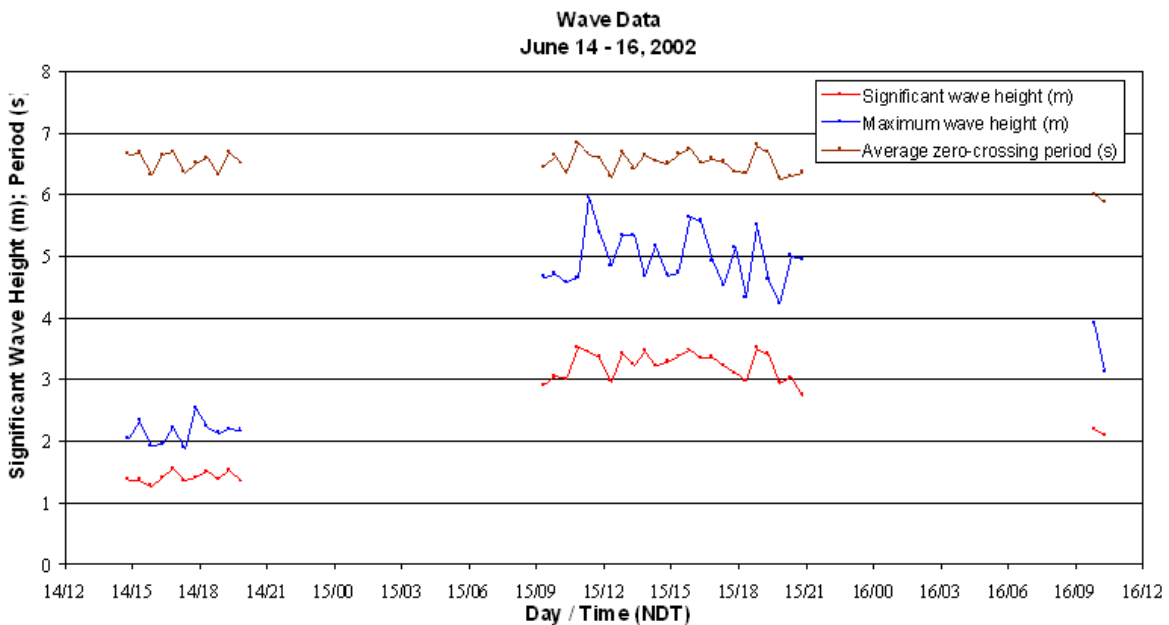


**Figure 5 Wave Height for June 14 to 16**

However, based on an assessment of the previous observations and the prevailing synoptic weather pattern, it is estimated that the sea state consisted of a northeasterly swell in combination with the northerly wind-sea. About mid-afternoon, the visibility improved sufficiently to visually estimate the sea state. At that point, the wind-sea was estimated to be near 2 m with a characteristic period of near 7 s, while a swell from the north-northeast was estimated to be near 3 m with a period of 10 to 11 s. The wind-sea lowered during the late afternoon to become near 1 m with a period of 4 s by the evening. The swell persisted, however, ranging from 2.8 to 3.3 m with a period near 10 s.

### 3.1 ICEBERG DATA

In-field notes of iceberg position as estimated visually or taken from the radar display were used to generate plots of iceberg position at specific times during a data collection. Figure 6 shows a set of iceberg plot data from June 14 at 17:45 NDT.

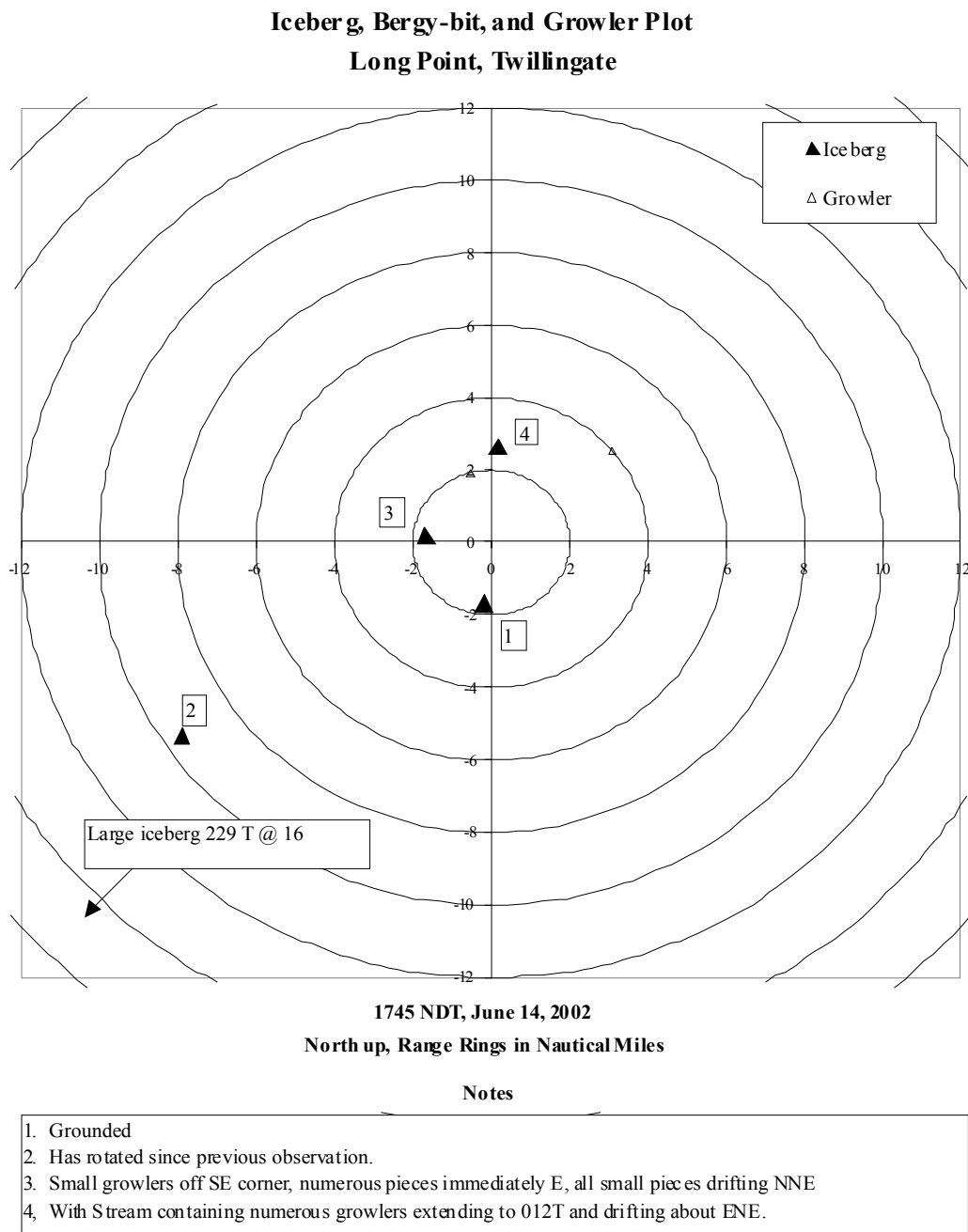


**Figure 6 Iceberg Position Plot, June 14**



This figure provides iceberg position data in graphical format with numbered notes. In Figure 6 there are three icebergs within 4 nmi. Each range ring is 2 nmi. Table 2 provides this same information in tabular format with actual target position information and description.

**Table 2 Iceberg Position and Identification**

Iceberg, Bergy-bit, and Growler Observation								
Declination: 23 deg W								
1745 NDT, June 14, 2002								
Number	Description	Bearing (deg M)	Range (deg T)	Range (nm)	Bearing (polar)	X (nm)	Y (nm)	Notes
1	Small dome	209	186	1.69	-096	-0.18	-1.68	Grounded. Position from radar.
2	large iceberg	252	229	16.00	-139	-12.08	-10.50	Distant
3	Large dry-dock	259	236	9.50	-146	-7.88	-5.31	Has rotated since previous observation Small Growler off SE corner, numerous small pieces immediately to east; all small pieces drifting generally north-northeastward. Position from radar.
4	Wedge	299	276	1.67	-186	-1.66	0.17	With stream containing numerous growlers extending to 035M(012T) and drifting about east- northeastward. Position from radar.
6	Tabular/Blocky	027	004	2.65	086	0.18	2.64	
5	Growler	008	-015	2.00	105	-0.52	1.93	
7	Growler / small bergy-bit	074	051	4.00	039	3.11	2.52	

The tabular iceberg listed in Table 2 as target number 6 is presented in Figure 7. This iceberg was grounded and fixed in this position during the June 14 to June 16 data collection period. The iceberg was north of the radar site at a range of 2.65 nmi and a bearing of 4° True. The photograph in Figure 7 was taken with at a focal length of 21.3 mm and a 3.6 times digital zoom, and the iceberg was measured from the digital photograph to be 24 m high and 120 m long. This size places the iceberg in the medium size category.

The wedge iceberg listed in Table 2 as target number 4 is presented in Figure 8. This iceberg was grounded and fixed in this position during the June 14 to June 16 data collection period. The iceberg was west of the radar site at a range of 1.67 nmi at a bearing of 276° True. The photograph of Figure 8 was taken with at a focal length of 21.3 mm and a 3.6 times digital zoom, and was measured from the photograph to be 20 m high and 96 m long. This size places the iceberg in the medium size category.

During the data collection numerous growlers and bergy bits calved from these icebergs, providing continuous opportunities for iceberg detection measurements. The wind was light (6 to 7 kn) and from the west on June 14. This resulted in the movement of the small pieces of ice to the east (to the right in Figure 7 and Figure 8).



**Figure 7 Iceberg to the North of the Radar Site**



**Figure 8 Iceberg to the West of the Radar Site**

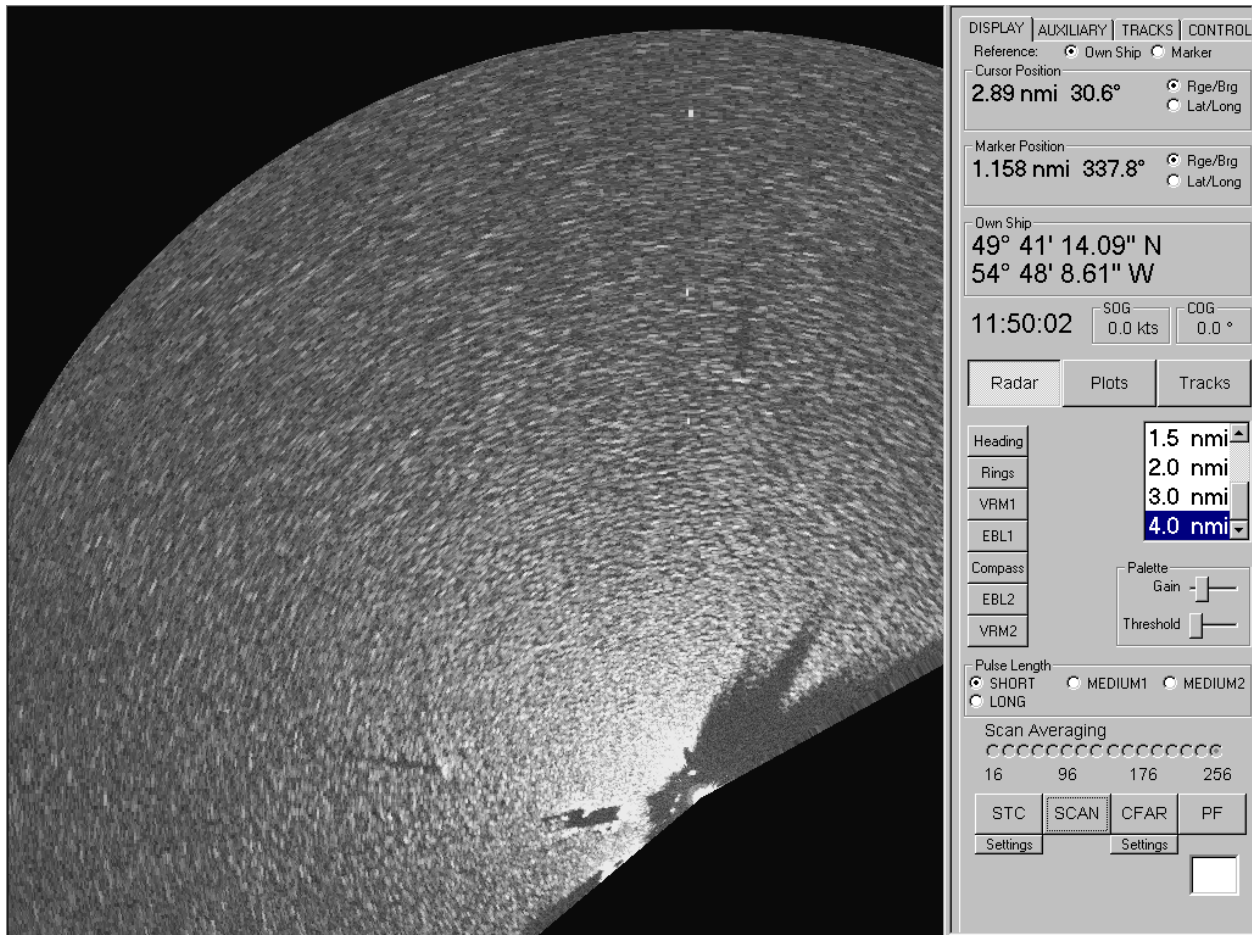
## 4 DETECTION PERFORMANCE

During the data trial it became clear that the system could detect all of the smaller pieces of ice within a 2 to 3 nmi range in the lower sea states. The only day that presented any problem for detection was June 15, when seas and winds were representative of a Douglas Sea State 6 or Beaufort Scale 7. The wind direction was from the north, so there was no limiting of wave height by shore effects or fetch. Given that these conditions were ideal for characterizing the system performance and the presence of the two grounded medium icebergs, it was considered that this data set should be the focus of the data analysis and system characterization.

Early in the experiment it was observed that under higher sea conditions detection did not seem to be as good as the trial that was conducted in 1999 using a 24 rpm antenna. The software had been configured to scan average process up to 64 radar scans. At 24 rpm this equates to 160 s of processing time. At 120 rpm 64 scans is only 32 s. It was speculated that for the 120 rpm system there was not sufficient time to allow the clutter to fully decorrelate. A modification to the software processing library was made to permit processing up to 256 scans, and this version was used for the field trial. This version did provide better detection performance than the 64 scan version. The Server PC had 2 GB of main memory and all of this was required for processing of 256 scans of 12-bit radar data.

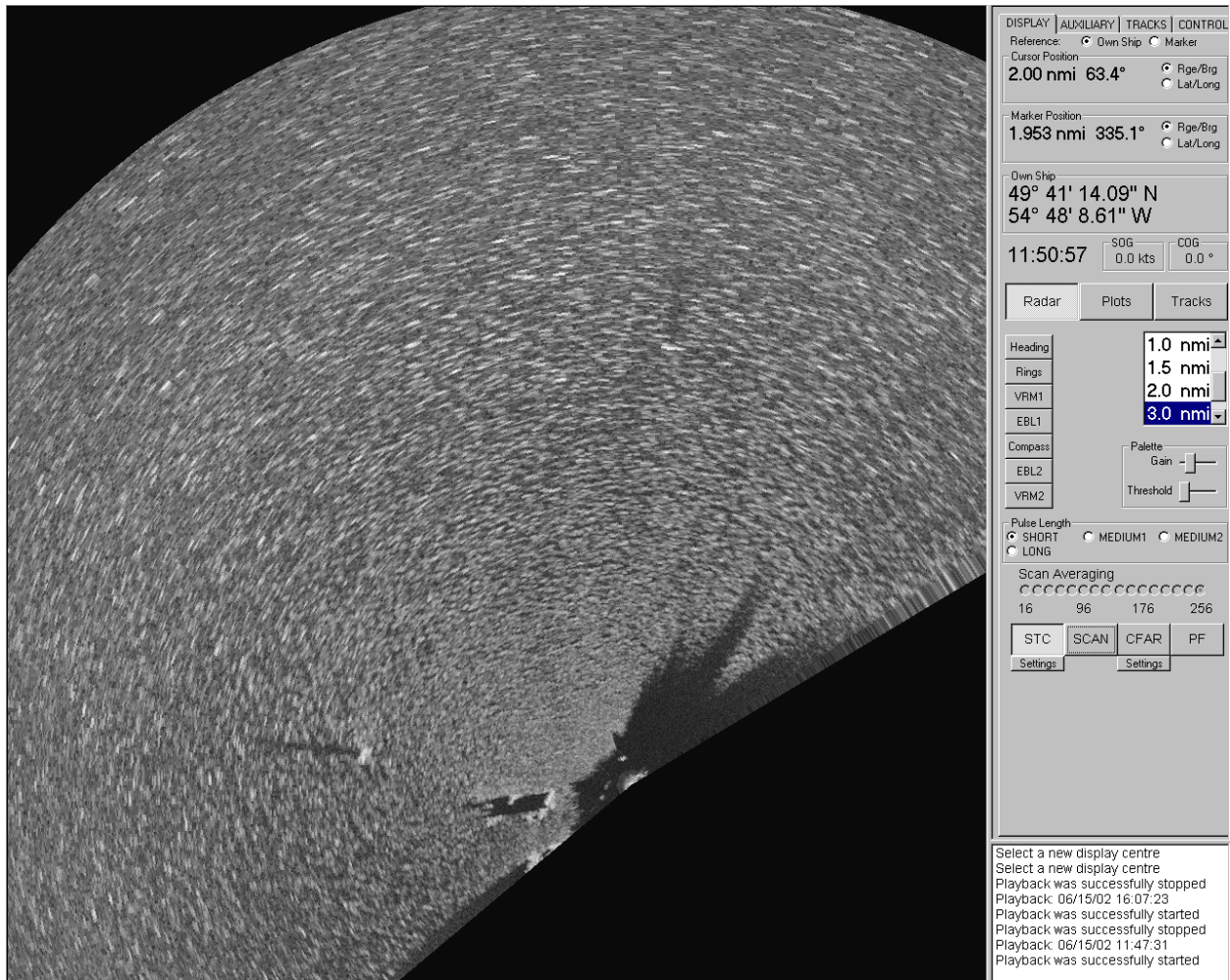
In order to get an overview of the conditions on June 15, it is informative to review some examples of the radar data and the effect of signal processing.

Figure 9 presents a raw image of the bergy bit and icebergs. It may be seen from the image that there is heavy clutter and even the larger icebergs are not obvious. The medium blocky iceberg at 2.6 nmi to the north is the iceberg in Figure 7. It is possible to see the shadow from the iceberg in the sea clutter. The medium wedge iceberg to the west is the iceberg in Figure 8.



**Figure 9 Icebergs in Sea Clutter on June 15 (Raw Data)**

Figure 10 presents the raw data with STC applied to remove some of the range dependence in the data.



**Figure 10 Raw Data with STC Applied**

Figure 11 presents results of 256 scans averaged (STC applied). The iceberg to the north and the one to the west become much more obvious. The bergy bit is showing up south of the iceberg to the north.

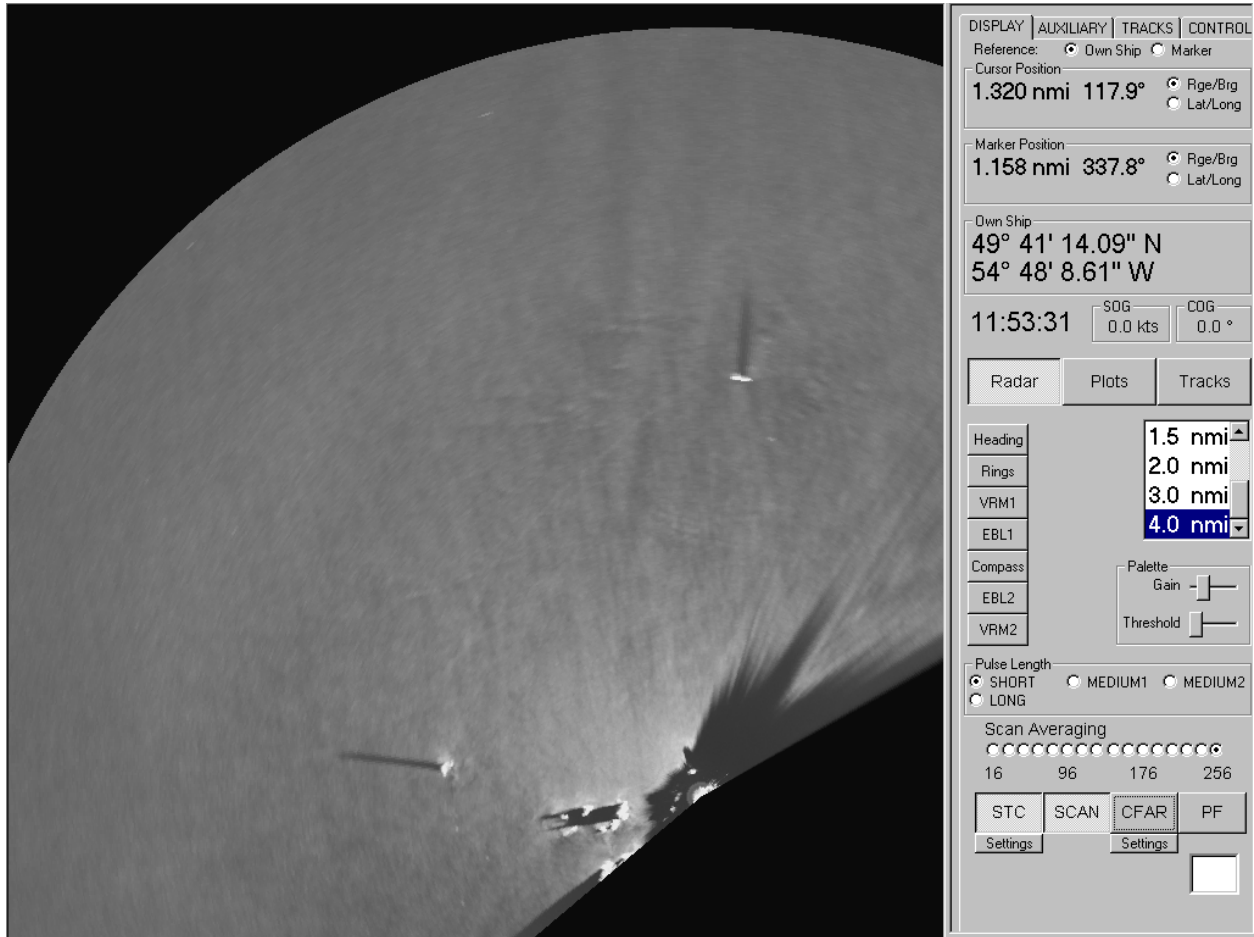
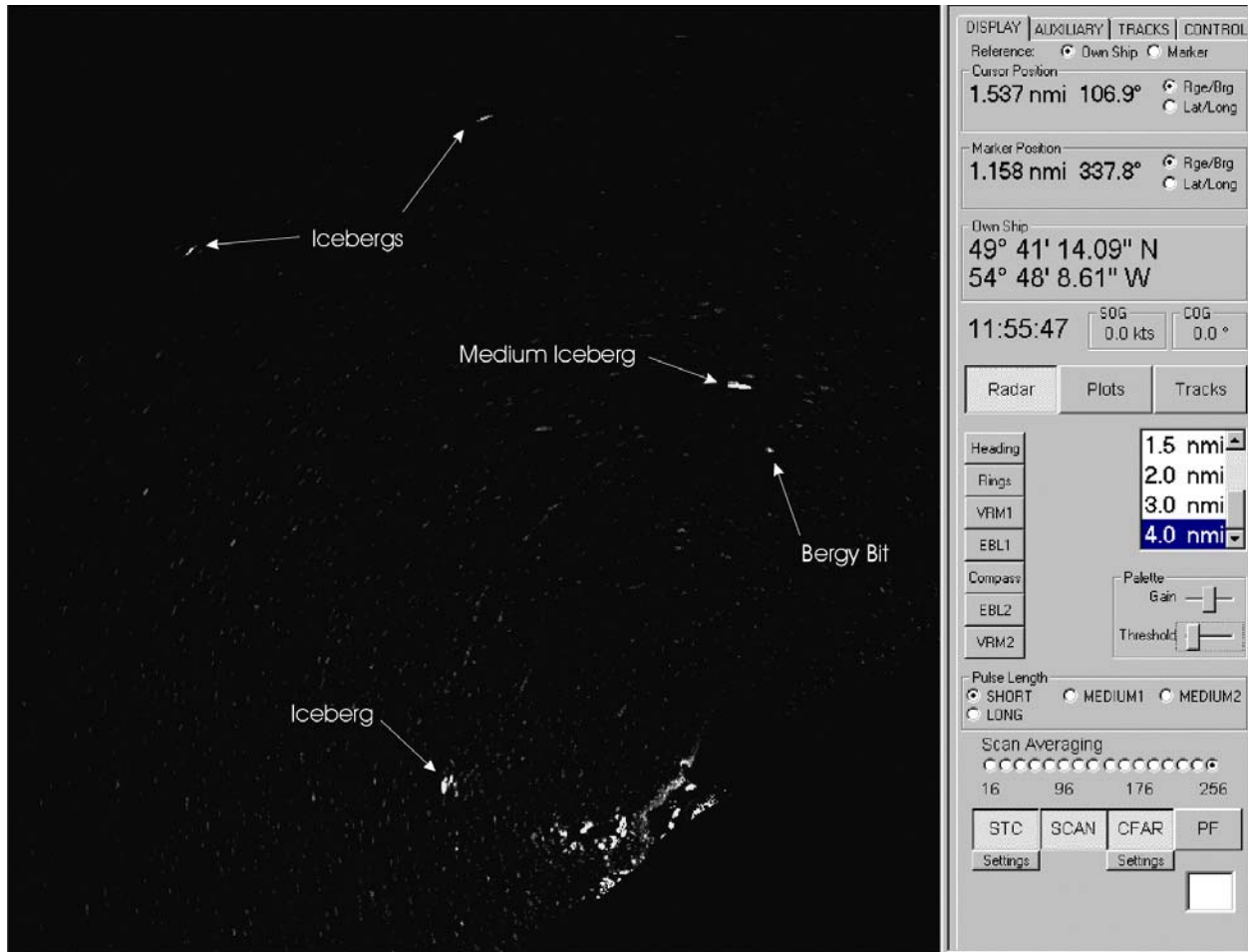


Figure 11 Scan Averaging and STC Applied

Figure 12 provides the results of full processing (STC and 256 scans averaged) with CFAR clutter removal. The bergy bit is now very clearly present along with other targets identified as icebergs. There are also bergy bits and growlers visible to the south of the iceberg to the west.



**Figure 12 Full Processing Applied**

Figure 12 shows the area and targets of interest. Throughout the day and into the evening of June 15, numerous bergy bits and growlers were monitored as they calved from these two larger icebergs and moved toward the radar. Sections 4.1 and 4.2 investigate the measured detection performance on these targets. Furthermore, the wave rider used for wave measurement proved to be a very challenging target and it too was used in the detection analysis.



## 4.1 ANALYSIS METHODOLOGY

Target detection performance is measured in terms of Probability of Detection (Pd) and Probability of False Alarm (Pfa). This means that for a given set of operational conditions and display and processor settings, a target will be visible or detected a percentage of the time and there will be a corresponding number of false alarms caused by system noise and clutter from sea and rain echos. There is a trade off in these two quantities. The higher the number of false alarms (higher Pfa) displayed, the higher the probability of detection (Pd) will be. In order to achieve optimal detection performance, a radar operator will normally set up the radar display and adjust the radar processing to display a small number of false alarms. This is similar to automatic detection systems where the tracker can tolerate and reject a small number of false alarms. If the system is set up so that there are no false alarms, then it is likely that detection performance will not be as good as possible, particularly for small targets such as icebergs in sea clutter.

A radar performance prediction model is often to predict probability of detection as a function of range for a given probability of false alarm for the particular radar parameters and prevailing environmental conditions. Under typical operating conditions, a probability of false alarm in the range of  $10^{-6}$  to  $10^{-4}$  is used. This means that in one radar scan, 1 to 100 false alarms will be displayed. A trained operator or sophisticated target tracker can tolerate this false alarm rate.

The 2002 Twilligate data was reviewed and targets that offered the best possibility of meeting the analysis objectives were selected for analysis. The targets selected were a bergy bit and a deployed wave rider buoy. These targets were selected as a long time series of recorded data was collected on them during the highest sea state.

Furthermore, the bergy bit moved from a range of 2.5 nmi to 0.9 nmi during the data collection period.

Data analysis software was used to automatically compute the target detection probability for the selected target and the false alarm probability for a region close to the target's position.

For each target analyzed, a target detection window was set up, and nearby a window for computing false alarms was set up. This method was used to analyze data from the 1999 Twillingate trial. The software processes a large number of radar scans and generates Pd and Pfa as the detection threshold is changed. Since it is not known prior to analysis what the best threshold is, it is necessary to sequentially change the threshold and log detections. This requires numerous runs of the data analysis software.

The detection threshold is the digital level (or analogue voltage) that must be exceeded by the radar signal before the signal can be counted as a detection or false alarm. At this point, the detection process does not know whether the signal exceeding the threshold is from a target or from noise or clutter. For example, in the case of receiver noise limited detection, as the detection threshold is lowered so that noise signal exceeds the threshold, the display and analysis software will count a higher number of false alarms. When there is a target present, as the threshold is lowered there is a higher probability that the target signal will exceed the threshold, so the number of target detections increase. The analysis software must count the number of detections in the target and clutter windows for each threshold analyzed. For the results to be operationally significant, a threshold must be found that gives a Pfa in the range of  $10^{-4}$  to  $10^{-6}$ .

## **4.2 ANALYSIS RESULTS**

This analysis concentrated on data from two targets collected on June 15, 2002. Data was collected continuously through the day from 09:00 until 21:00 (NDT). Over this 12-hour period, data on many growlers and bergy bits were collected. Six data tapes were collected, totalling 360 GB of data. The bergy bit selected here for analysis was detected at 10:44 in heavy fog. The target was assumed to be an iceberg, as it was first detected at a position very close to a grounded medium iceberg (Figure 7). This berg was monitored by radar throughout the day, although it was not observed visually until 15:35. The iceberg was first identified at a range of 2.6 nmi and bearing of 5.7° (True). The wind and waves at the time were from the north, so the iceberg was being driven toward the radar from a direction of maximum sea clutter. It took the iceberg, later identified as a small bergy bit (Bergy Bit 1 in Table 2), 5 hours to travel 1.6 nmi, giving it an average speed of 0.3 kn or 0.15 m/s.

The other target selected for analysis was a deployed wave rider buoy. The wave rider represents a very challenging target from a detection point of view as it is physically small and half submerged. This target was deployed at a range of 1.9 nmi from the radar. Bergy Bit 1 passed very close to the wave rider as it moved toward the radar, so wave data is expected to be very accurate for both the wave rider and bergy bit detection analysis.

### **4.2.1 Wave Rider Detection**

In order to further test the radar performance, it was decided to analyze data from the deployed wave rider buoy, as it represented a controlled target that was present during the entire trial. The wave rider has physical diameter of 0.9 m, of which half is submerged. The calculated radar cross section of this target is 0.3 m<sup>2</sup>. This would correspond roughly to the size of a large growler (1 m high by 6 m long) or close to that of the small bergy bit to be considered in the analysis. The wave rider was detectable on most days, but was not obviously detected during the data collection of June 15. It

was, however, identified during the detection analysis of the bergy bit. This target would therefore seem to represent close to the detection limit of the system for this set of environmental conditions.

For each target it is possible to configure the processing for different levels of scan processing. This, coupled with the large amount of data collected on each target, requires a selection of the processing and specific data segments to optimize the time required to analyze data collected. Data analysis was conducted on specific data points to investigate the effects of antenna speed and processing levels on detection. More detailed analysis was conducted on targets over longer periods of time for investigation of detection as a function of range as the iceberg moves towards the radar. The wave rider data is analyzed over time to measure detection as a function of time and environmental parameters.

#### 4.2.2 Wave Rider Analysis with 256 Scans Processed, 120 rpm

Figure 13 presents detection analysis results for the wave rider buoy as a function of time for short pulse. In this case, 1000 scans of data were processed at each time window. The target was stationary and so did not move during the processing other than that permitted by its watch circle. At 120 rpm, 1000 scans represents 500 s or 8.3 minutes of data, and the processing interval represents 128 s (256 scans at 120 rpm). Eight data segments were analyzed. Detection was found to be poor early in the day

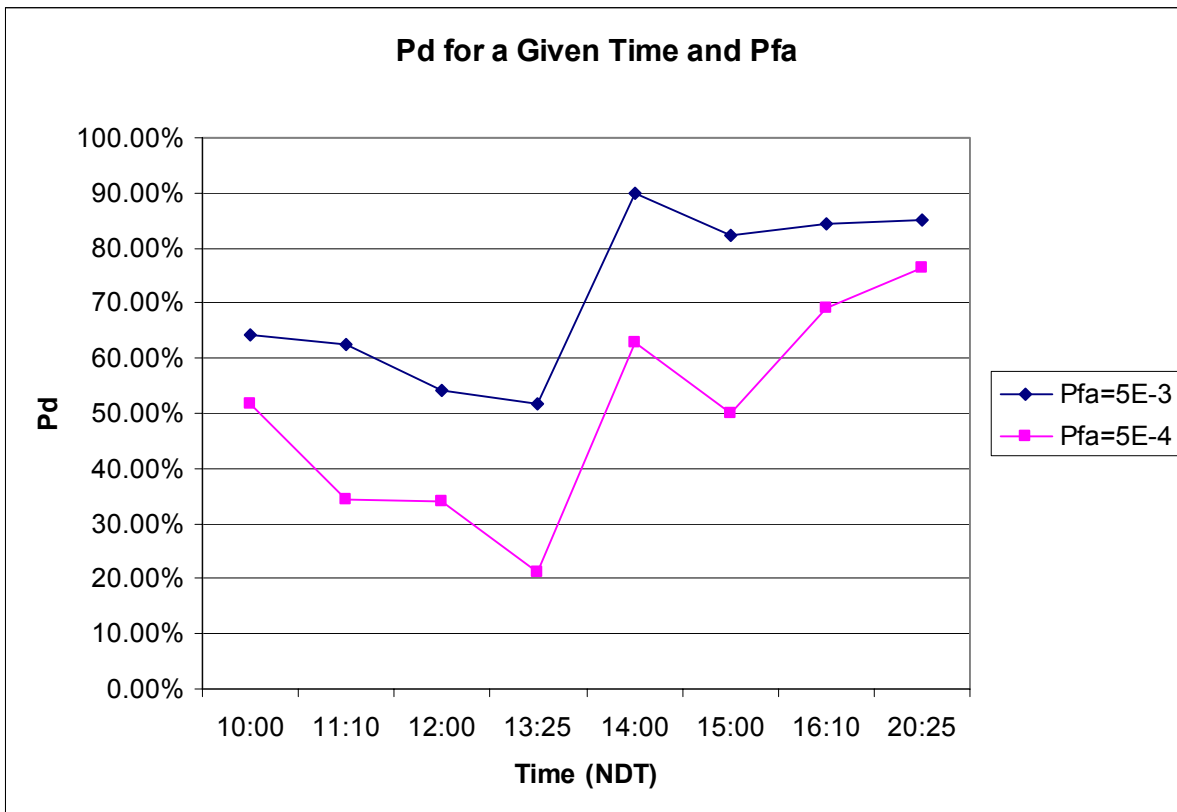


**Figure 13 Probability of Detection of Wave Rider Buoy, 256 scans, 120 rpm**

and improved later in the day as the wind speed dropped. Reviewing the environmental data, it can be seen that the wind speed drops and swings to the northwest between 14:00 and 15:00. This provides excellent agreement with the change in detectability. It would appear that even though the wave height remained high throughout the day, it became more swell dominated in the later hours. This is very significant as it demonstrates that even this small a target (0.5 m out of the water) can be detected in

wave heights that far exceed its own height (maximum seas remained in the 4.5 to 6 m range over the entire time). Furthermore, the data illustrates the effect of wind speed on detection for near constant wave height.

It should be noted in this case that the best detection for Pfa of  $10^{-3}$  was in the range of 80 to 90 percent. This would be quite acceptable, although the high Pfa would result in up to 300 false alarms in one scan and this may exceed the operational capabilities of the operator and tracker. The lower false alarm rate of  $10^{-4}$  provides detection in the 70 to 80 percent range in the best case, and it is expected that this target would be detectable over this range. During the morning, when maximum wind speed and wave height was encountered, the target would not be detected in an operational context with this level of processing. The data collected on the wave rider can therefore be considered to bracket the detection/no detection limit of the scan average processing. There were no detections of the wave rider when medium pulse was used.

#### **4.2.3 Wave Rider Analysis with 64 Scans Processed, 120 rpm**

In order to investigate the effect of scan average processing on the 120 rpm antenna, the same data segment was analyzed only processing 64 scans of data. Figure 14 presents results from this analysis as a function of time. In this case, 1000 scans of data were processed at each time window. The target was stationary and so did not move during the processing other than that permitted by its watch circle. At 120 rpm, 64 scans represents 32 seconds of data. Eight data segments were analyzed and detection was found to be poor over the whole day. As was observed for the 256 scans processed, better detection was observed later in the day, but nowhere does detection exceed 50 percent. It is clear that the 256 scans are required if detection is to approach reasonable levels. It was noted in the analysis of data from the 1999 Twillingate trials that 48 scans processed provided very good results in similar sea conditions to those encountered here. It is expected that this is related to the relative time duration of the

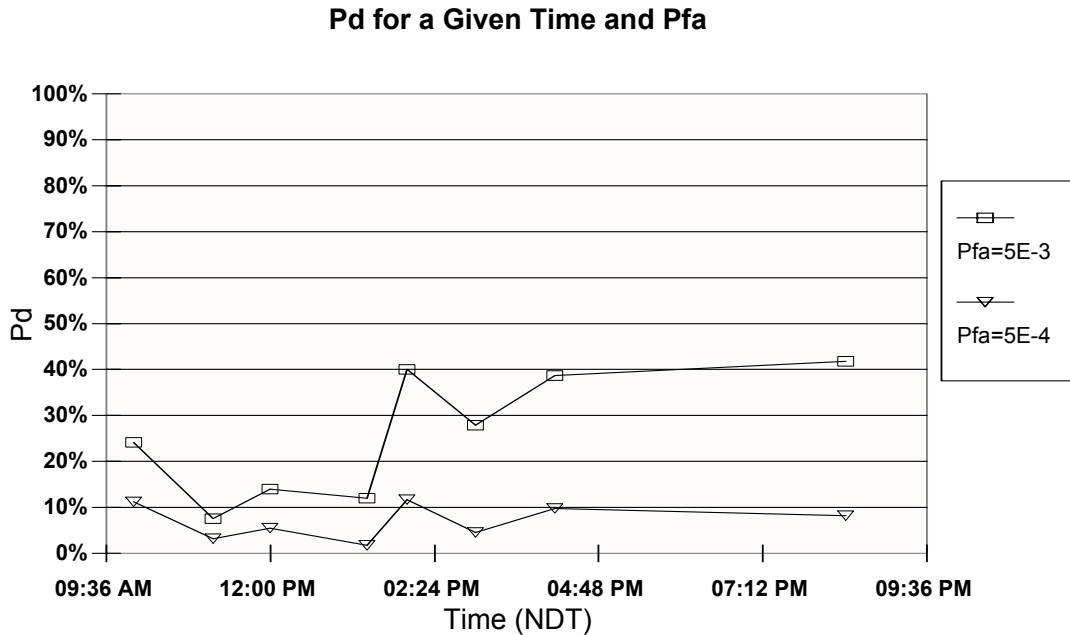


**Figure 14 Probability of Detection of Wave Rider Buoy, 64 scans, 120 rpm**

processing and not the number of scans processed. This is investigated further in section 4.2.7 of this report.

#### 4.2.4 Bergy Bit Detection

This section summarizes the detection results for Bergy Bit 1 over a 5 hour period. The bergy bit selected here for analysis was detected at 10:44 in heavy fog. The target was assumed to be an iceberg as it was first detected in the vicinity of a grounded medium iceberg (Figure 7). This berg was monitored by radar throughout the day, although it was not observed visually until 15:35. Figure 15 and Figure 16 provide ground truthing pictures of the bergy bit taken with a digital camera. The camera was calibrated over its zoom range so that accurate target size measurements could be made. Each photograph contains all data on camera settings, including focal length and digital zoom factor, if used. Table 3 presents measurements on the bergy bit. When a review of the photographs was conducted, it was noted that a small growler-sized piece of ice was

located to the west (left of the bergy bit). This target was not observed in the field and no other obvious targets had been detected in the vicinity of the bergy bit during the field trial. The smaller target identified in the photograph was a growler and its size information is also presented in Table 3.



**Figure 15 Growler and Bergy Bit Targets, 15:45 NDT**



**Figure 16 Growler and Bergy Bit Targets, 15:46 NDT**

This growler, described in Table 3 and shown in Figure 15 and Figure 16, was not detected in the field or in the analysis of the bergy bit in to a range of 1 nmi. It was therefore assumed that the growler was not detectable, even with full radar processing. In order to confirm this, the data was re-analyzed and reviewed as close as possible to the radar. It was found that between 15:25 and 15:32, the target that had been tracked actually split into two targets and this was verified in the processed radar video (Figure 17). Furthermore, this shows that both the bergy bit and growler presented in Table 3 and shown in Figure 15 and Figure 16 were both detectable. This clarifies the



situation of the non-detection of the growler and means that the target detection results presented in this section apply to a slightly larger bergy bit than that presented in Table 3.

**Table 3 Iceberg Measurements from Photographs**

Date	Time(NDT)	Photo	Length(m)	Height(m)	Description
06/15	15:45:13	4923	6.3	1.8	Bergy Bit 1
06/15	15:45:19	4924	4.5	1.5	Bergy Bit 1
06/15	15:46:17	4925	4.9	1.4	Bergy Bit 1
Average Dimension(m)			5.2	1.6	Bergy Bit 1
Date	Time(NDT)	Photo	Length(m)	Height(m)	Description
06/15	15:45:13	4923	2.5	0.7	Growler 1
06/15	15:45:19	4924	3.2	0.5	Growler 1
06/15	15:46:17	4925	2.5	0.4	Growler 1
Average Dimension(m)			2.7	0.5	Growler 1

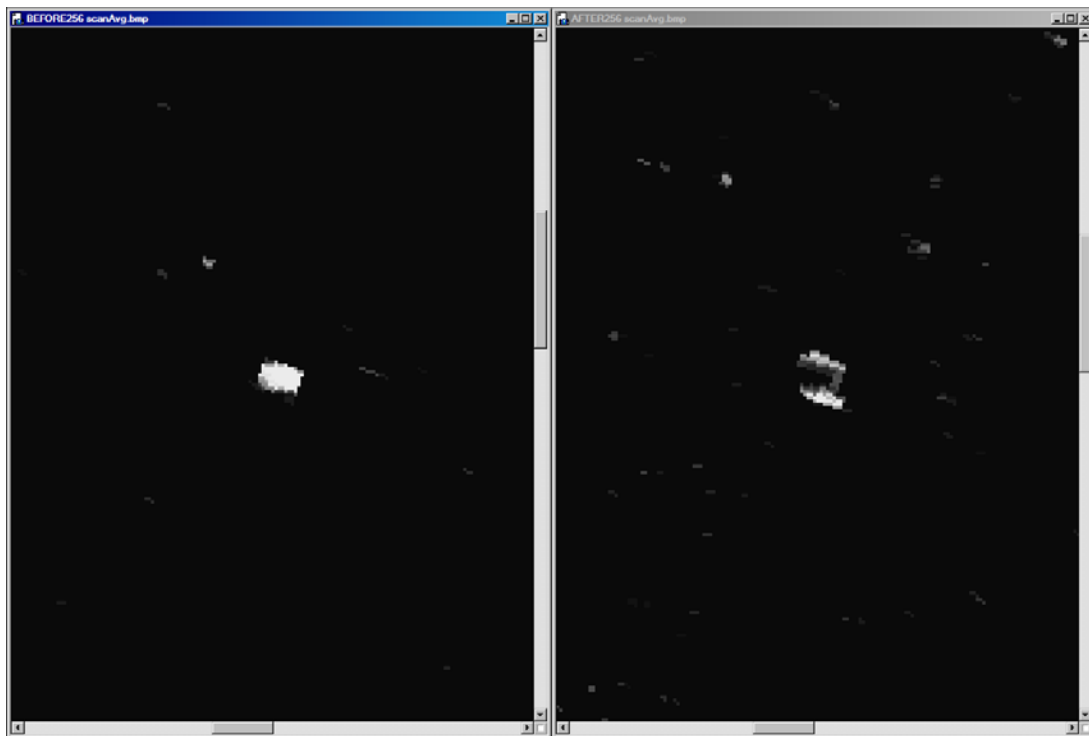


**Figure 17 Radar Image Before (Left) and After (Right) Bergy Bit Split**

#### 4.2.5 Bergy Bit Analysis with 256 Scans Processed, 120 rpm

Figure 18 presents detection analysis results for Bergy Bit 1 as a function of range. In this case, 1000 scans of data were processed at each range window. The target was permitted to move through a detection window during the processing. At 120 rpm, 256 scans represents 128 seconds of processing time. Eleven data segments were analyzed and detection was found to be excellent over the entire range. Data was not analyzed at 2 nmi as the wave rider was too close to the bergy bit and contamination of

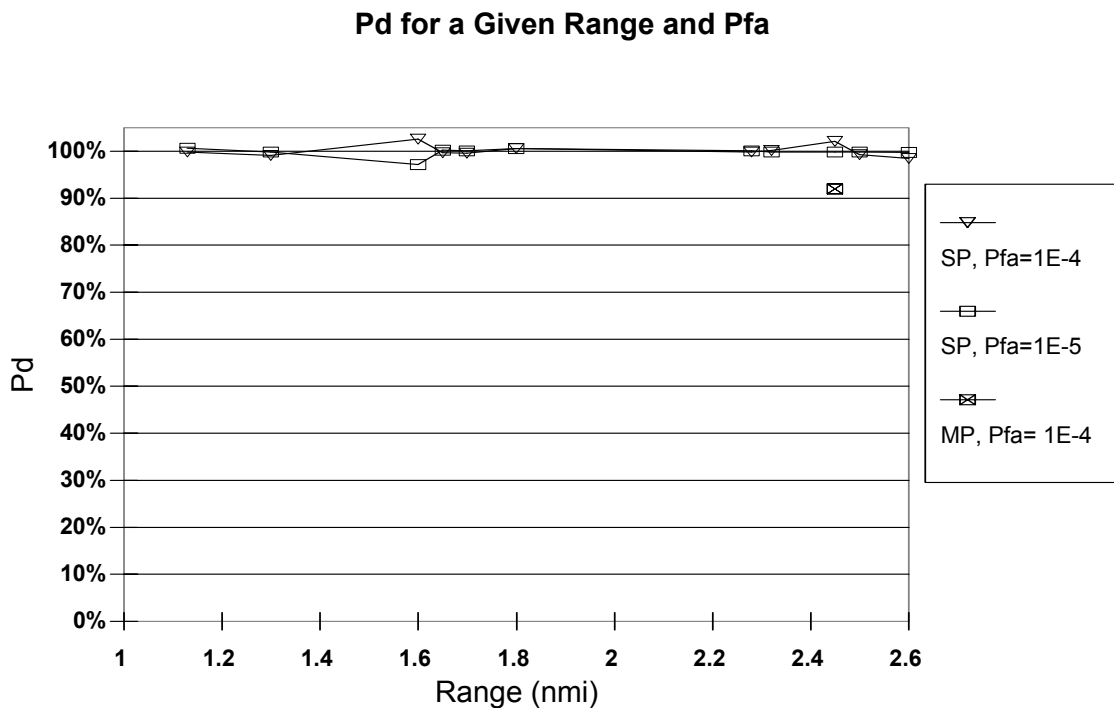


**Figure 18 Probability of Detection of a Bergy Bit, 256 scans, 120 rpm**

detection results was noted. Most of the data analyzed was for short pulse. It was noted in the field that detection on medium pulse was intermittent and that it was much easier to follow the target on short pulse. Most data was collected on short pulse as it was expected that it would provide the best data for analysis. Four medium pulse data segments were collected and one was analyzed for this report. When the iceberg was at 2.4 nmi, medium pulse gave a Pd of 92 percent for a Pfa of  $10^{-4}$ . This is a bit lower than short pulse and supports the field observations.

#### 4.2.6 Bergy Bit Analysis with 64 Scans Processed, 120 rpm

Figure 19 presents detection analysis results for Bergy Bit 1 as a function of range. In this case, 1000 scans of data were processed at each range window. The target was permitted to move through a detection window during the processing. At 120 rpm, 64 scans represents 32 seconds of processing time. Seven data segments were analyzed and detection was found to be very good over the entire range. The iceberg was moving toward the radar, so the maximum range was during the higher wind conditions. It may be noted from the figure that while detection is good, it is less than

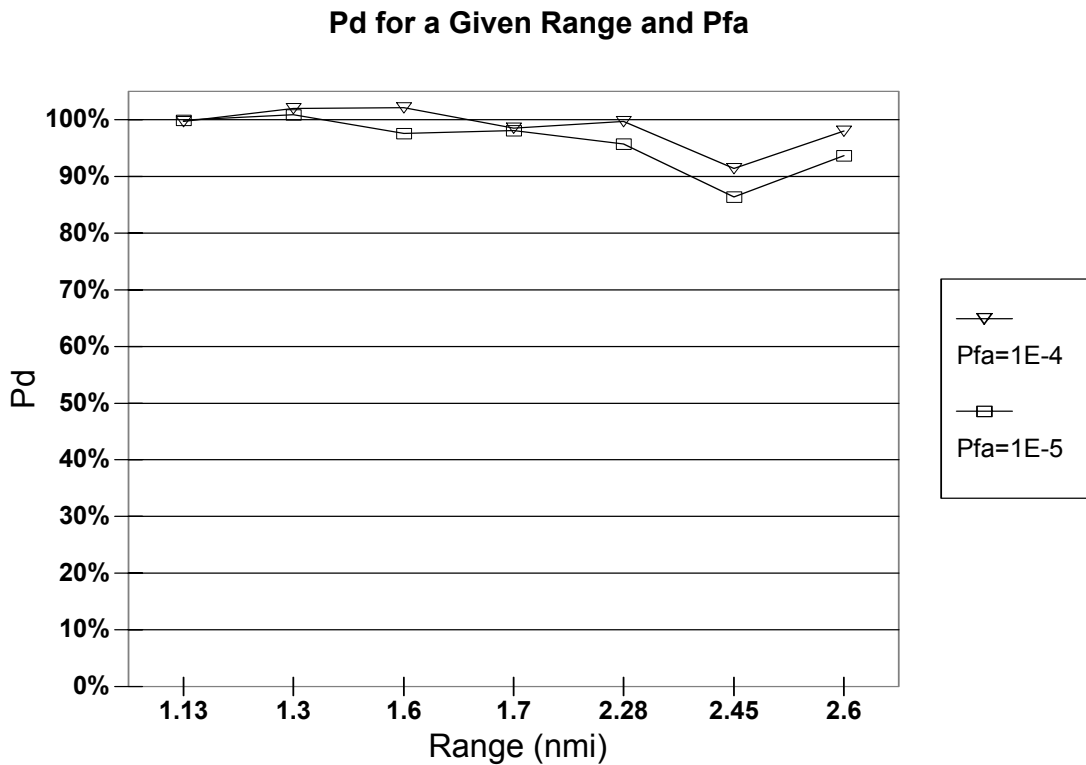


**Figure 19 Probability of Detection of a Bergy Bit, 64 Scans, 120 rpm**

100 percent at the longer range during the higher wind and wind-wave conditions. It is expected that this iceberg would be detected at ranges greater than 2.6 nmi. Data was not analyzed at 2 nmi as the wave rider was too close to the bergy bit and contamination of detection results was noted.

#### **4.2.7 Examination of the Effect of Antenna Speed**

The experimental radar used for the field trial was developed to aid in research into optimum antenna speeds for small target detection in high sea states. It is observed that a small target that is very low in the water compared to the prevailing wave height will often be obscured by the intervening waves and so will not be visible to an observer and to the radar. The visibility of the target will depend on the wave height, period and wave direction with respect to the radar. Looking up or down sea will be the worst case. Given that the target will only be visible for short intervals, the high-speed antenna will maximize the number of scans on the target while it is visible and therefore improve detectability.

Most shipboard radars operate in the 24 to 30 rpm range with newer high-speed antennas required for high-speed craft (HSC) operating in the range of 40 to 50 rpm. For a 30 rpm antenna, the same patch of ocean will be scanned by the radar every 2 seconds. If the sea has a period of 12 s, the radar will sample the wave 6 times as it passes a specific point. A small target could be hidden 50 percent of the time and would therefore be visible for 3 scans every 6 scans. In the case of a 120 rpm antenna, the target would be visible for four times that, or 12 scans every 24 scans. This is a very simplistic view of the situation. In reality the waves are much more complex in nature and obscuring of the target may not be as severe as this.

Furthermore, the only effective signal processing technique available for small target detection in clutter is scan-to-scan averaging. In order to achieve beneficial improvement in detection, the scan-to-scan processing interval must be long enough to average out the large variations in sea clutter echoes. In practice it has been found that this means processing anywhere from 16 to 64 radar scans on a normal low-speed scanning radar. In the case of a marine radar scanning at 30 rpm, this equates to 32 to 128 seconds of processing time. During this period of processing time, a small target

will inevitably be obscured by waves and detection will depend on the average signal displayed from the target versus the average clutter level.

Antenna height or height of eye will also affect whether a target will be obscured by waves. The higher the antenna and the closer the target is to the radar the less it will be obscured.

Sections 4.2.7.1 to 4.2.7.3 are directed toward the estimation of the effect of antenna speed on target detection.

#### *4.2.7.1 Simulating Different Antenna Speeds*

The experimental radar had a fixed 120 rpm antenna speed and as such does not directly permit the measurement of effect of antenna speed on detection. The only modification to the radar was to increase the antenna speed from a nominal speed of 24 rpm. This resulted in a reduced number of transmitted radar pulses per radar beam width from normal operation. In the case of the high-speed antenna this is compensated for by the increased scan rate coupled with scan-to-scan processing.

On short pulse, the pulse repetition frequency (prf) for the radar is 3000 Hz, resulting in 4 pulses per radar beam width for the 120 rpm antenna. Pulse-to-pulse integration in the radar processor will result in improved signal-to-noise ratio and better detection in noise-limited cases such as long-range target detection. In the case of clutter-limited detection, pulse-to-pulse processing does not provide much benefit in detection as the clutter remains correlated from pulse to pulse. In this case, scan-to-scan processing is considered more important, so the sacrifice in pulse-to-pulse processing is given up to increase scan-to-scan processing. It is generally accepted that, for effective radar performance, a minimum of 3 to 4 pulses per radar beam width is required. This means that in the case of a 3000 Hz prf and a 1 degree beam width, 120 rpm is the maximum speed that may be used without further modification to the radar to increase the prf.

An approximation of the change in antenna speed may be obtained by sampling the data prior to processing. If every fourth radar scan is processed, then the 120 rpm data could be used to emulate a 30 rpm antenna. Similarly, if every second scan is taken, a 60 rpm antenna may be simulated.

A custom version of the Sigma S6 software was configured to permit the selection of the number of scans to be skipped when processing the data. This would permit the simulation of antenna speeds of 60, 40 and 30 rpm along with the basic speed of 120 rpm.

The data analyzed in this study was taken from an eight-minute time period starting at 12:00 on June 15, 2002. This data was chosen because of its potential to test the effect of antenna speed on detection. This was the case as the wave rider target was marginally detectable due to poor weather conditions at that time.

The test was performed in two stages. The first was to investigate detection for a constant processing period for different antenna speeds. In this case, the number of radar scans was varied to meet the requirement of the processing period. The second was to investigate detection for a constant number of scans-to-average.

#### *4.2.7.2 Constant Processing Period*

The processing or averaging time was restricted to 128 seconds and the data set was analyzed at various antenna speeds. In order to simulate the effect of a changing antenna speed, the number of scans to skip was selected prior to scan averaging. Skipping one scan resulted in a scan interval of one second so only 128 scans were processed to meet the 128 second constant processing time. This would simulate a 60 rpm antenna. Similarly, if three scans were skipped, the scan interval would be two seconds and the simulated antenna speed would be 30 rpm. In this case, 64 scans would be processed to give the 128 second processing time.

Figure 20 shows the results of this test. It may be clearly seen that detection performance increases continuously with increasing antenna speed. It is important to point out that, in the case of slow moving targets, processing or averaging time is limited by the time a target stays in a particular radar resolution cell. Therefore, the faster the scans can be accumulated the better. There will be a limit to the maximum antenna speed where the clutter remains correlated from scan to scan. From the performance shown in Figure 20 it appears that this limit is greater than 120 rpm.

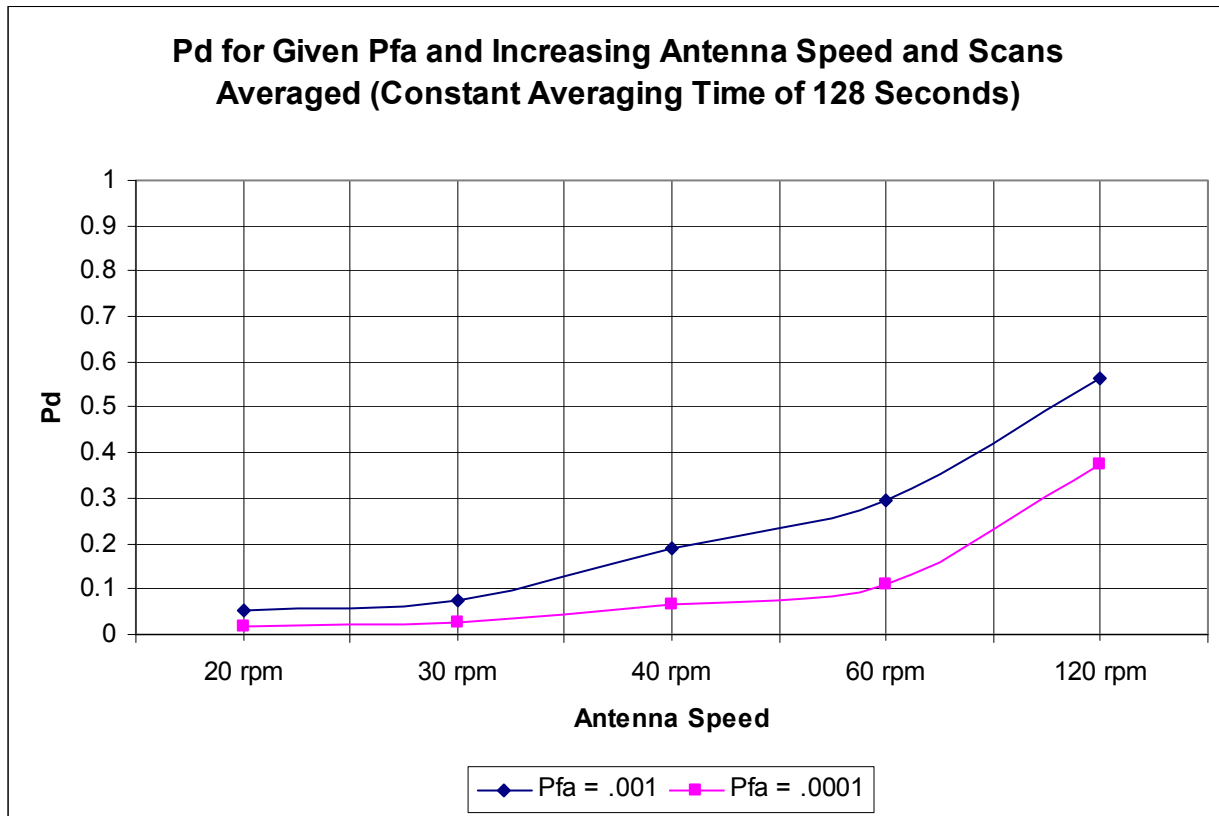


**Figure 20 Detection vs. Antenna Speed - Constant Average Time, 12:00 NDT**

#### 4.2.7.3 *Constant Scans-to-Average Value*

To further investigate the effect of antenna speed on target detection, the data set was again analyzed over a range of antenna speeds, keeping the number of scans-to-average constant at a value of 256. In this test, the number of scans processed remains constant so the processing, or time over which the average is computed, will decrease with increasing antenna speed. For example, 256 scans at 30 rpm results in 512 seconds of integration time, 256 scans at 60 rpm results in 256 seconds of integration time, and 256 scans at 120 rpm results in 128 seconds of integration time. In the case of moving targets it is preferable to minimize processing time.

Figure 21 presents the results of this test. It can be clearly seen that in the case of the stationary wave rider target, there is no benefit in increasing the antenna speed. A 30 rpm antenna can provide the same results as a 120 rpm antenna, but with four times the processing time. In the case of moving targets and early warning of a collision, the 120 rpm antenna is expected to provide a significant advantage over the 30 rpm antenna, as is illustrated in Figure 20. Further, the results of Figure 21 illustrate that even at 120 rpm the sea clutter is sufficiently decorrelated so that the full benefit of the scan processing is achieved. One might speculate that an even higher antenna speed might achieve this performance and therefore provide further improvement in target detection.



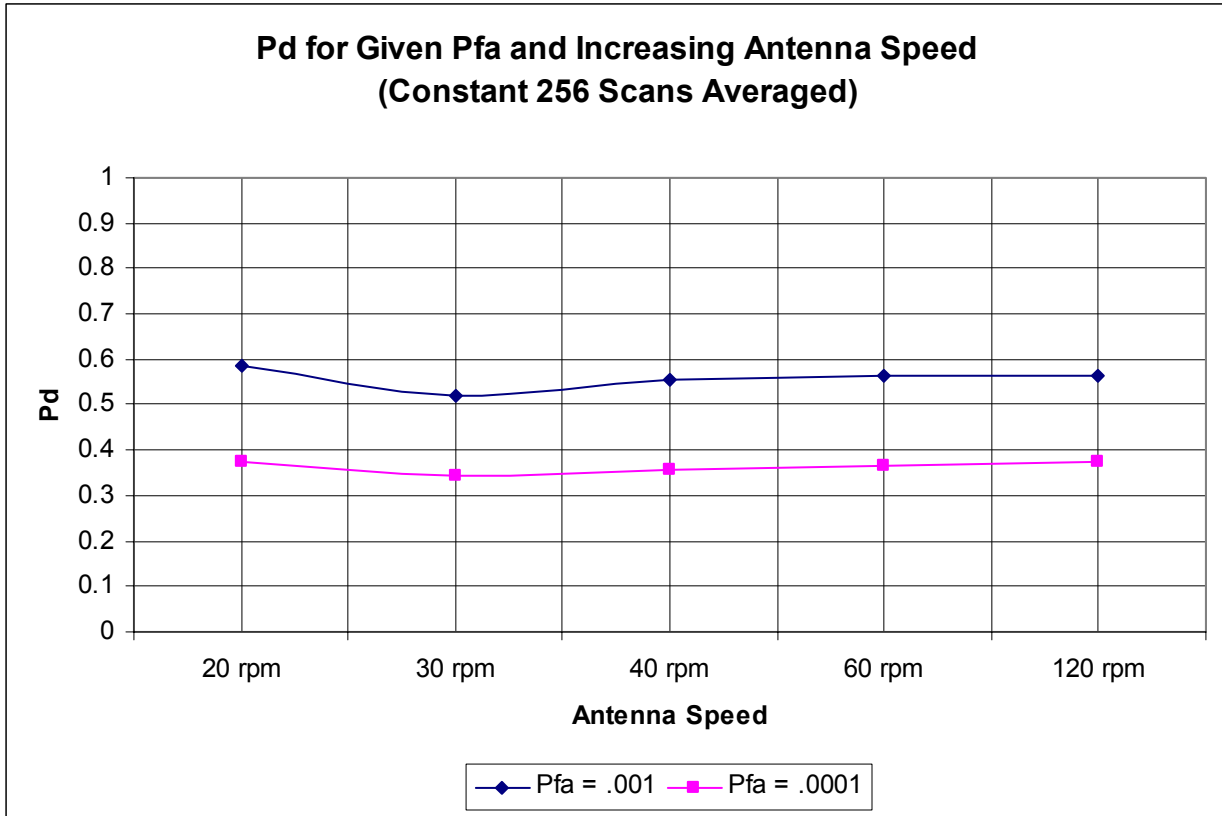


**Figure 21 Detection vs. Antenna Speed - 256 Scans Averaged, 12:00 NDT**

The data in Figure 20 was from the period of time when the wave rider was marginally detectable. Later in the day the sea conditions eased somewhat and detection improved, as shown in Figure 13. Figure 22 presents results for a constant averaging time of 128 seconds taken at 16:10. In this case, detection is better than in Figure 20, but follows the same trend of increasing detectability with increasing antenna speed.

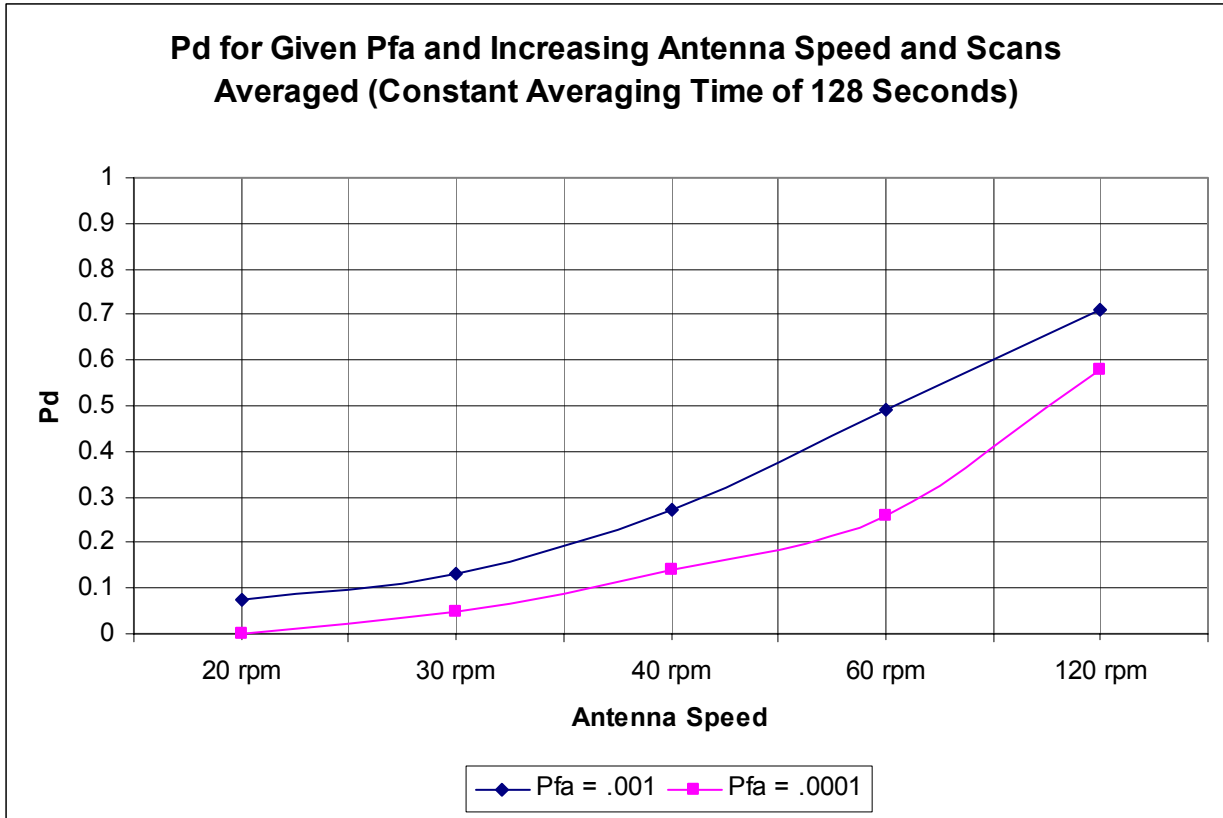


**Figure 22 Detection vs. Antenna Speed - Constant Average Time, 16:10 NDT**

From these trials we can easily see the benefit of faster antenna speeds. Two clear inferences can be made directly from the results of the experiment:

- 1) Higher values of scans-to-average will most likely correspond to better target detection.
- 2) Faster antenna speed means less processing time needed for desired Pfa and Pd values.

These two inferences indicate that, at higher antenna speeds, it becomes significantly easier to attain acceptable target detection, especially in cases of limited processing time on slow-moving targets such as drifting icebergs.

#### **4.2.8 Analysis of Close Range Bergy Bits and Growlers**

During the evening of June 15, 2002, numerous bergy bits and growlers that had calved from the iceberg to the north of the radar (Figure 7) moved toward the radar and along in front of the radar. This unique situation provided continuous opportunities to detect and collect data on these icebergs. In this case most of the data of interest was within 2.5 nmi and photographs from shore were acquired as the radar data was collected.

The data was collected over a period from about 18:00 to 21:00. This data offered the opportunity to review detection performance on very small targets in moderately rough sea conditions. By 18:30 the wind had dropped to about 17 to 18 kn from the northeast and combined seas were in the 3 m range, with maximum wave heights in the 5 m range. Swell height was about 3 m from the north ( $10^\circ$ ). From the afternoon, when the sea was being driven by a northerly wind, the evening saw the wind drop and swing around to the east. The swell direction remained northerly. This condition resulted in the icebergs tracking south toward the radar and then moving west.

Consistent with the analysis methodology in this project, all data was analyzed (using the **S6** plot extractor) in 8-minute segments at increasing threshold levels. For each target, an individual set of target and clutter zones was developed and an independent segment start time was determined. All data was analyzed at 256 scans averaged and 120 rpm. Detection points of interest were again at the  $P_{fa}=10^{-3}$  to  $P_{fa}=10^{-5}$  marks as these correspond to practical operational false alarm levels.

#### **4.2.9 Close-Range Target #1**

The first close-range target can be seen in the field photographs presented in Figure 24. At this time the target was at 1.4 nmi. The target was photographed later that evening (picture is provided in Figure 23). These photographs were used to estimate the target size. This target (Target #1) was analyzed in two 8-minute segments: one starting at 18:15, and another starting at 20:07.



**Figure 23 Field Photographs of Close-Range Target #1 at 20:13 NDT (0.8 nmi)**



**Figure 24 Field Photographs of Close-Range Target #1 at 17:58 NDT (1.6 nmi)**

Figure 25 and Figure 26 demonstrate the detection behaviour of Target #1 for both analyzed data segments. Both graphs show detection levels at 100 percent or a Pd of 1 over the range of Pfa. This illustrates very good detection on this target over the range from 1.4 to 0.8 nmi. Measurements from the photographs are provided in Table 4 and confirm the target to be less than 1 m in height and about 4 m in length. This places the iceberg in the growler size category.

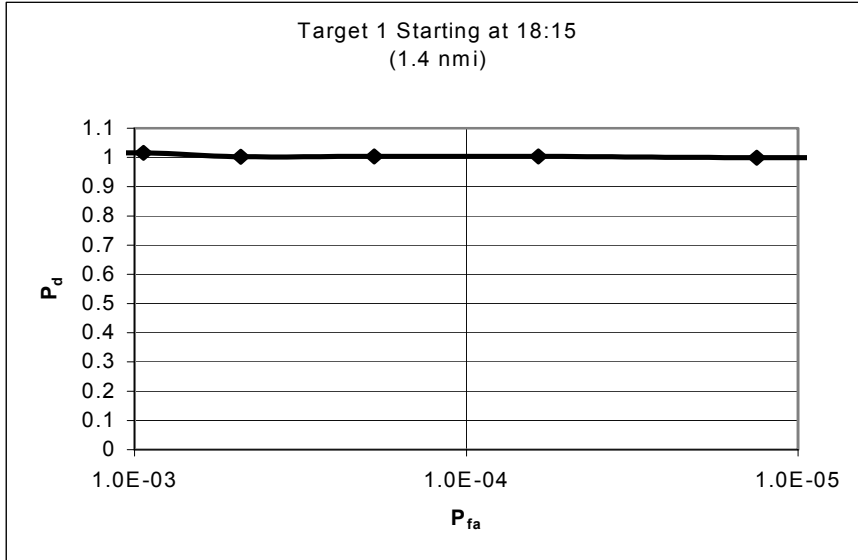


**Figure 25 Detection Performance for Target #1 at 1.4 nmi**

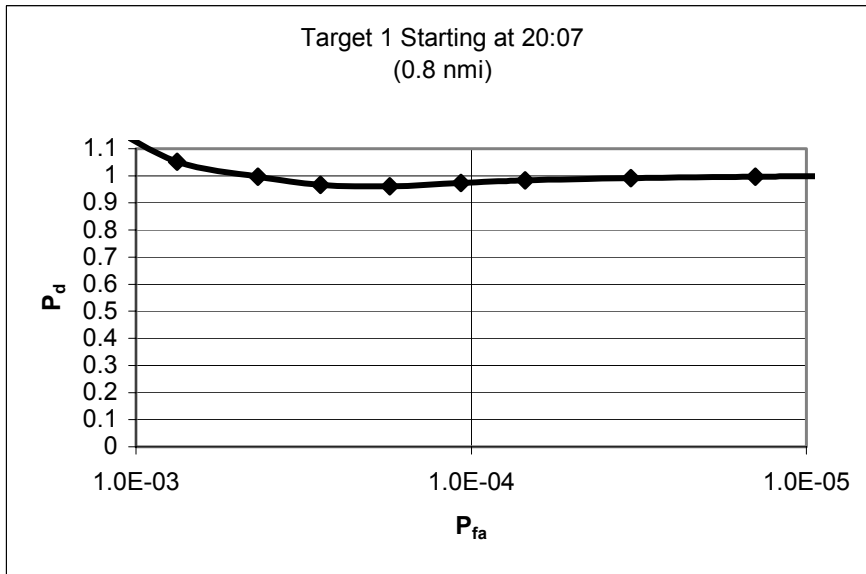


**Figure 26 Detection Performance for Target #1 at 0.8 nmi**

#### 4.2.10 Close-Range Targets #2 and #3

Two other close-range targets were analyzed. These targets are seen in the field photographs in Figure 27 and Figure 29. The field photographs were both taken at 20:18, but because of the targets' relative proximity to each other and other targets, the most accurate analysis segments started at 20:28:20 (target #2) and 20:30 (target #3).



Figure 27 Photograph of Target #2 at 20:18 NDT (1 nmi)

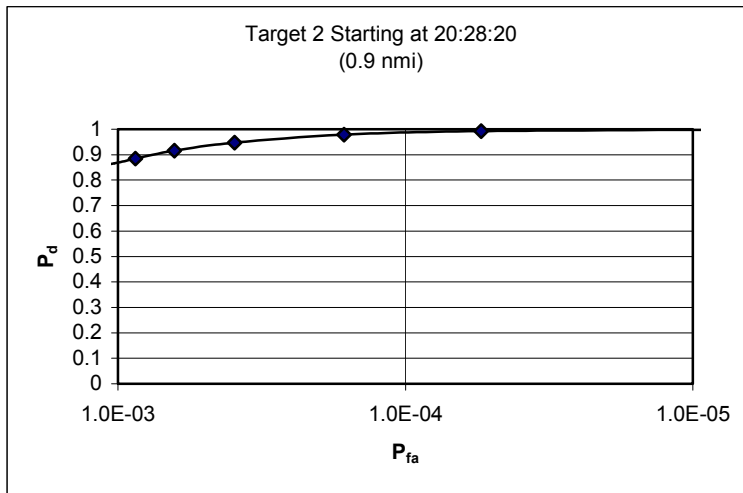


**Figure 28 Detection Performance for Target #2 at 0.9 nmi**

Figure 28 and Figure 30 demonstrate that  $P_d$  for both targets #2 and #3 rose to and stabilized at 100% as  $P_{fa}$  declined. This again confirms very good detection of these targets with the **S6** system.



**Figure 29 Photograph of Target #3 at 20:18 NDT (1.2 nmi)**

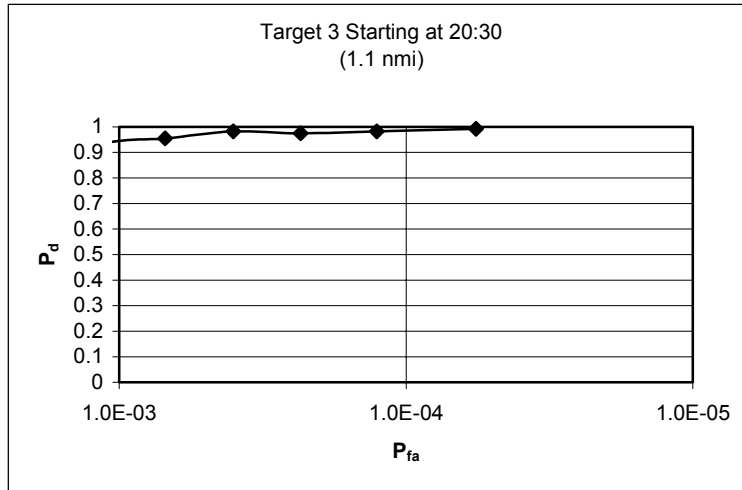


**Figure 30 Detection Performance for Target #3 at 1.1 nmi**

Measurements of the sizes of Targets #2 and #3, provided in Table 4, confirm them to be just over growler size and they would be classed a small bergy bits.

#### 4.2.11 Verification of Close-Range Targets using S6 Image Processor

Table 4 summarizes size and coordinate information for each of the analyzed close-range targets, corresponding to the field photographs.

**Table 4 Target Size Summary**

Target #	Range (nmi)	Size L x H (m)	Time
1	1.6	3.6 x 0.9	17:58
1	0.8	4.4 x 0.8	20:13
2	1.0	8.7 x 1.0	20:18
3	1.2	7.0 x 1.5	20:18

Figure 31 is an image capture of the processed data taken from this data set at 20:16. The circled targets are the close-range targets presented in this section. This figure visually verifies the detection and position of these close-range targets, and also demonstrates the ability to detect these targets using scan averaging. Table 5 summarizes the detection results and presents target size information.



**Table 5 Close-Range Target Detection Summary**

Target	Pd for Pfa = 0.001	Pd for Pfa = 0.0001	Range (nmi)	Size L x H, m	Time of Analysis
1	1.0125	1.003399	1.4	3.6 x 0.9	18:15
1	1.193845	0.973485	0.8	4.4 x 0.8	20:07
2	0.866267	0.978238	0.9	8.7 x 1.0	20:28:20
3	0.944179	0.982813	1.1	7.0 x 1.5	20:30

Detection probabilities of greater than 1 (100%) indicate a strong influence of clutter in the data at the lower Pfa. This is a result of false alarms being counted as detections in the target detection window. The analysis method estimates the number of false alarms that will occur in the target window and subtracts that number from the target count. As this is an estimate it will, on average, be correct but may cause some false target counts in individual scans, particularly at the higher false alarm rate (higher Pfa).

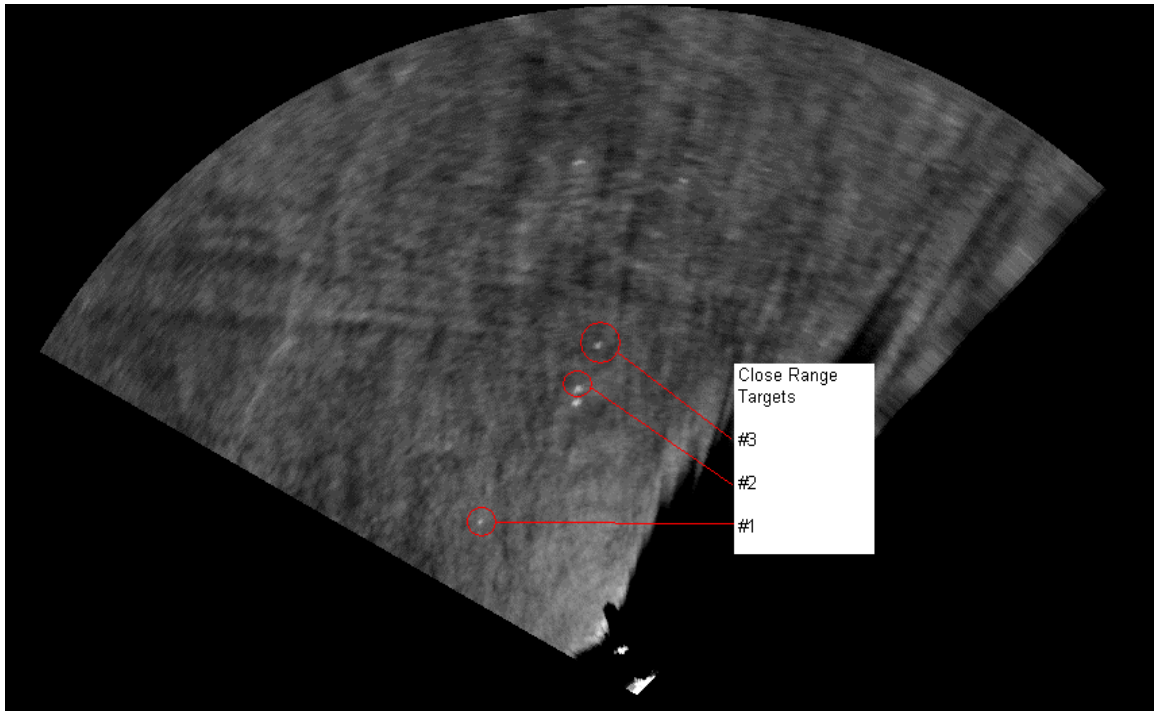


**Figure 31** Close-Range Targets at 20:16 NDT, Viewed with 256 Scans Averaged

#### **4.2.12 Close-Range Detection Conclusions**

On June 14 and 15, 2002, numerous growlers and bergy bits came within a 3 nmi range of the radar site. While it was not possible to document detection performance on all of these targets, it is clear from the analysis conducted that the S6 processor is capable of detecting these small targets in the conditions encountered.

## 5 PHASE 2 – DSP ENHANCED PROCESSING

### 5.1 DIGITAL FILTER REVIEW

The current **S6** method for scan processing is scan averaging. This is a digital filtering technique where subsequent scans are simply averaged to produce an output image. This method was implemented and used without technical considerations such as frequency response of the filter.

In Phase 2 of this analysis project, technical parameters and characteristics were used to evaluate current and prospective digital filtering methods.

First, it was determined that radar filtering requires a low-pass filter (which scan averaging satisfies). Using low-pass filter design tools, new digital filters were developed and implemented. Several filter parameters were used to compare the design of these new filters to that of scan averaging, and technical filter characteristics were used to compare the performance of corresponding filters.

Configurable filter parameters included:

- Order: Refers to the number of stages and consequently the required storage for the filter. Order has a direct effect on charging time and processing delay. As order increases, required charging time increases significantly, and memory (processor) requirements become more constricting.
- Attenuation: Refers to the suppression of signals at specified frequencies (in the case of low-pass filters, frequencies higher than the 3 dB frequency). Higher attenuations at specific bandwidths force higher filter orders.
- Bandwidth: Equal to the 3 dB point of the filter, the bandwidth is inversely proportional to the charging time of a digital filter (if the bandwidth is doubled, charging time decreases by 50 percent).

As mentioned above, technical filter characteristics were used to evaluate each digital filter design. These determining characteristics included:

- Group Delay: This is the average delay (in samples) as a function of frequency. Most often, practical filter charging time is equivalent to twice the maximum group delay value.
- Impulse Response: The rise and settling times, overshoot, and ripple of a filter's impulse response help to determine how effectively the filter can be expected to process data scan-by-scan.
- Step Response: The rise and settling times of a digital filter's step response indicate required charging time. The overshoot and ripple help to determine how efficiently the filter can process transient data signals. Specifically, it is expected that fewer oscillations and less overshoot in the step response will result in more predictable results from processing of time varying radar data.
- Frequency Response: The slope of a filter's frequency response indicates the efficiency of attenuation (suppressing unwanted signals).

The overall goal of this project phase was to determine the limiting factors for efficient digital filter design, and to use that information to design a digital filter with optimum target detection capability.

## 5.2 FIR (Non-Recursive Filters)

One of two basic forms of digital filters is the FIR (finite impulse response). This is a NON-RECURSIVE filter, meaning the output depends on inputs only (no feedback). Here, inputs are stored, weighted, and added together to yield an output. The transfer function for an FIR filter looks like:

$$y(n) / x(n) = b_0 + b_1z^{-1} + b_2z^{-2} + \dots + b_Mz^{-M} \quad (1)$$

where  $y(n)$  and  $x(n)$  are the current input and output,  $b_0 - b_M$  are the pre-determined coefficients (multipliers for stored inputs), and  $z^{-m}$  represents a delay of  $m$ -samples.

Figure 32 is a physical representation of the operation (time-storage, weighting, and summation) of an FIR filter.

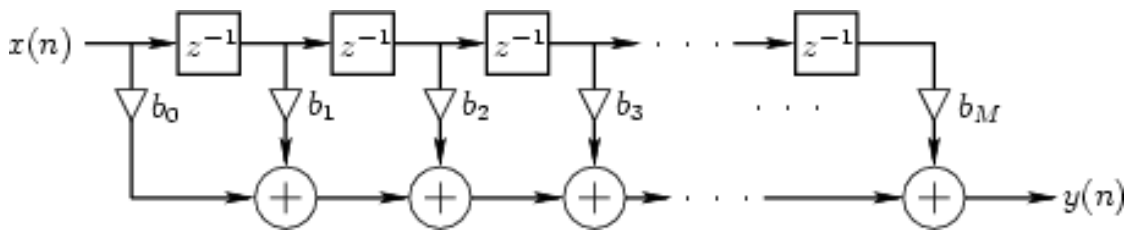


**Figure 32 Physical Representation of General FIR Filter**

For the case of the SCAN AVERAGING filter, all of the coefficients are of equal value ( $1/(M+1)$ ), so the filter operation works out to be a simple averaging of subsequent scans.

The ORDER of an FIR filter is defined as the number of previous inputs (stored) and used to calculate the output. Therefore, in general, we can say that this type of filter is of order  $M$ .

### 5.3 IIR (Recursive Filters)

The second category of digital filters is IIR (infinite impulse response). These filters are RECURSIVE, which means the output depends on previous inputs and outputs (feedback). The transfer function for a recursive filter looks like:

$$y(n) / x(n) = (b_0 + b_1z^{-1} + b_2z^{-2} + \dots + b_Mz^{-M}) / (a_0 + a_1z^{-1} + a_2z^{-2} + \dots + a_Nz^{-N}) \quad (2)$$

where all representations are the same as in the non-recursive case, with the addition of the terms  $a_0 \dots a_N$ , which are the coefficients for the stored outputs. In most cases,  $a_0 = 1$ .

The ORDER of an IIR filter is equal to the greater value of the numbers of stored inputs and outputs. In other words, if  $M > N$ , then the filter is of order  $M$ ; if  $N > M$ , then it is of order  $N$ . The main advantage in using IIR filters is that they can meet performance requirements using lower orders than a corresponding FIR filter. This is due to the feedback components of IIR filters.

Two forms of IIR filters were tested during the analysis: Butterworth and Bessel.

#### 5.3.1 Butterworth

For the design of Butterworth filters, a method known as the bilinear transform was used to produce coefficients. The structure of the filter was designed using a multi-stage biquadratic approach. The transfer function for a biquadratic filter is:

$$y(n) / x(n) = (b_0 + b_1z^{-1} + b_2z^{-2}) / (a_0 + a_1z^{-1} + a_2z^{-2}) \quad (3)$$

A multi-stage biquadratic filter can be visualized as shown in Figure 33. Each stage of the filter consists of a gain block, followed by a biquadratic filter block. Each stage is unique, meaning each stage has unique gain and coefficient values. After the final stage, one final gain is applied.

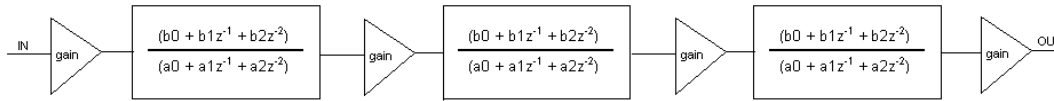


**Figure 33 Block Representation of Multi-Stage Biquadratic IIR Filter**

Each stage of the filter is either of order 1 or 2 (depending on whether all coefficients are non-zero). The order of the IIR filter is equal to the sum of all individual stage orders.

### 5.3.2 Bessel

Analog low-pass Bessel filters retain practically constant group delay throughout the pass band, allowing filtered signals to retain their wave shape through the pass band. To attain this useful response from a digital Bessel filter, the *matched-z transform* is required. The more traditional bilinear transform cannot produce a digital Bessel filter with the linear group delay characteristic.

For the design of Bessel filters, the matched-z transform was used instead of the bilinear transform. With the matched-z transform, there are no zeros in the z-plane. The transfer function therefore becomes:

$$y(n) / x(n) = (b_0) / (a_0 + a_1z^{-1} + a_2z^{-2} + \dots + a_Nz^{-N}) \quad (4)$$

with filter order N.

### 5.3.3 Comparison of FIR and IIR Filtering Characteristics

The typical frequency responses for FIR and IIR filters are quite different, as can be seen Figure 34, which illustrates some of the differences and benefits of the IIR filter. The IIR filter presented is a second order Butterworth having a 3 dB bandwidth of 0.0034 Hz (IIR O2 0034 in Figure 34). This is the same 3 dB bandwidth of the scan average process (FIR256 in Figure 34). Note the lobing on the scan average frequency response. This is due to the equal weight coefficients in the filter. Shown for comparison is a 256 order FIR filter with Blackman Harris weighting on the filter coefficients (FIR256BH). This has the beneficial effect of controlling the lobes in the frequency response at the expense of the broadening of the pass band.

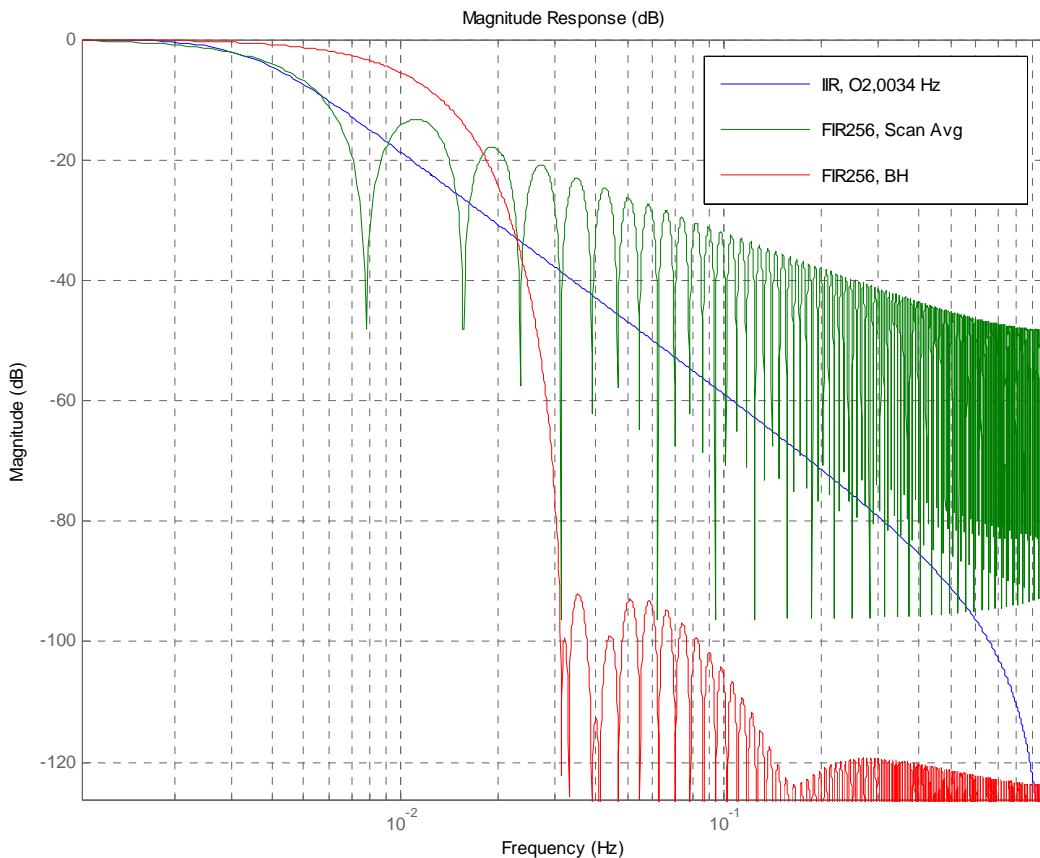
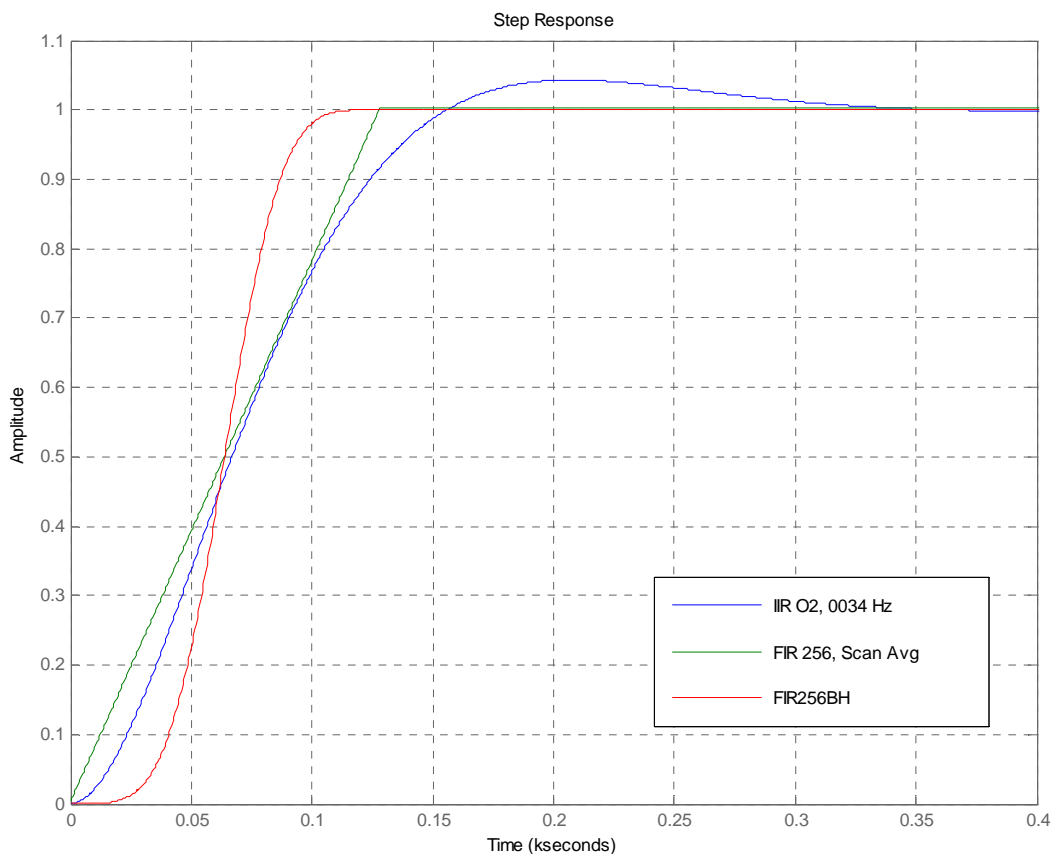


Figure 34 Digital Filter Frequency Response for Various Filters



Figure 34 demonstrates some advantages of IIR filtering. For a filter with the same cut-off frequency, the IIR filter offers much better attenuation at the higher frequencies. The presentation of all digital filters in this section is based on a 2 Hz sampling frequency, putting the Nyquist frequency at 1 Hz, the maximum frequency plotted in Figure 34. Note the better attenuation in the IIR curve (no residual lobes).

Figure 35 and Figure 36 present step and impulse responses of the filters in Figure 34.



**Figure 35 Step Response for Various Digital Filters**

These step and impulse responses illustrate the time-domain behaviour of these filters. The FIR scan-average filter has a very well behaved time-domain response with a linear step response and a flat impulse response. Of course, the penalty for this is the poor frequency domain behaviour. The Blackman-Harris weighted FIR provides a very well

behaved time-domain response and much better frequency domain behaviour at the expense of a wider bandwidth, as illustrated in Figure 34. The IIR filter offers a compromise, with this Butterworth example having not quite ideal time-domain behaviour due to overshoot and undershoot in step and impulse responses, but good frequency domain behaviour.

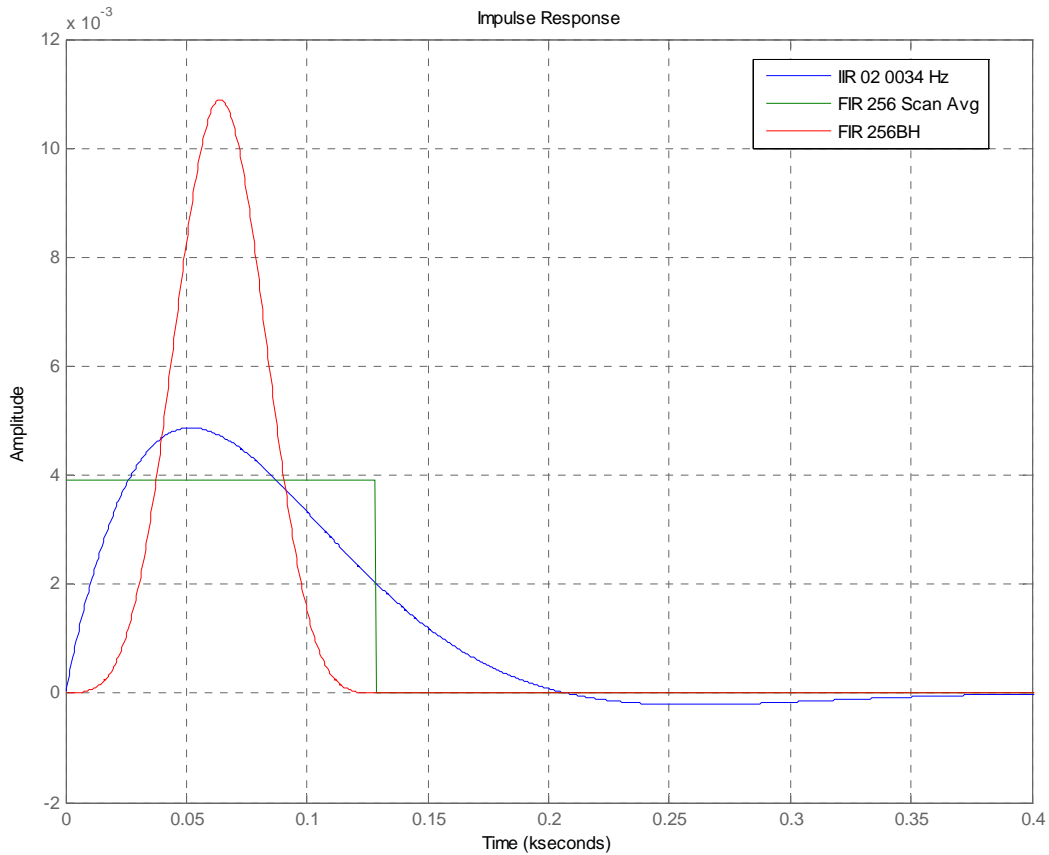


**Figure 36 Impulse Response for Various Digital Filters**

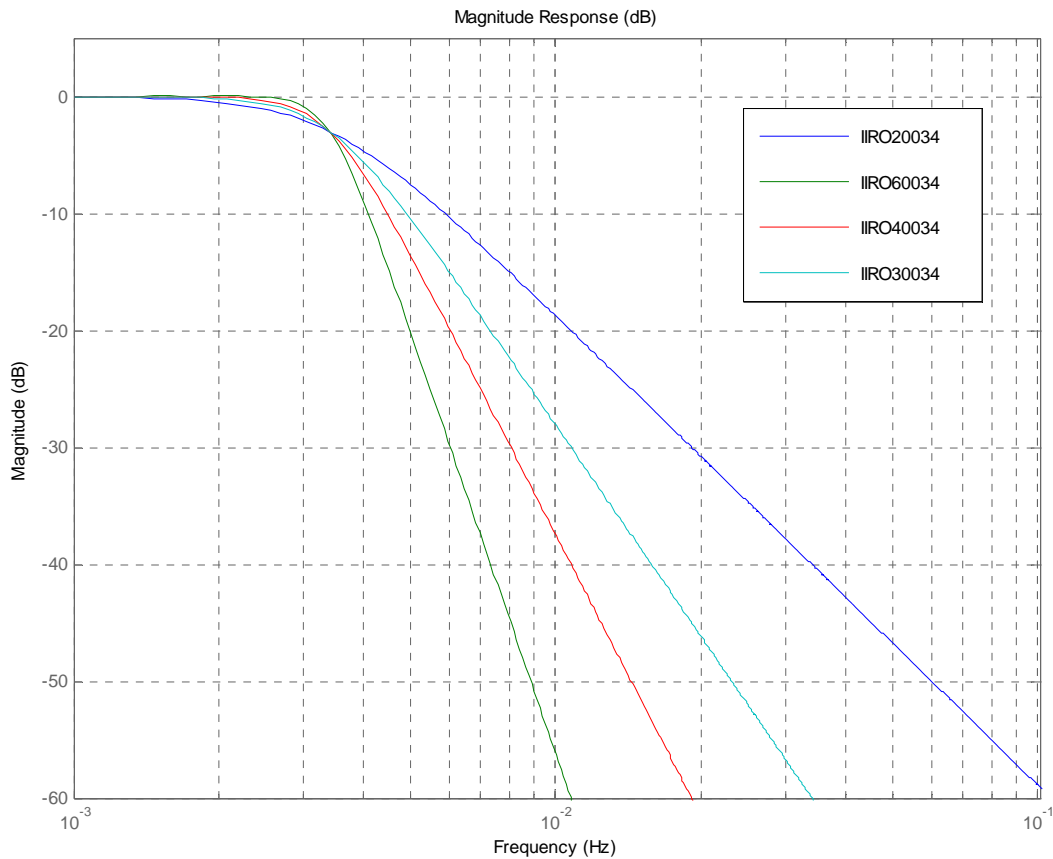


**Figure 37 IIR Digital Filter Frequency Response for Increasing Order**

It can be seen in Figure 37 that, for a given cut-off frequency (in this case 0.0034 Hz), the higher order Butterworth filters offer sharper roll-off in the frequency response and higher corresponding attenuation in the stop-band of the filter. This is a desirable behaviour as we are seeking to suppress time-varying noise and clutter signals. The penalty in this is again in the resultant time-domain step response. Figure 38 shows that as the filter order is increased, the ringing on the response becomes more severe. This will be of concern in the target detection scenario as changing clutter behaviour may create time-domain artifacts that persist for long periods of time. Note that in Figure 38 the order 6 filter ringing persists for over 600 seconds.

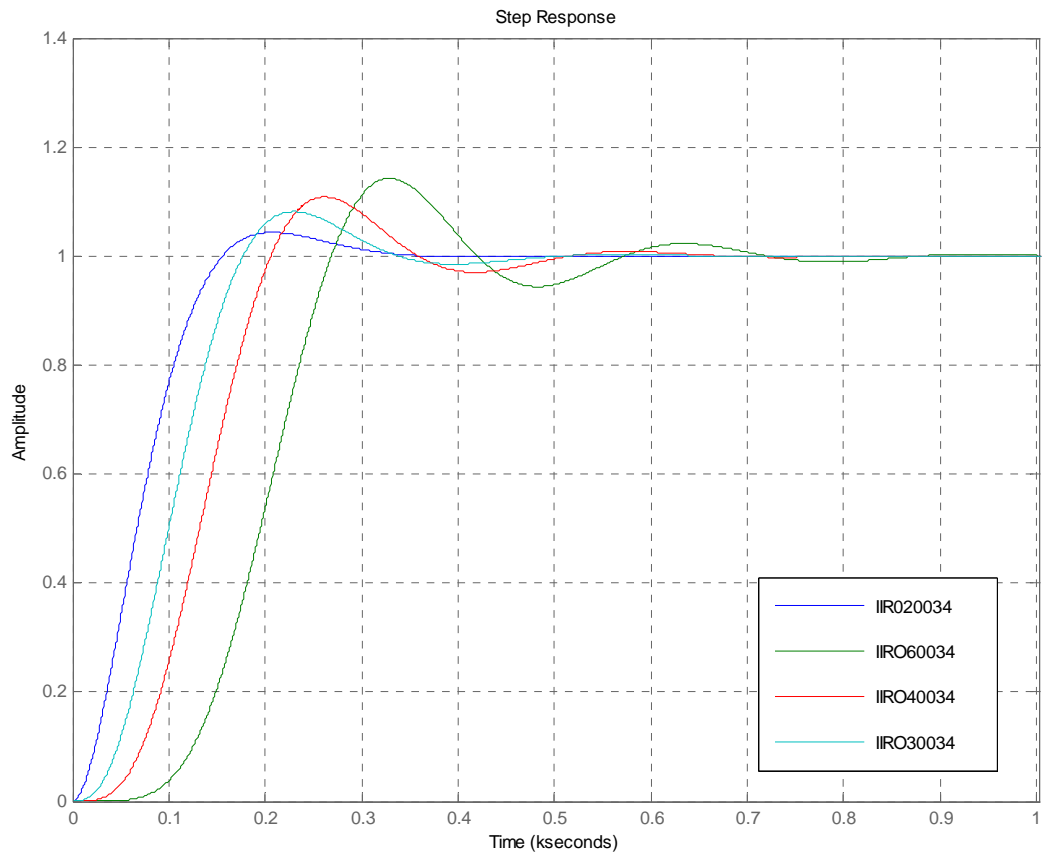


**Figure 38 IIR Digital Filter Step Response for Increasing Order**

## 5.4 FILTER DESIGN AND IMPLEMENTATION

FIR and Butterworth IIR filters were designed using the MATLAB Filter Design and Analysis (FDA) Tool from MATHWORKS. Bessel filters were designed using an online filter design tool ([www-users.cs.york.ac.uk/~fisher/mkfilter/trad.html](http://www-users.cs.york.ac.uk/~fisher/mkfilter/trad.html)), since the FDA Tool does not support the design of digital Bessel filters.

In the cases of both design tools, filter parameters (order, bandwidth, etc.) are selected for the particular filter under consideration. These tools will then generate the filter coefficients and response curves. The response curves were used to determine the effective charging time of the filter, and the coefficients were used in a digital filter software framework built into a test versions of the Sigma S6 plot extractor and image processors.

Two approaches were taken to designing new filters:

1. Attempting to match some form of scan averaging filter in terms of parameters such as bandwidth or charging time. This approach investigated the possibility of increasing filter performance without sacrificing practicality of implementation.
2. Pushing practical boundaries by designing filters with exceptionally long charging times, high orders, or narrow bandwidths in search of supreme performance.

The design constraints dictated that the filters be low-pass with low cut-off frequency and high attenuation. When designing new digital filters, parameters were chosen in an attempt to keep bandwidth as narrow as possible and attenuation as high as possible. In addition, filter order was kept low to limit processing delays.

## 5.5 PRELIMINARY ANALYSIS

As with previous analysis, the data analyzed in Phase 2 was taken from June 15 data and, for consistency, the same 8-minute data segment, starting from 14:00, was analyzed. Once again the target of interest for analysis was the wave rider buoy. The methodology for analyzing this data was identical to the methodology described in Section 4.1.

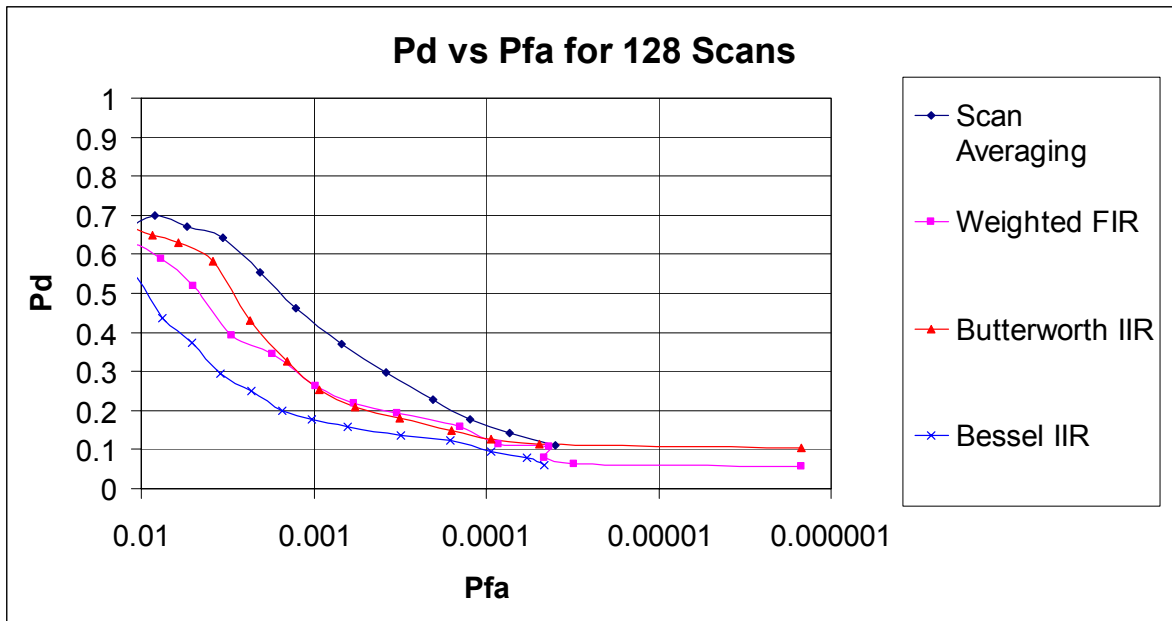


**Figure 39 Detection Performance for Fixed Processing Time (128 scans)**

Initially, new digital filters were designed by matching charging times with those of existing scan averaging filters. Specifically, versions of weighted FIR, Butterworth IIR, and Bessel IIR filters with charging times of 128 samples were analyzed against the standard 128 scan averaging filter.

Figure 39 presents plots summarizing the detection performance of each 128-scan filter. This figure demonstrates that at 128 scans processed, the scan averaging filter performs best; however, in the usable Pfa range of  $10^{-4}$  there is very little difference in the performance of these filters.

Figure 40 demonstrates similar results for 256 scans processed. The weighted FIR could not be tested for 256-scan processing because of impractical memory requirements. Two versions of each IIR design were tested: lower order and higher order. Since all filters were of equal charging time, variations of order correspond to variations of bandwidth in the analyzed IIR filters (low order – narrow bandwidth, high order – wide bandwidth).

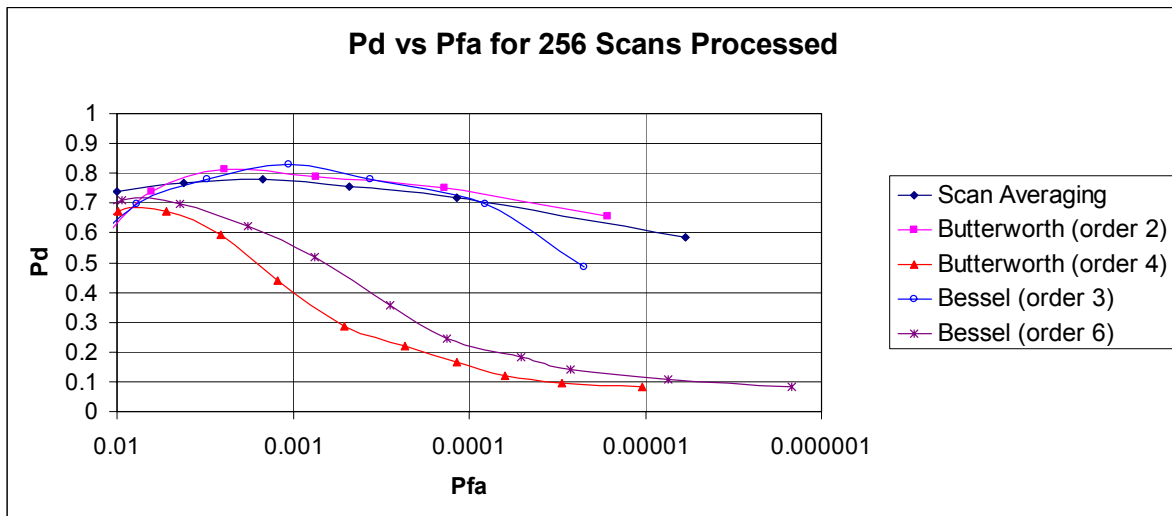


**Figure 40 Detection Performance for Fixed Processing Time (256 scans)**

Figure 40 demonstrates that the IIR filters can perform as well as scan averaging. It is also evident that for a given processing time, lower order IIR filters have superior performance characteristics over the higher order filters. Since IIR filters of different orders also have different bandwidths, the true limiting factor of IIR filter performance cannot be determined from the above results alone.

From this preliminary analysis, three conclusions were made:

1. Weighted FIR filtering cannot improve detection within the practical limits of real-time radar signal processing and therefore would not be further analyzed.
2. IIR filter performance is dependent on filter parameters, not charging time.
3. Further analysis should involve researching how each filter parameter affects filter performance. This information should then be used to create optimum-performance filters.

## 5.6 IIR FILTER ANALYSIS

As mentioned in Section 5.4, the three significant parameters of digital filter design are filter order, bandwidth, and attenuation. To determine the exact effect of these parameters on filter performance, three specific studies were performed on specially designed digital filters. These three studies included analysis of filters with:

- Matched Bandwidth: Bandwidths for two scan averaging filter types (128 and 256 scans) were found from the filters' frequency response curves. Various IIR filters with these bandwidths were designed and analyzed against the corresponding scan averaging filters. IIR filters were further tested at other constant bandwidths.
- Matched Order: IIR filters of common order and varying bandwidth were grouped and analyzed.
- Matched Attenuation: Similar to the matched bandwidth analysis, filters were grouped and analyzed according to common 50 dB and 75 dB attenuation points.

To make filter analysis easier, it was decided that only one form of IIR filter would be developed and compared to the scan averaging filter. This was acceptable since the performances of the Butterworth and Bessel filters in the preliminary analysis were virtually identical.

A summary of the Butterworth filters designed and analyzed in this project phase are shown in Table 6. In all, 16 filters were used in the segment of the analysis.



**Table 6 Summary of Order - Bandwidth Combinations of Butterworth Filters**

	3 dB BANDWIDTH (Hz)	0.0068	0.0045	0.0034	0.0025	0.0017	0.0012	0.0008
ORDER 2	Charging Time (scans)	160	256	320	420	640	904	1350
	50 dB Point (Hz)	0.1195	0.0796	0.061	0.0456	0.031		0.014
	75 dB Point (Hz)			0.243	0.18126	0.125		0.06
	Max Group Delay (scans)	80	120	160	217	320	452	675
ORDER 3	Charging Time (scans)	256	388	512	700	1024	N/A	N/A
	50 dB Point (Hz)	0.0462	0.0306	0.023	0.0171	0.012		
	75 dB Point (Hz)			0.06	0.0443	0.031		
	Max Group Delay (scans)	128	194	256	349	512		
ORDER 4	Charging Time (scans)	366	552	732	1000	N/A	N/A	N/A
	50 dB Point (Hz)	0.0287	0.019	0.014	0.0107			
	75 dB Point (Hz)			0.02954	0.0216			
	Max Group Delay (scans)	183	276	366	498			

The two scan averaging filters used as benchmarks for bandwidth were the 128 and 256 scan versions. These filters have 3 dB bandwidths of 0.0068 Hz and 0.0034 Hz, respectively. In order to make the analysis more thorough, additional scan averaging filters were analyzed to demonstrate the general performance trends exhibited by scan averaging. Table 7 presents a summary of all scan averaging filters analyzed.

**Table 7 Summary of Scan Averaging Filters**

BANDWIDTH (Hz)	0.0136	0.0068	0.0051	0.0041	0.0034
Charging Time (scans)	64	128	170	214	256
50 dB Point (Hz)	NA	NA	NA	NA	NA
75 dB Point (Hz)	NA	NA	NA	NA	NA
Max Group Delay (scans)	32	64	85	107	128

It is interesting to note that the frequency response of these scan average filters never reached 50 dB attenuation. In this major filter analysis, the familiar 8-minute data segment from 14:00 (June 15) was analyzed using each filter implementation. Again, the analysis methodology determined and used in Phase 1 was used for this data analysis, and the analyzed target was the wave rider buoy.

## 6 DSP DETECTION PERFORMANCE

### 6.1 FILTER BANDWIDTH ANALYSIS

As can be seen in Table 6, seven bandwidths of IIR filters were tested: 0.0068 Hz (matched to 128 scan averaging), 0.0045 Hz, 0.0034 Hz (matched to 256 scan averaging), 0.0025 Hz, 0.0017 Hz, 0.0012 Hz, and 0.0008 Hz. Figures 41 to 45 demonstrate the performances of filters with matched bandwidths. The bandwidth values of 0.0012 Hz and 0.0008 Hz are not represented. This exclusion is due to the fact that these bandwidths require significantly long charging times and could only be implemented in order 2 filters.

From Figures 41 to 45, it may be seen that there is little difference in the performance of different filter designs in the Pfa range of  $10^{-4}$ . However, the results also suggest that the best-performing filter for a specified bandwidth is the Butterworth, order 2.

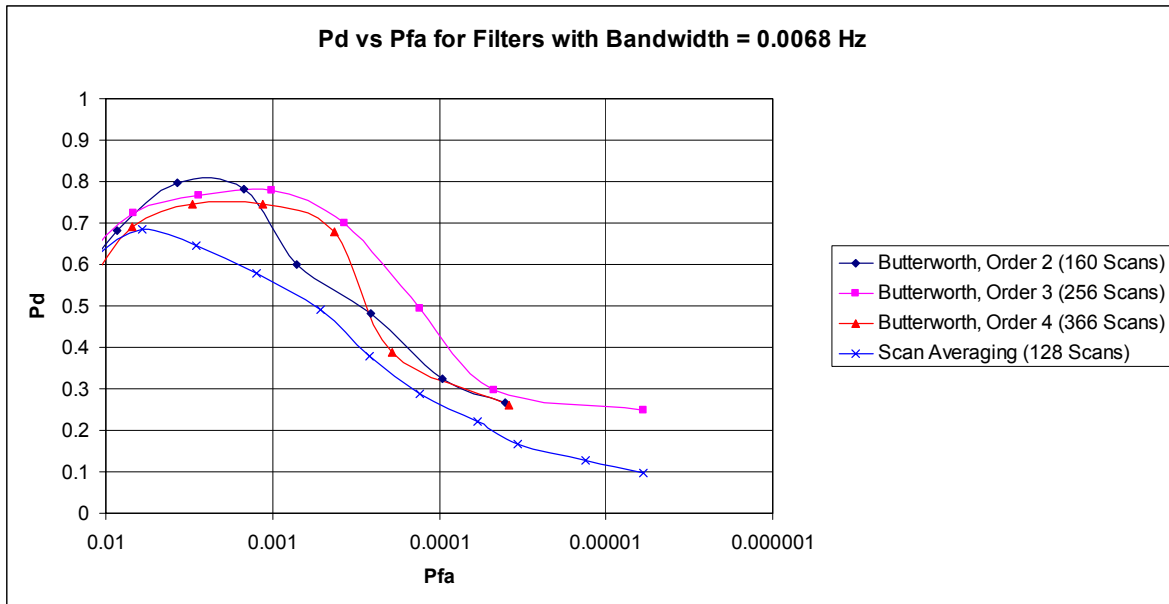
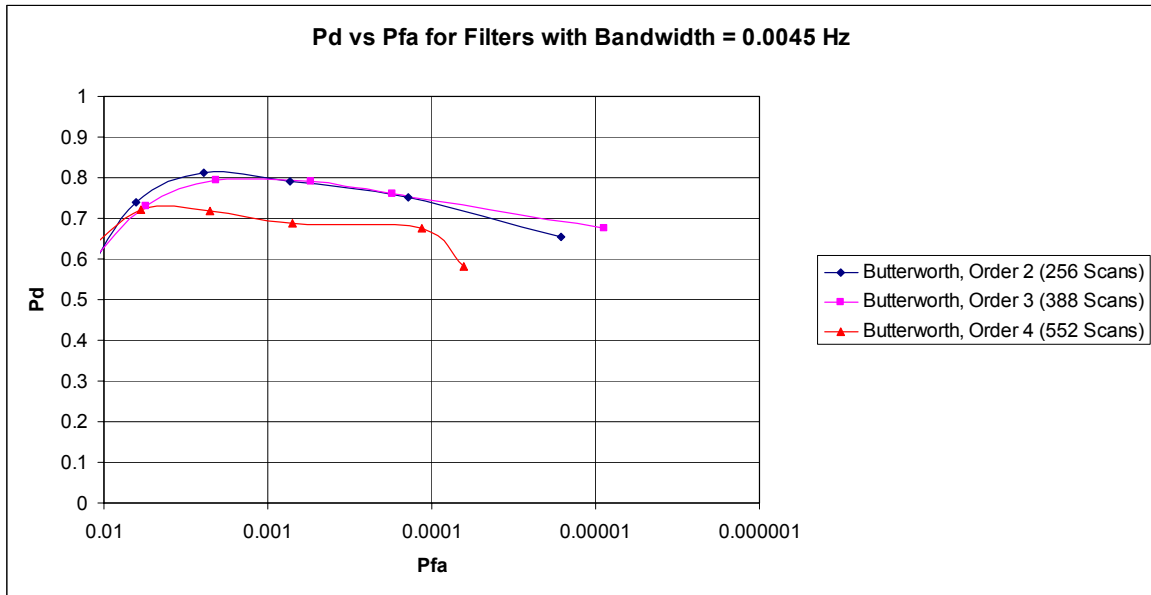
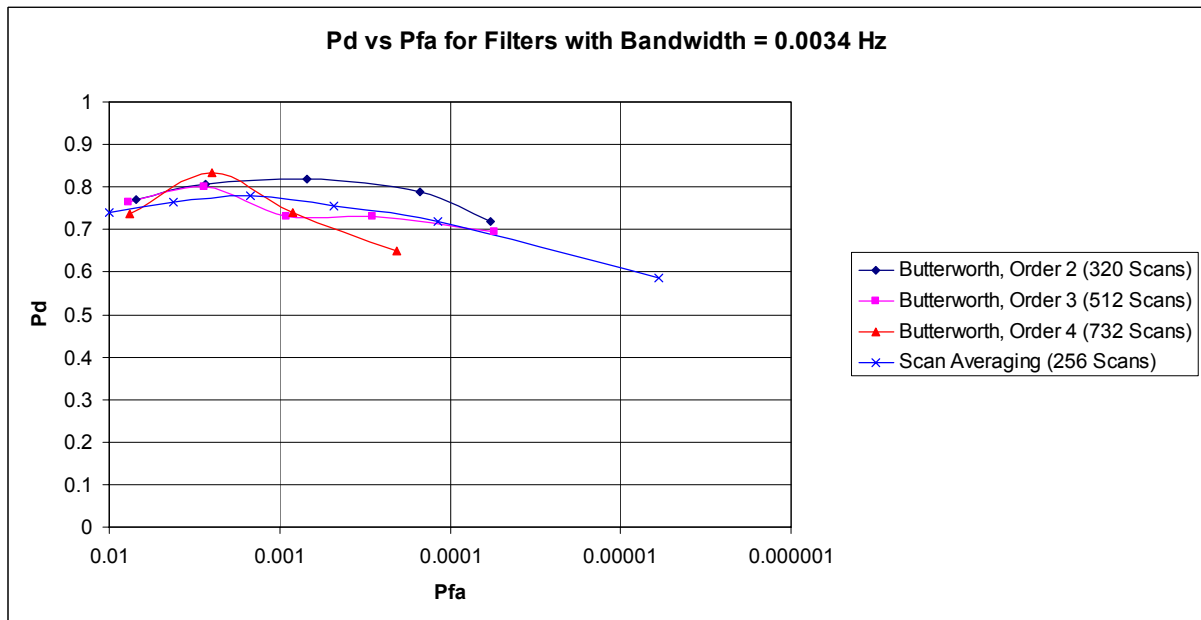


Figure 41 Performance of Filters with Bandwidth = 0.0068 Hz



**Figure 42 Performance of Filters with Bandwidth = 0.0045 Hz**



**Figure 43 Performance of Filters with Bandwidth = 0.0034 Hz**

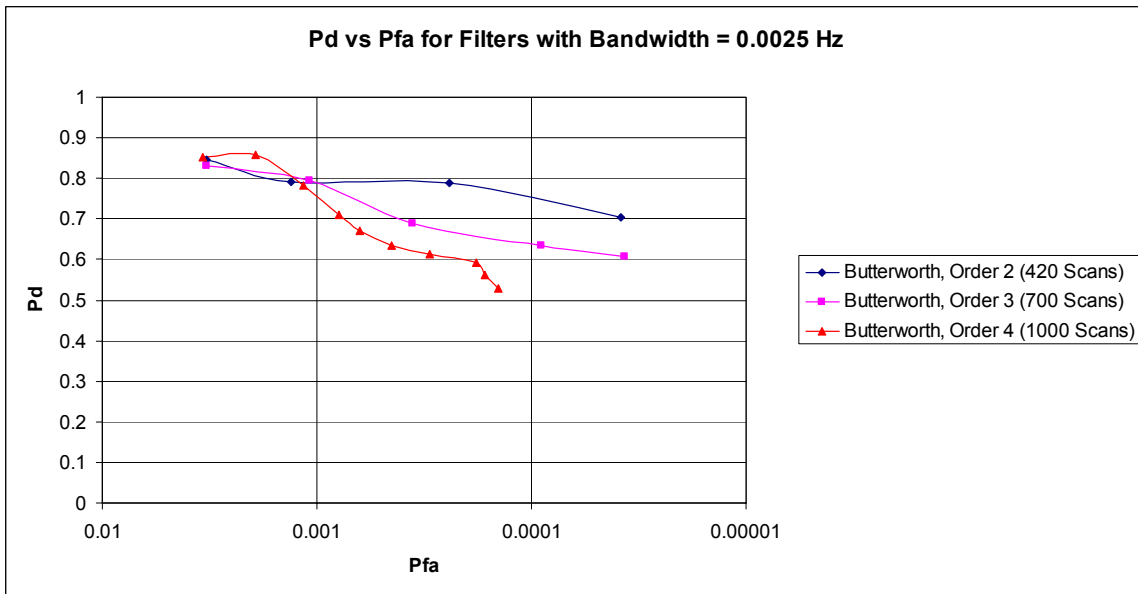


**Figure 44 Performance of Filters with Bandwidth = 0.0025 Hz**

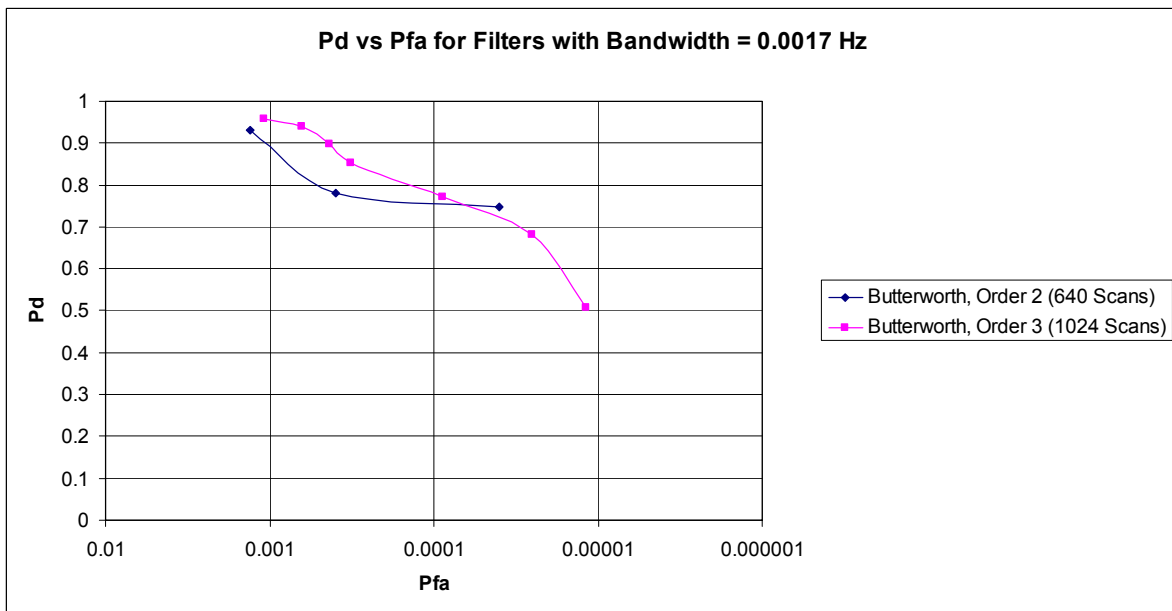


**Figure 45 Performance of Filters with Bandwidth = 0.0017 Hz**

## 6.2 FILTER ORDER ANALYSIS

This section presents the performance results of Butterworth filters in terms of matched filter order. There are three sets of results in this section: order 2, order 3, and order 4. At each order, several bandwidths are represented. More bandwidths are present in the order 2 results since lower filter orders allow for narrower bandwidths within a specified window of charging time.

Figure 46 through 51 present the results of Pfa and Pd in separate figures. This was done because both Pd and Pfa are affected by the filter performance and it is informative to see how each responds to filter bandwidth. The measure of Pfa as a function of detection threshold actually shows how well the filter is able to attenuate clutter returns. A lower threshold value for a constant Pfa tells us that the filter is achieving higher attenuation because a lower detection threshold may be used to achieve the same Pfa.

It is also informative to present Pd this way as, often, when the threshold is increased, the Pfa may fall to zero due to a zero count in false alarm. Plotting Pd as a function of threshold therefore shows the complete detection picture.

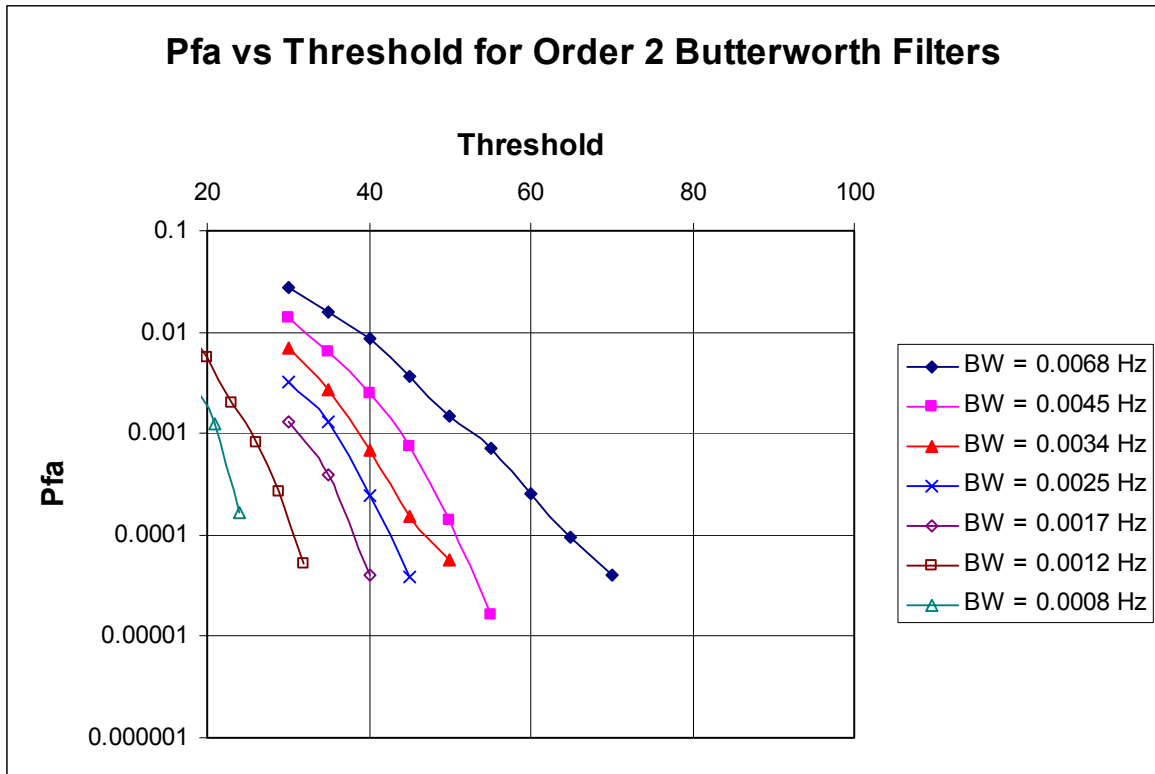


**Figure 46 Pfa Performance of Second Order Butterworth Filters**

Figure 46 is one of the most informative views of how the digital filter affects Pfa. This data from the second order Butterworth filter shows that as the filter bandwidth is narrowed, the threshold may be lowered to achieve the same Pfa. This means, of course, that the clutter returns are being suppressed by higher attenuation. For example, for a Pfa of  $0.0001(10^{-4})$ , the threshold may be reduced from 65 to 23 when going from the 0.0068 Hz filter to the 0.0008 Hz filter. This reduction in threshold permits higher target detection levels, as is shown in Figure 47. It is also informative to note from Figure 46 how the Pfa decreases at a constant threshold as lower filter bandwidths are used.

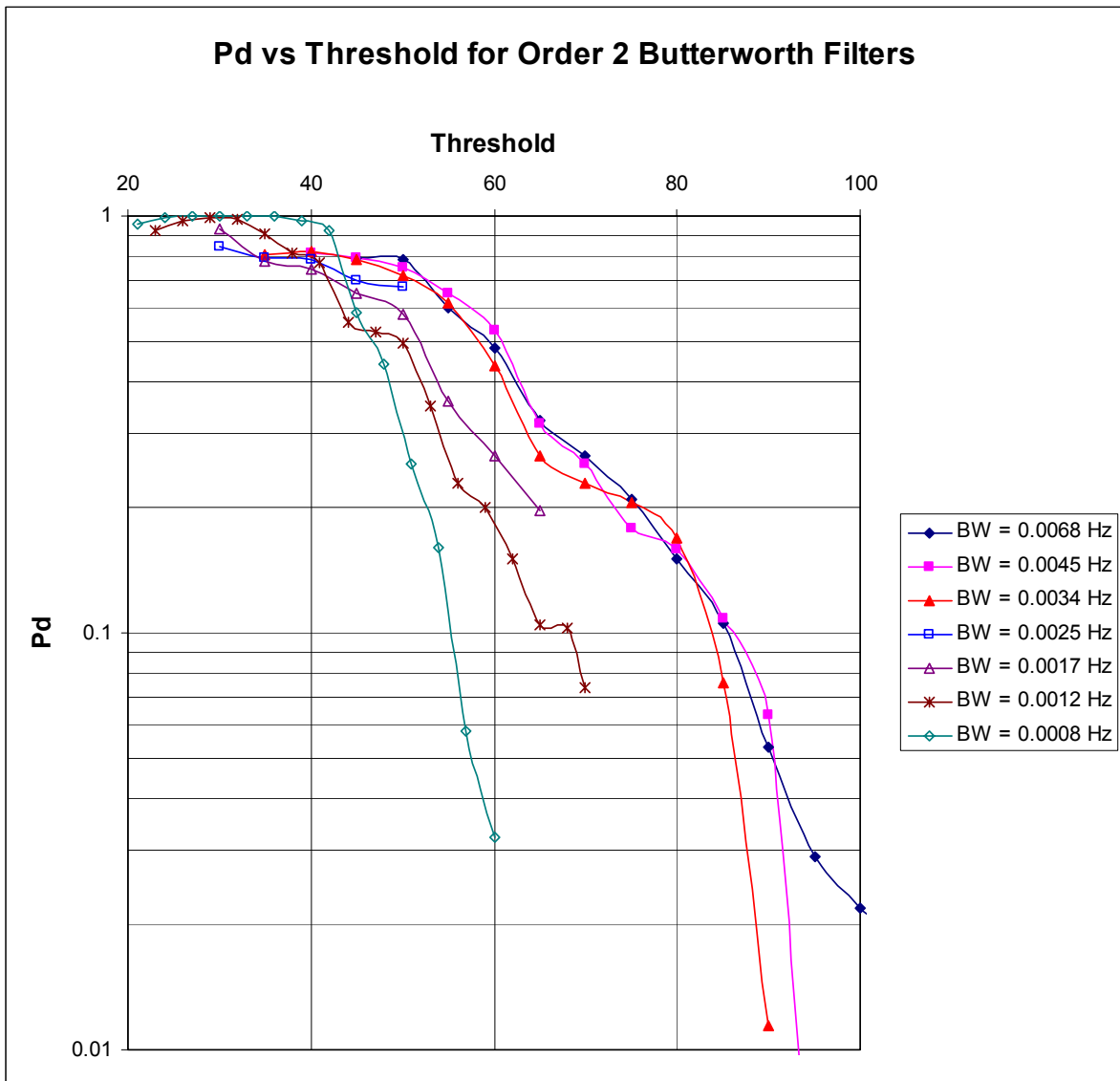


**Figure 47 Pd Performance of Second Order Butterworth Filters**

Figure 47 shows Pd as a function of threshold. In this case it is also clear that as the threshold is decreased, the Pd increases and maximum Pd is obtained for the narrowest filters. Note that for the 0.0008 Hz filter the Pd is 1 (100% detection) over the threshold range of 20 to 40. This is a very impressive result, as Figure 46 showed that the Pfa in this range is very low and over 30 is actually zero. This is ideal detection – high probability of detection with zero probability of false alarm.



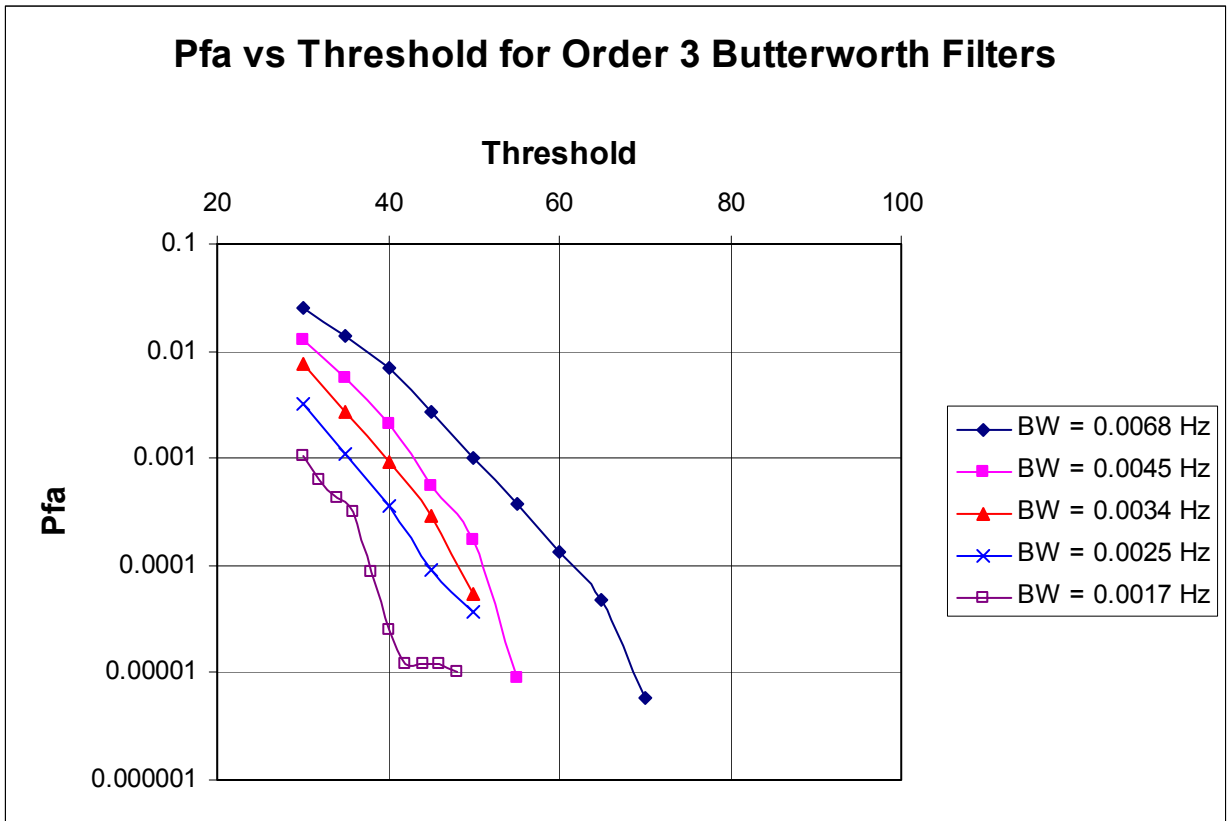


**Figure 48 Pfa Performance of Third Order Butterworth Filters**

The trend shown in Figure 46 and Figure 47 is further illustrated in Figure 48 and Figure 49 for the third order Butterworth filters, with the exception that the probability of detection never achieves the same high level as for the second order filter. Note in this case it was not possible to run the 0.0008 Hz filter due to the processing time exceeding the time available in the data segment (charging time too long).

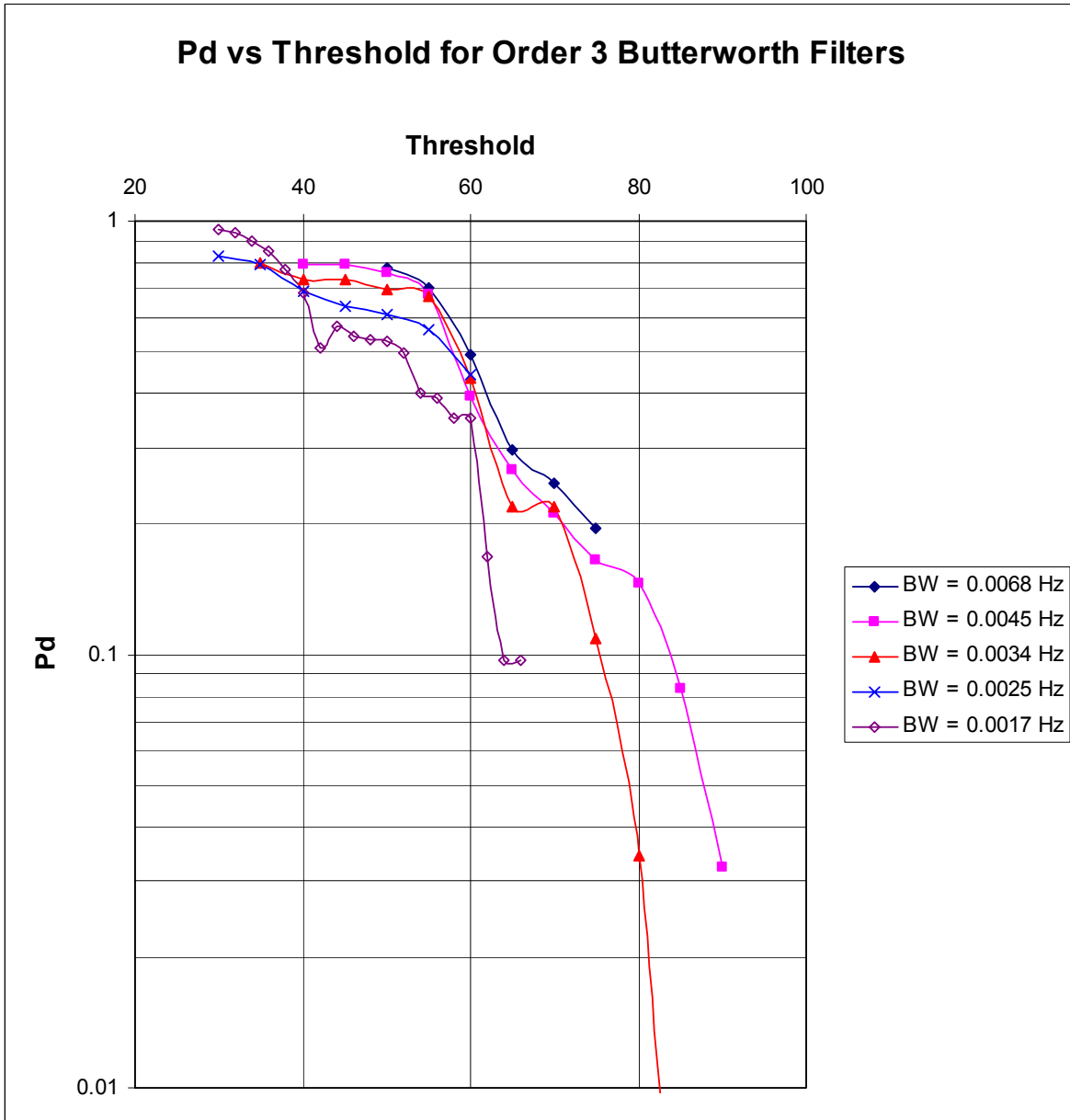


**Figure 49 Pd Performance of Third Order Butterworth Filters**

Close examination of Figure 49 for the 0.0017 Hz filter and comparison with the same filter in Figure 47 shows comparable detection performance between the second and third order filters for this bandwidth.

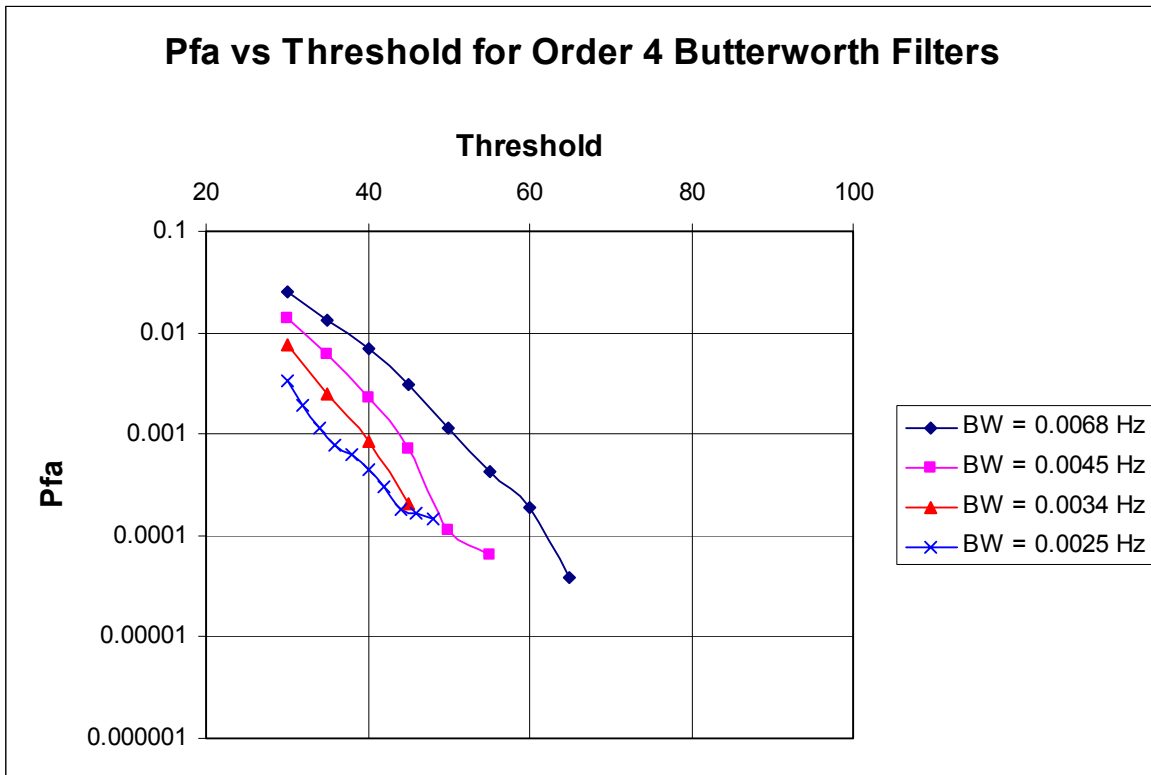


**Figure 50 Pfa Performance of Fourth Order Butterworth Filters**

The trend shown in Figure 46 and Figure 47 is further illustrated in Figure 50 and Figure 51 for fourth order Butterworth filters. In this case it was not possible to run the narrowest bandwidth filters due to the processing time exceeding the time available in the data segment (charging time too long).

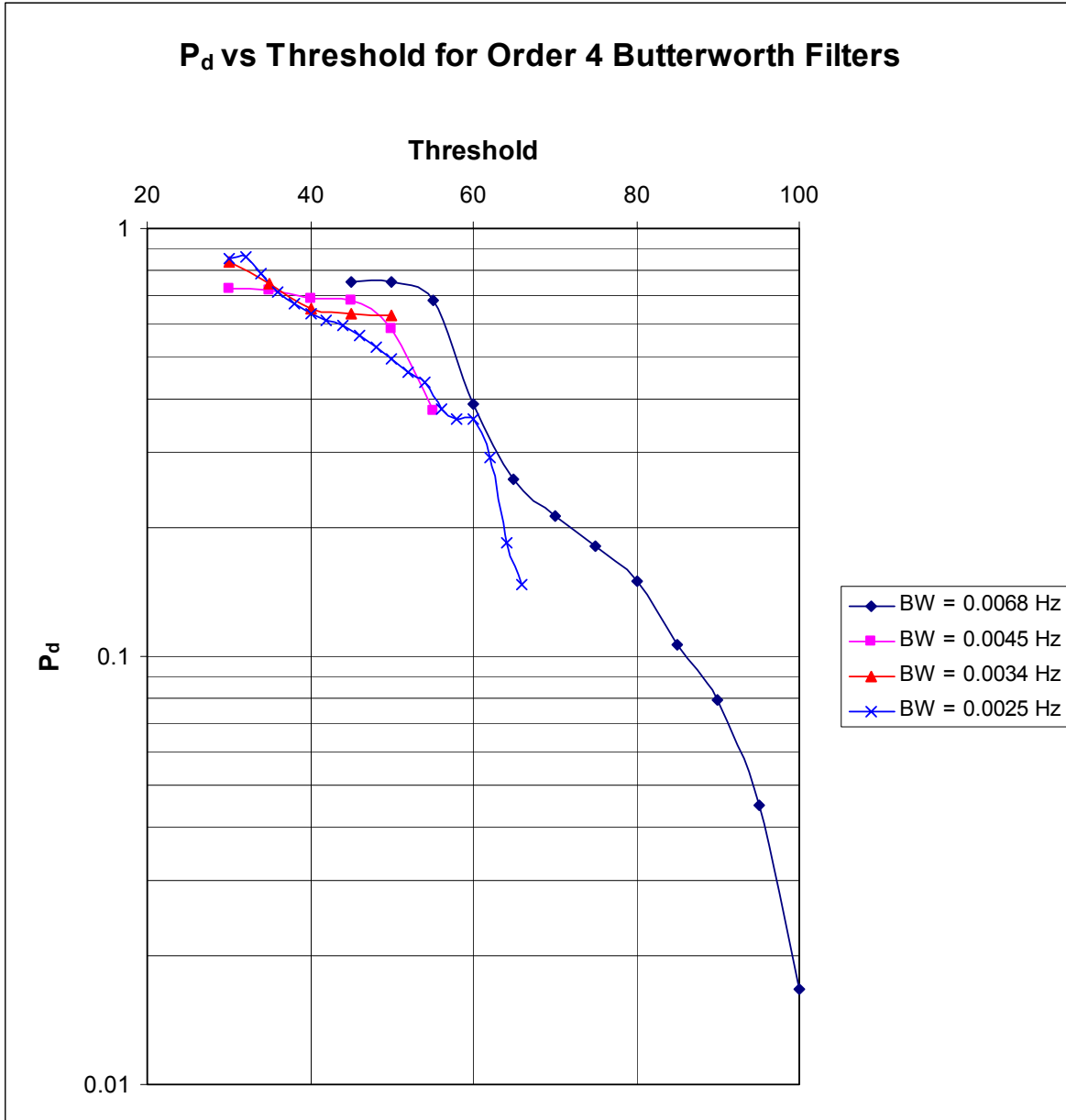


**Figure 51 Pd Performance of Fourth Order Butterworth Filters**

Close examination of Figure 51 in comparison to Figure 49 for the 0.0025 Hz filter shows comparable detection performance between the fourth and third order filters for this bandwidth.

This section reviewed the effect of bandwidth (3 dB) on filter detection performance. The main conclusion from this review is that bandwidth appears to be the important

parameter and that narrower bandwidths achieve the best performance. It is also clear that due to transient response considerations, the lower order filter offers the better response time (see also Figure 38 for filter step response).

### 6.3 FILTER ATTENUATION ANALYSIS

In the first section of IIR filter analysis, filters were grouped according to bandwidth. Effectively, this analysis concerned filters matched at -3 dB points (frequency value at which signal is attenuated by 3 dB). Filter attenuation analysis is an extension of this -3 dB point comparison. In this section of filter analysis, filters with common -50 dB points and -75 dB points were grouped and compared.

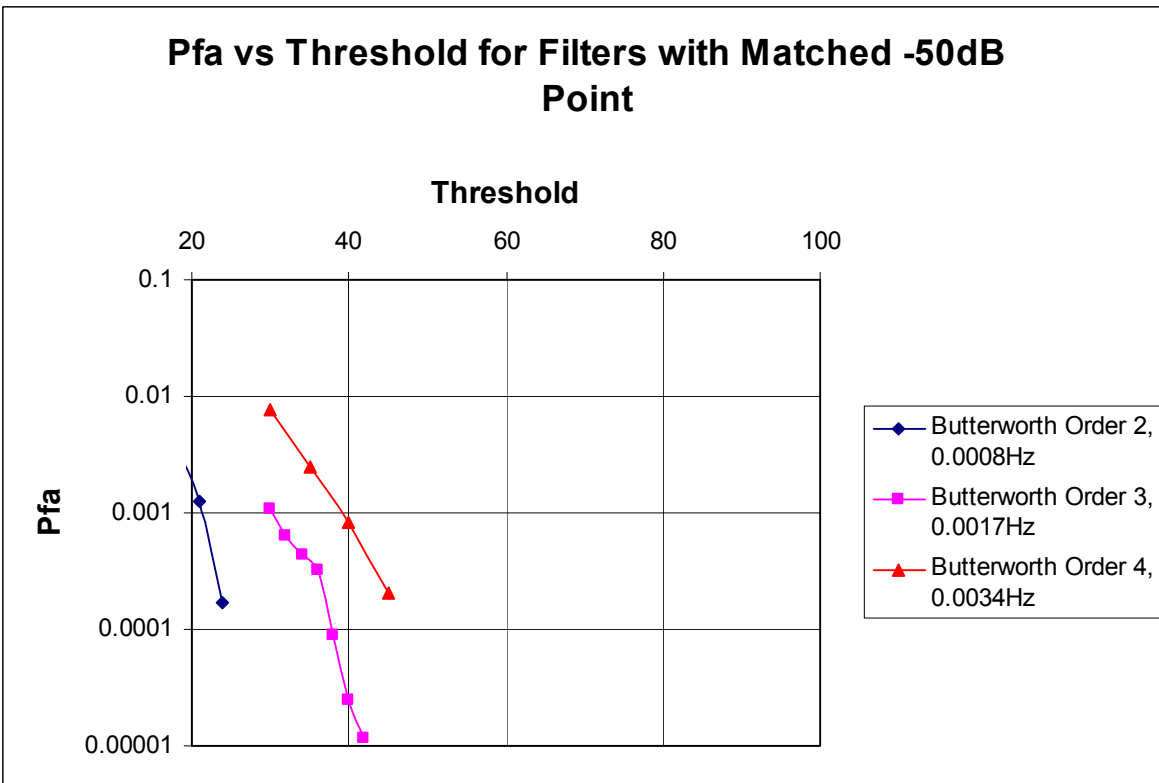


**Figure 52 Pfa Performance of Filters with Matched 50 dB Attenuation**

Figure 52 presents Pfa for filters having a common -50 dB attenuation point. In this case it is clear that filters having the narrower 3 dB bandwidth offer the best performance. This is due to the fact that as the filter order is increased, the difference between -3 dB and -50 dB point becomes smaller. Matching higher attenuation points therefore results in wider filters and poorer performance.

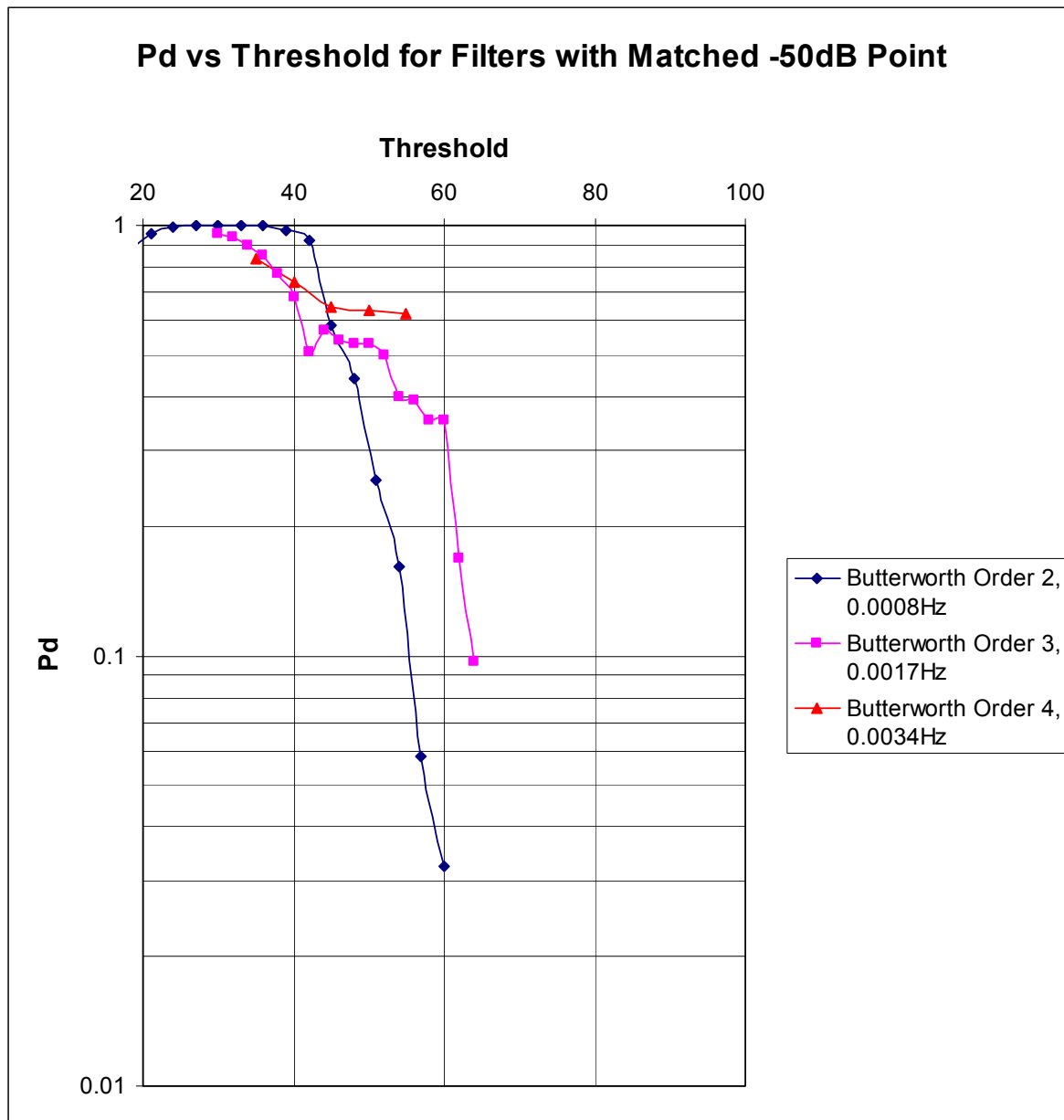


**Figure 53 Pd Performance of Filters with Matched 50 dB Attenuation**

Figure 53 demonstrates the same effect, with the narrow bandwidth filter outperforming the higher order filters.

Figure 54 and Figure 55 present detection performance for filters matched at the -75 dB point. The same trend can be seen in these figures, with the narrower filters performing better.

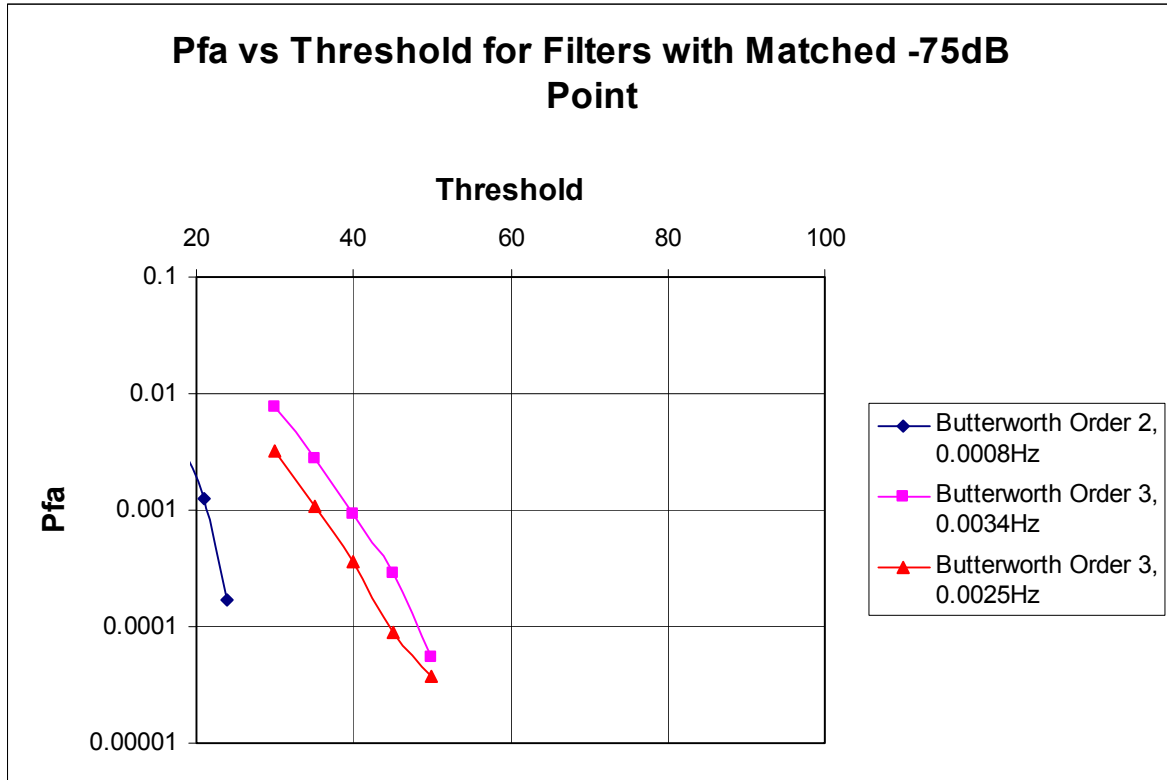


**Figure 54 Pfa Performance of Filters with Matched 75 dB Attenuation**

It is clear that the key to better performance is narrow bandwidth. The second order filter offers sufficient attenuation in the stop band, and so the higher order filters offer no real advantage.



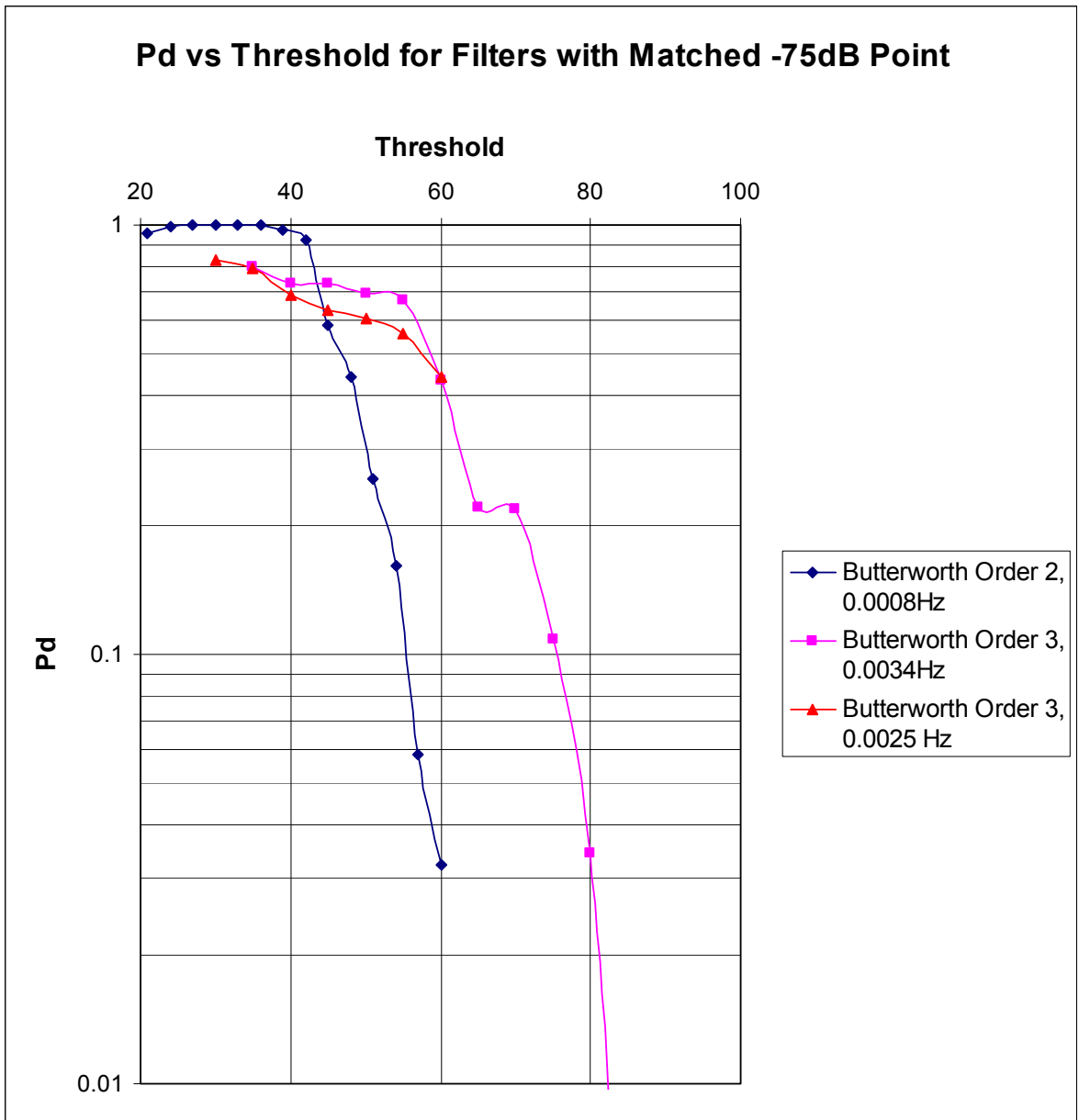


**Figure 55 Pd Performance of Filters with Matched 75 dB Attenuation**

## 6.4 STATIONARY TARGET CONSIDERATIONS AND CONCLUSIONS

Since the position of the wave rider buoy was fixed, the major analysis results from Sections 6.1, 6.2 and 6.3 offer information suitable to draw conclusions about IIR filter performance regarding stationary targets.

From the performed analysis, three summarizing statements can be made:

1. Low IIR filter orders yield the most satisfactory performance.
2. Attenuation is not a major contributor to filter performance.
3. Narrower bandwidths offer better detection.

Since low filter orders allow for narrower bandwidths, the above statements can be replaced with one simple IIR filter design rule:

Bandwidth is the limiting factor for IIR filter performance in detecting stationary targets: the narrower the bandwidth, the better the detection of static targets. Filter orders must be kept low to allow for practical use of narrow bandwidths (narrow bandwidths and high orders both force long charging and processing times, which can become impractical for target searching).

To verify this conclusion, a secondary analysis trial was performed on the wave rider target. The target was analyzed using the 8-minute data segment from 12:00 on June 15. This data segment was chosen since it contained some of the heaviest sea clutter (see Figure 13).

Figures 56, 57 and 58 display the results from analyzing the 12:00 data (with wave rider target) using four filters: 128 scan averaging (0.0068 Hz), 256 scan averaging (0.0034 Hz), and 0.0034 and 0.0008 Hz bandwidth Butterworth filters. These figures show detections of 100 percent using the narrowband Butterworth filter, where the scan averaging approach is only capable of a maximum probability of detection of 55 percent.

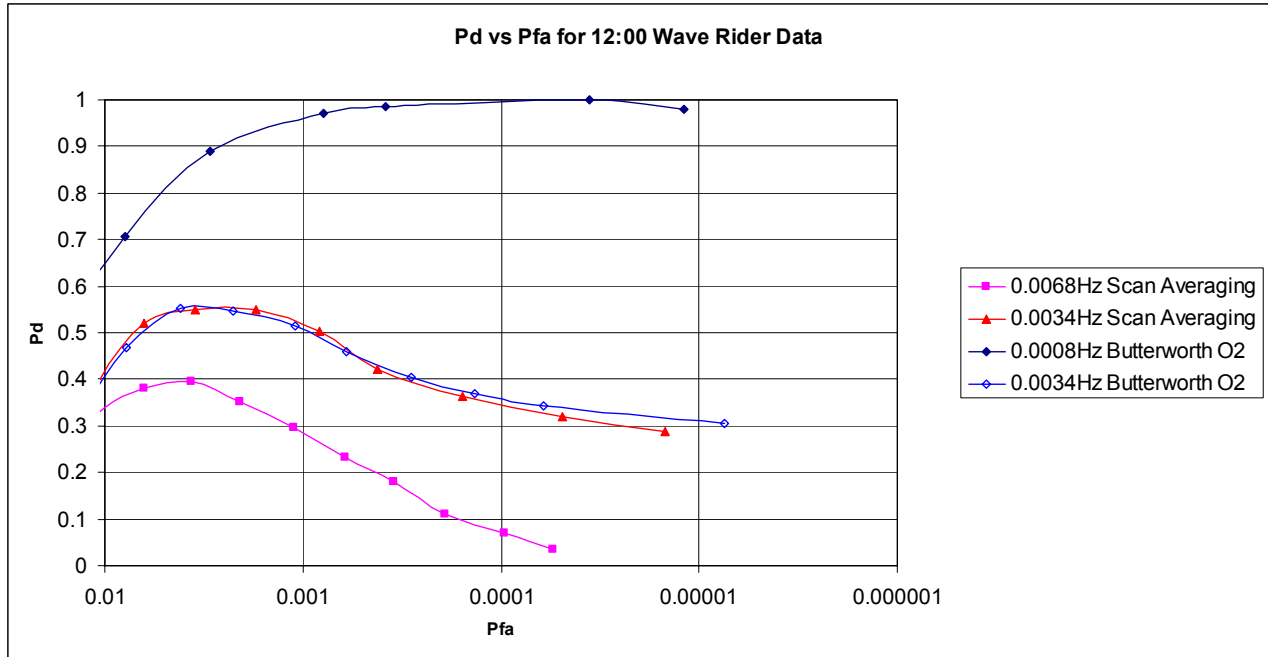


**Figure 56 Pd versus Pfa for the Wave Rider in High Sea Clutter (IIR Filter)**

Figure 56 presents Pd vs Pfa for the four filters. The IIR filter is clearly superior, offering 100 percent target detectability for a Pfa in the  $10^{-4}$  to  $10^{-5}$  range when the 256 scan average filter provides unacceptably poor detection.

This point is further illustrated in Figure 57 and Figure 58, plotting Pfa and Pd versus threshold for the same data. Again, it can clearly be seen that the IIR filter offers better performance. It is important to note that the second order Butterworth filter having the same bandwidth as the 256 scan average (0.0034 Hz) provides exactly the same performance. This clearly indicates the enhanced detection offered by the narrowband IIR filter is as a result of the bandwidth limitation.

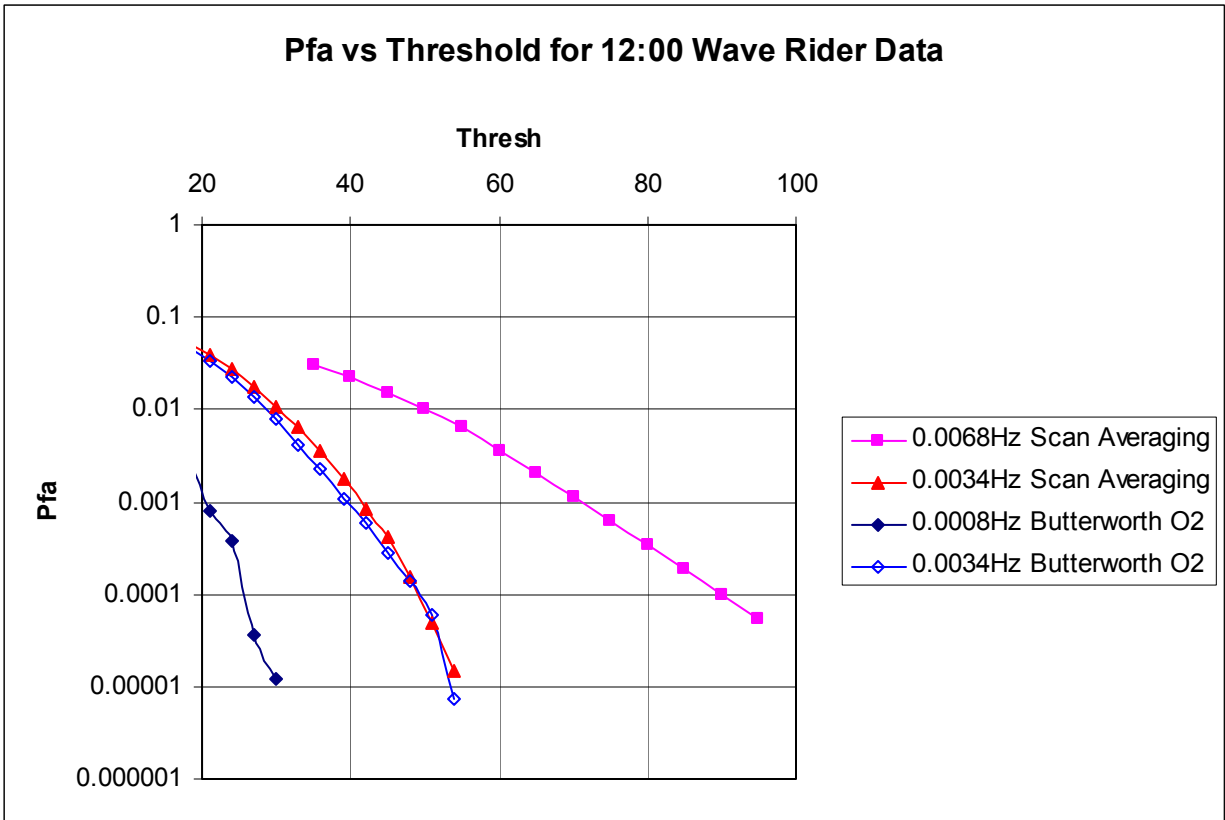


**Figure 57 Pfa versus Threshold for the Wave Rider in High Sea Clutter (IIR Filter)**

From these results, it is conclusive that filters with narrower bandwidths offer better detection of stationary and very slow-moving targets. Furthermore, these results show that the detection of stationary targets can be vastly improved through the use of IIR filtering instead of FIR (specifically, scan averaging) filtering due to the very narrow bandwidths that may be achieved in practice.

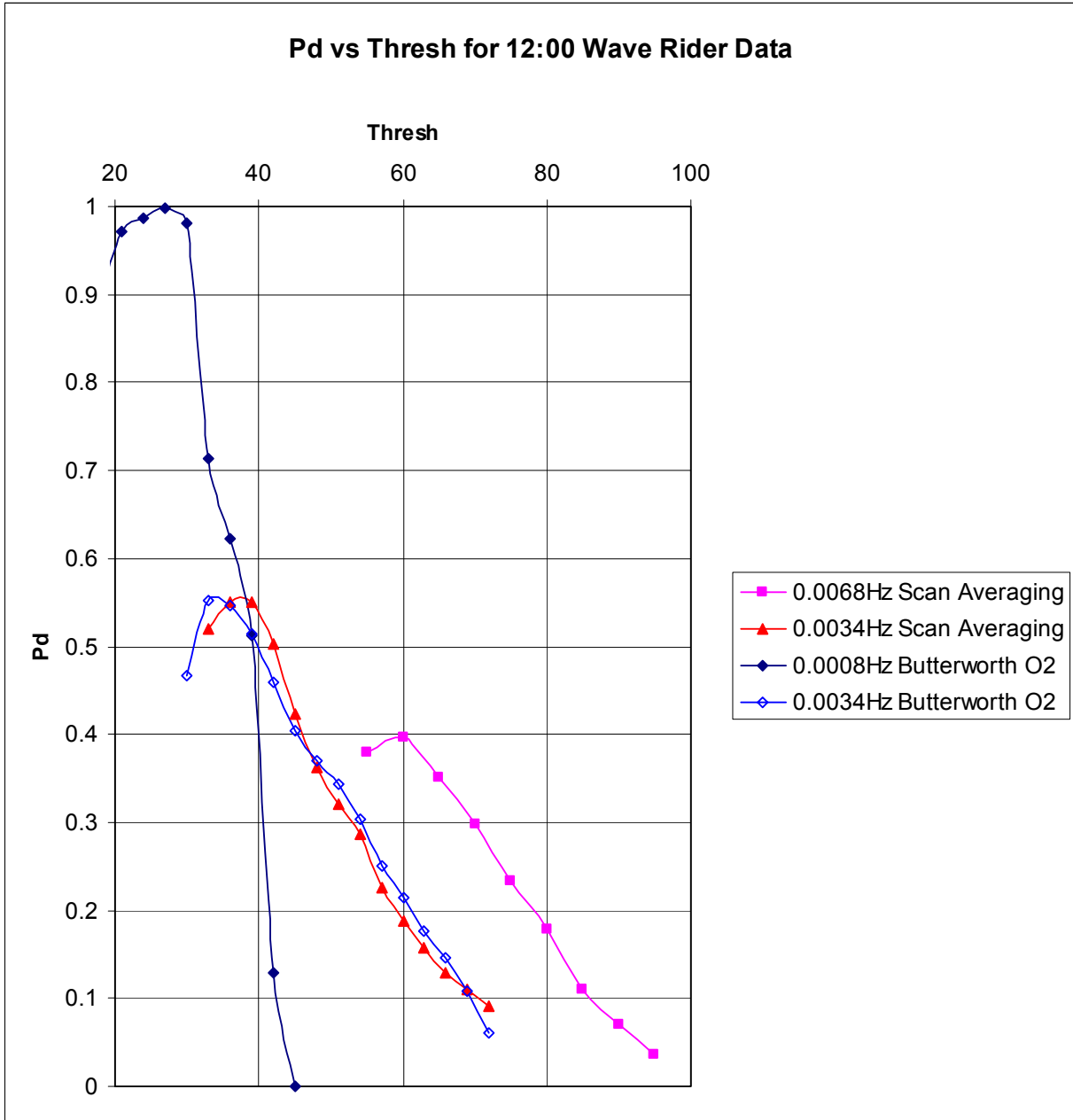


**Figure 58 Pd vs. Threshold for the Wave Rider in High Sea Clutter (IIR Filter)**

## 6.5 MOVING TARGET CONSIDERATIONS AND CONCLUSIONS

In practical application, most targets of interest are not stationary. Accounting for this reality, an additional detection trial was devised to investigate detection of moving targets. It was decided that for this analysis, a visual approach would be most practical.

The moving target analysis included implementing various FIR and IIR filters to process a common segment of data, and capturing screen shots at a specified time with consistent display settings. The SeaView display client was used to display this data. The data analyzed was taken from the June 15 data set, and all screen shots were captured at 20:16. The targets of interest were a collection of close-range bergy bit and growler targets analyzed in section 4.2.8.

In this brief trial, the Bessel IIR filter design was also used and tested. This was to ensure all filter designs involved in the project were fully and properly investigated. It was hypothesized that, again, no distinct advantage of Bessel filtering over Butterworth filtering would be found through this analysis.

Figures 59 and 60 display the results from the moving target analysis. As a reference, Figure 59 presents the results of three levels of scan averaging on three moving targets. The approximate speed of the targets has been estimated to be 1 kn or 0.5 m/s. The targets are about 1 nmi from the radar, moving in a southwest direction. The radar beam is 32 m wide at that range and the targets are about 5 to 8 m in length (Table 4).

It can be seen from Figure 59 that the targets in the 128 scan average (Middle) are slightly sharper than in the 256 scan average image (Left), but that the clutter is smoother in the 256 scan average image over both the 128 and 64 scan averaged data. This image shows some of the trade-offs when using scan averaging and the necessity to be able to adjust the number of scans averaged to match the target speeds of interest.

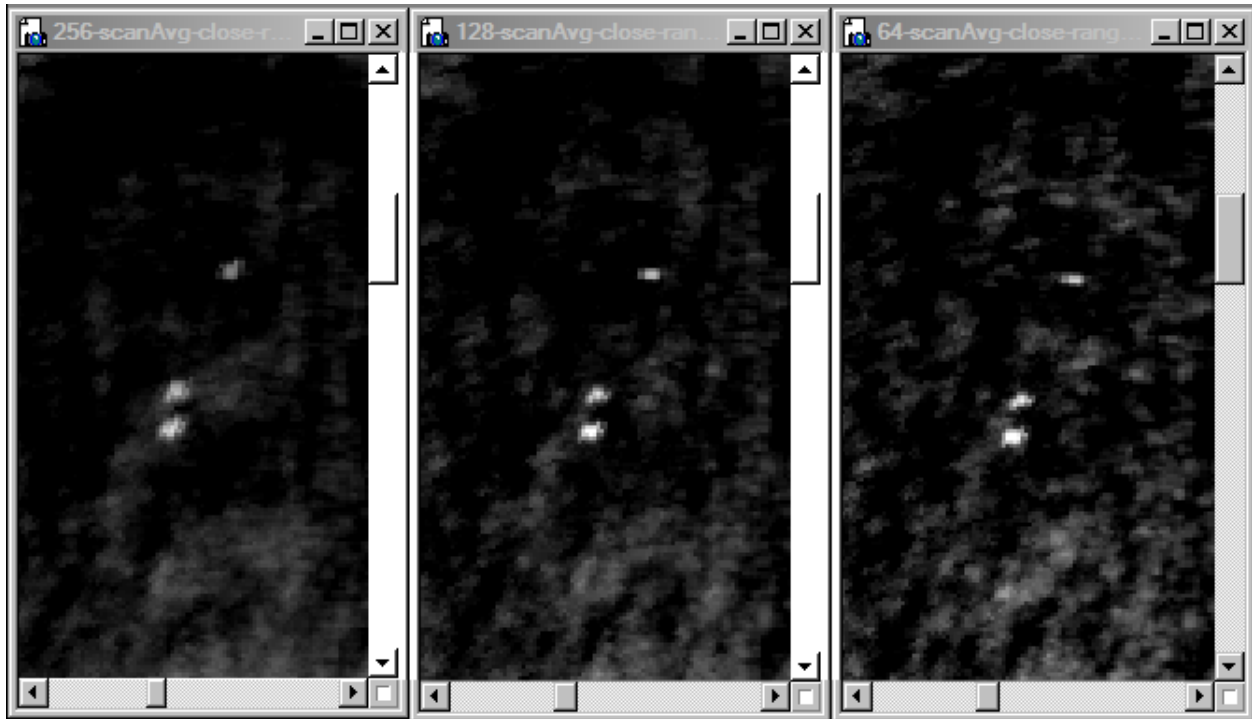


**Figure 59 Scan Average Processing on Moving Targets**

Figure 60 shows the effect of IIR filter (Butterworth Order 2) bandwidth on moving target detection. It can be seen clearly that once the bandwidth of the filter is decreased to less than 0.00017 Hz the targets become almost too smeared to be separated and detectable. Even the 0.0017 Hz filter is starting to show some degradation of signal sharpness and amplitude. Of course, the sea clutter will also be suppressed by the narrow filter response as well.

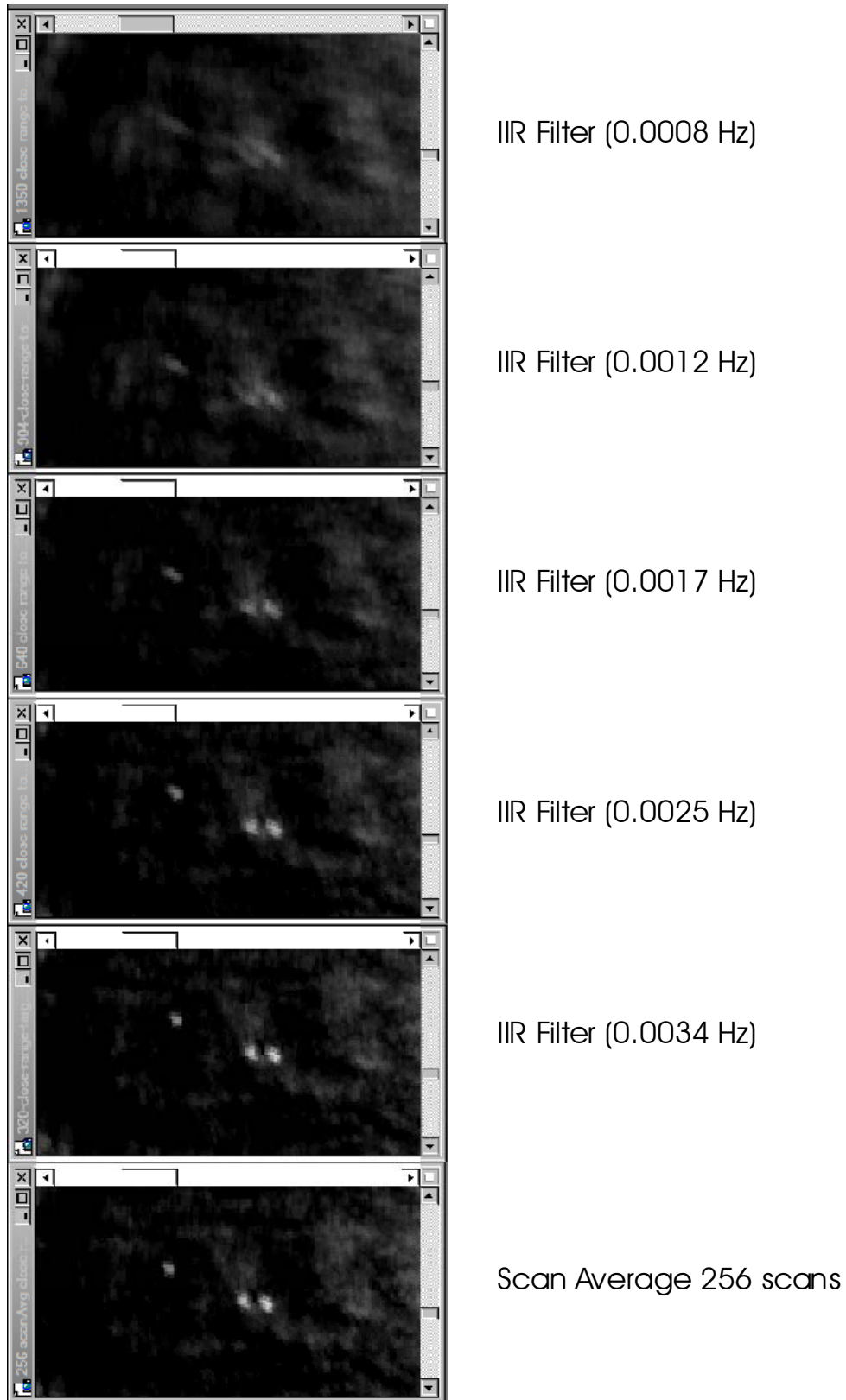


**Figure 60 Filter Bandwidth Effect on Moving Target Detection**



The preceding analysis demonstrates the trade-off of clutter suppression versus target enhancement when moving targets are involved. On a stationary target it was seen that the longer processing time (and narrower filter bandwidth) resulted in better detection performance. In the case of moving targets it is necessary to choose wider bandwidth filters to limit target smearing. It was shown in Section 4.2.7 that increasing the antenna speed provides increased opportunities for detection and this high speed scanning coupled with scan average processing produces the best detection performance. Revisiting Figure 21, it was shown that for a constant number of scans averaged; detection performance was independent of antenna speed. This result means that detection is also independent of bandwidth and the most important quantity is the number of independent samples that are processed by the filter. In the context of the narrowband IIR filter this means that detection could be improved on moving targets by further increasing the antenna rotation speed. Figure 60 shows that on a growler or bergy bit the minimum bandwidth of the IIR digital filter would be in the range of 0.0034 to 0.0025 Hz corresponding to 256 and 385 scans averaged in a scan average type filter. Increasing the antenna speed to 240 rpm would provide double the number of scans in the same time period and would permit the use of the 0.0017 Hz filter. Further increasing the antenna speed to 480 rpm would permit the use of the 0.0008 Hz filter. This approach would then provide performance on the moving iceberg targets equivalent to that presented in Figure 58. This would be a significant improvement over what is achievable with conventional scan averaging type filters.

## **7 COMPARISON OF DSP PROCESSING TO CONVENTIONAL RADAR**

In the past it has been difficult to demonstrate the benefit of advanced radar signal processors over conventional marine radar displays, as a side-by-side operational test is often only witnessed by field personnel during experimental data collection. It is possible with the Sigma S6 processor and raw radar recorder to play back full bandwidth radar video onto a PC display, demonstrating the effect of the signal processing, but this does not show how an off-the-shelf marine radar display would respond. This task in the project was dedicated to addressing this situation.

Rutter has a high-resolution radar output board, RSo4000, developed for its airport surveillance radar recorder. This board is capable of converting digital radar video and associated synchronization signals back into analogue form. It was proposed that this board be used to play back recorded radar video from the Twillingate trial into a marine radar display. In order to do this, the Sigma S6 radar playback software was used as a digital radar server to the digital-to-analogue output module. The output module was modified to permit the generation of generic radar signals for compatibility with typical radar display inputs.

### **7.1 TEST SETUP**

The Canadian Coast Guard made its facilities available for the test. The Ships Electronic Workshop (SEW) has X and S band radars available that the Coast Guard uses for testing and maintenance purposes. The display selected for use was from a BridgeMaster II.

In order to play the recorded video into the BridgeMaster display it was necessary to configure the signals to be electrically compatible with the display inputs. This meant outputting the azimuth data as a 90 count pulse and the heading pulse as a normally negative signal rising to zero volts when the antenna points at ships head. Video was configured as inverted with a nominal 5 V range. Comparative tests were made of

video levels coming from the BridgeMaster receiver to make sure proper setting of noise levels and maximum video levels was achieved.

One of the issues encountered was that the Twillingate data was recorded using a Raytheon Pathfinder MK2 modified to run at 120 rpm. It was therefore necessary to be able to configure the output module to reformat the Raytheon data into a format compatible with the BridgeMaster display manufactured by Sperry. The Pathfinder data was recorded on short pulse at a 3000 Hz pulse repetition frequency sampled at 40 MHz. With the radar operating at 120 rpm, this resulted in 1500 pulses per antenna rotation. The Sigma S6 server was configured to format the 1500 pulses into 2048 pulses per scan using its internal azimuth gating process. In this case pulses are replicated as necessary to provide the 2048 output pulses at equal azimuth intervals. The output card was configured to output these pulses and associated azimuth data at a 1200 Hz pulse repetition frequency. This results in a playback speed of 35 rpm into the BridgeMaster display. The data is therefore played back at approximately one quarter speed but remains compatible with the BridgeMaster timing. The output sample rate was set to 40 MHz for compatibility with the recorded data. The BridgeMaster display was placed on 3 nmi range and short pulse.

With the ability to play data back into the BridgeMaster display in place, it was necessary to have a method of capturing the high-resolution display video for comparison purposes. In order to provide very high fidelity, a video capture module was used from Rutter's VDR product. This frame grabber module provides a full RGB capture of the 1024 x 768 radar display image. The video capture quality in this module has met the IEC61996 Test Standard for video quality and is a faithful representation of the displayed video.

## 7.2 COMPARATIVE TEST

With the playback system connected to the signal input connectors of the BridgeMaster display and the video capture module connected to the slave video output of the BridgeMaster display, the test was started. A data segment from the June 15 data collection was used for the test. Figure 61 presents a video capture of the radar display with Gain set to 2 (maximum 10) and SEA clutter control set to 3 (maximum 10). In this case it is possible to see the extent of the sea clutter. The icebergs to the north and west are visible and their shadows may also be seen. See Figure 9, Figure 10, Figure 11 and Figure 12 for comparison.

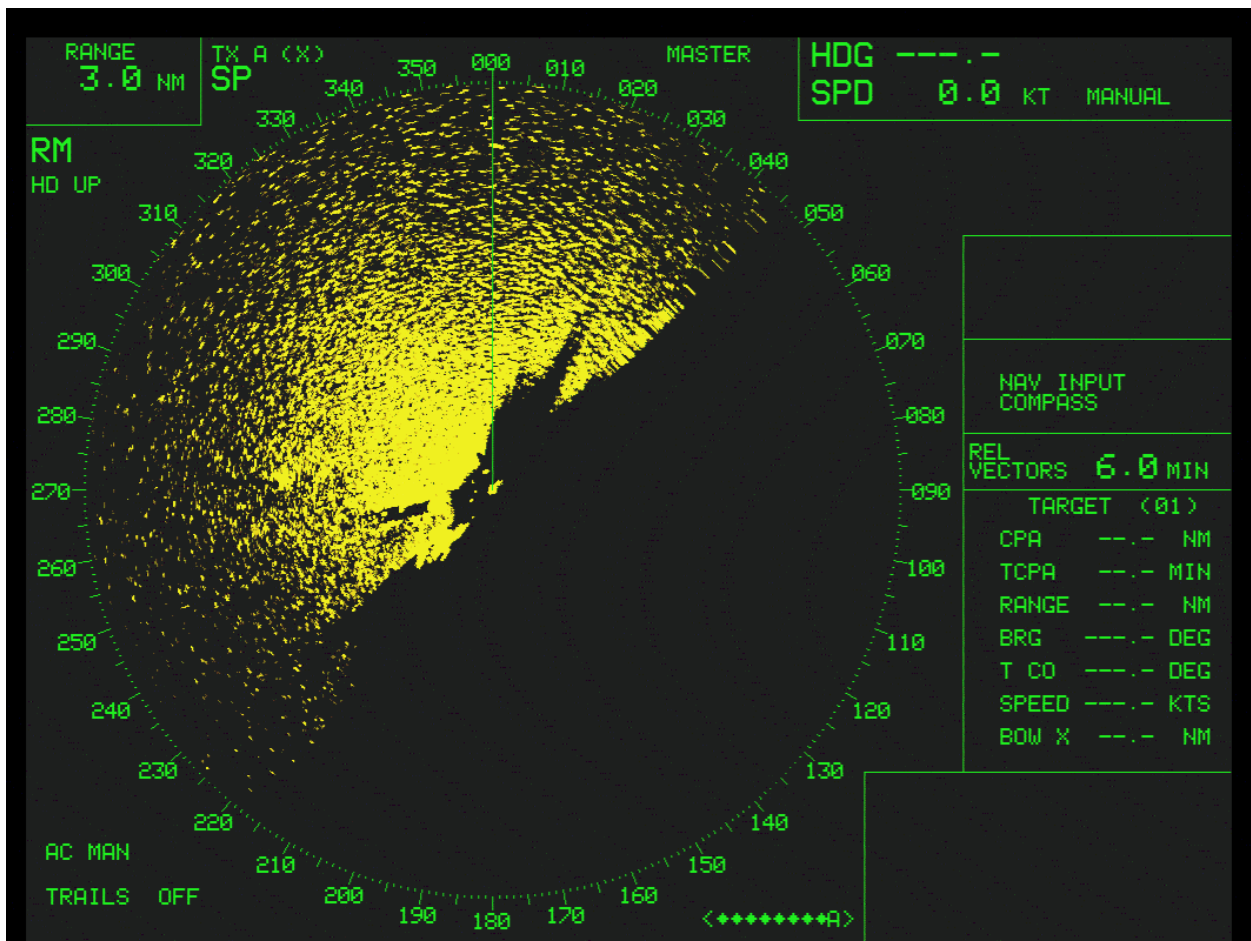
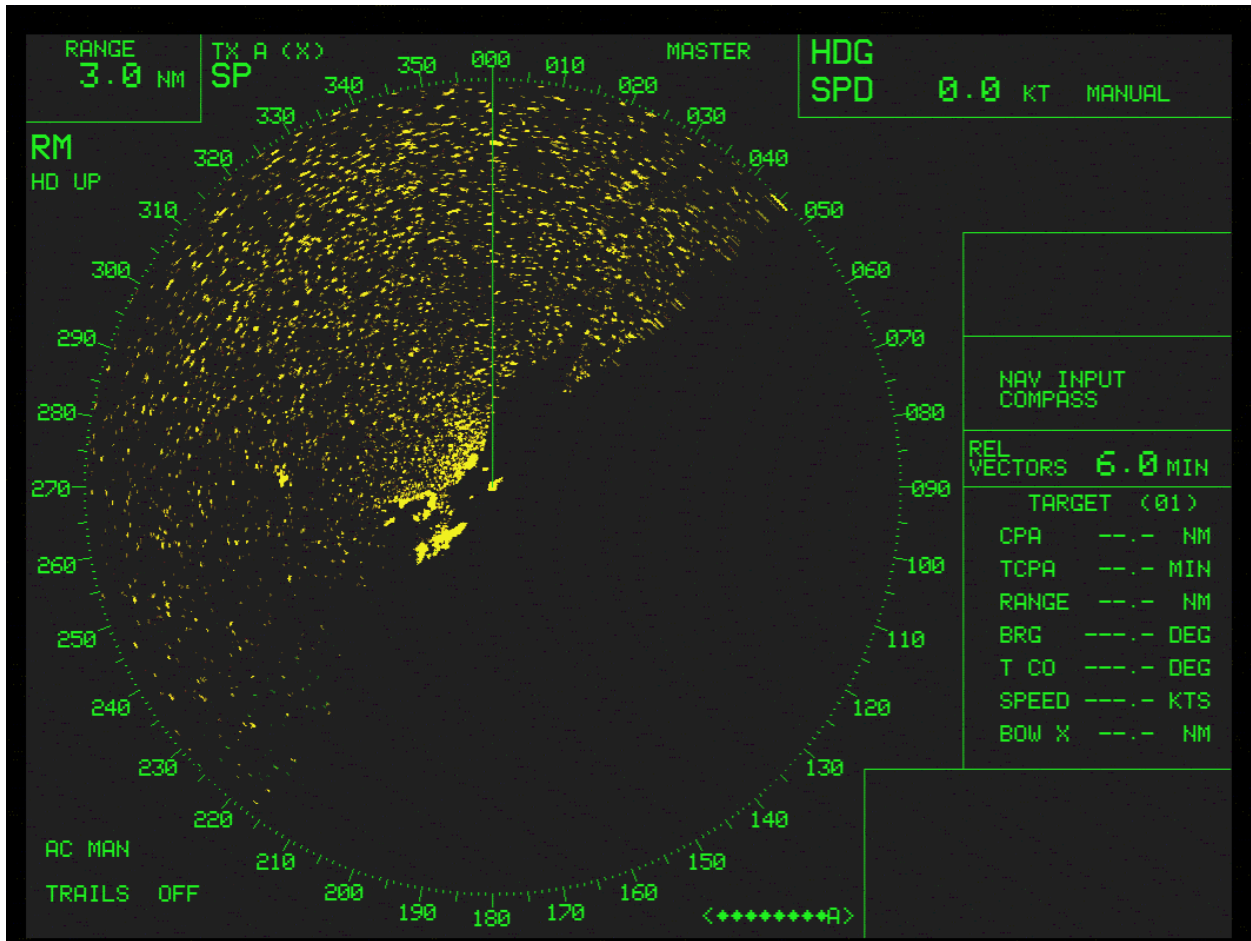


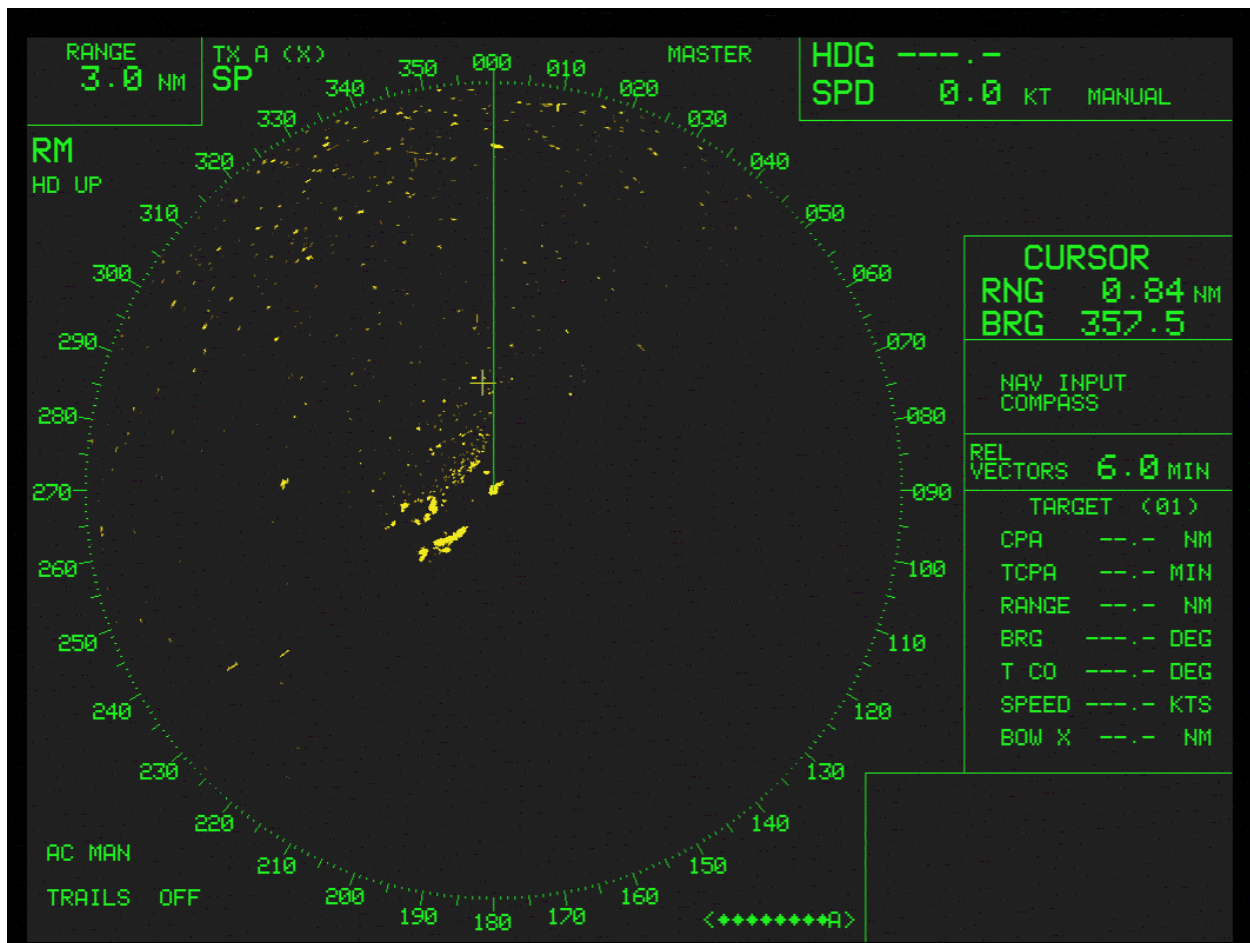
Figure 61 Marine Radar Display Video - Gain 2, SEA 3

In the following sequence, various display settings were used to provide the best presentation of the targets in the image.



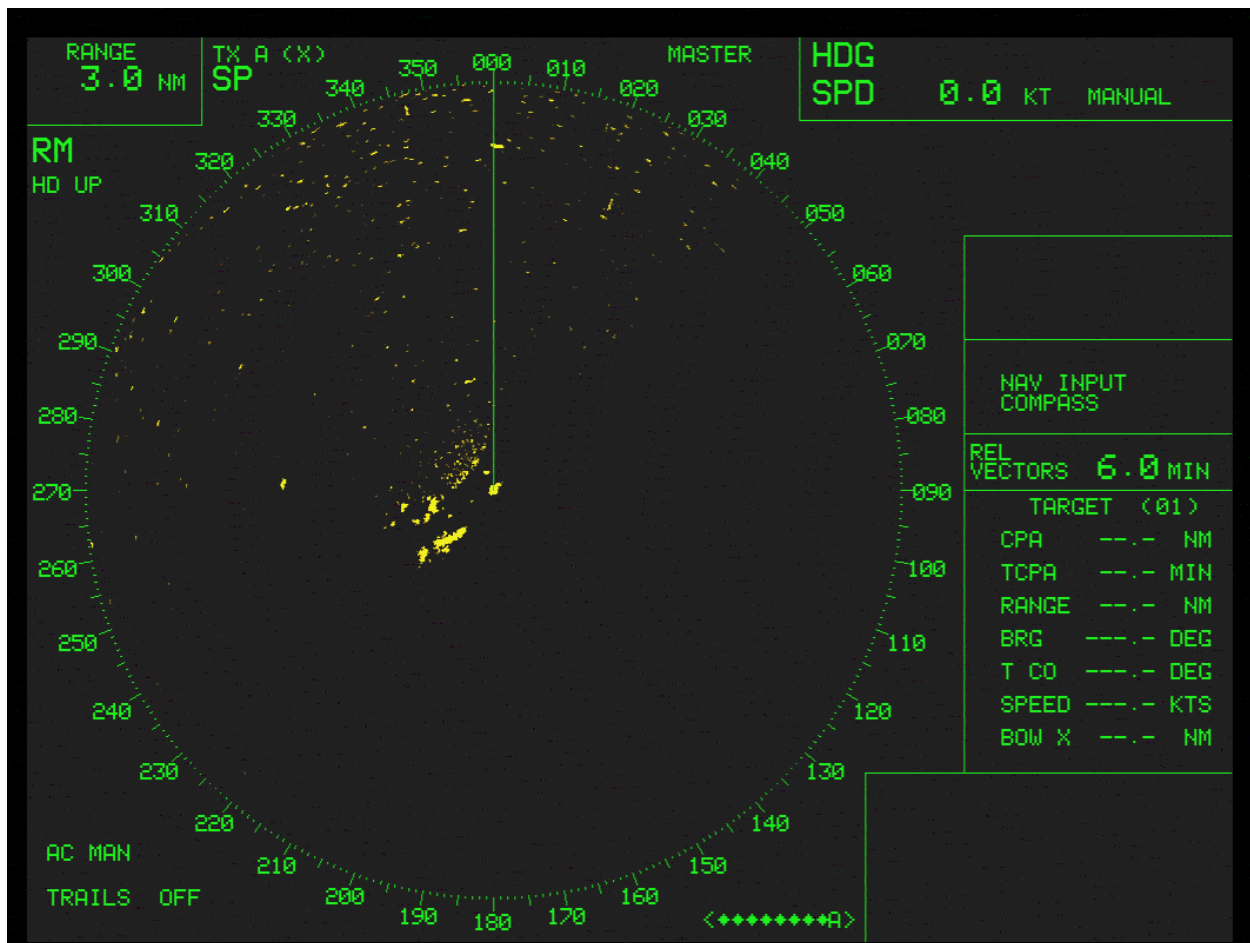
**Figure 62 Marine Radar Display Video - Gain 2, SEA 5**

Figure 62 shows the effect of increasing the sea clutter control to 5. The clutter response is becoming more even across the screen; however, there is still considerable sea clutter displayed. The bergs to the north and west are more visible in this display.



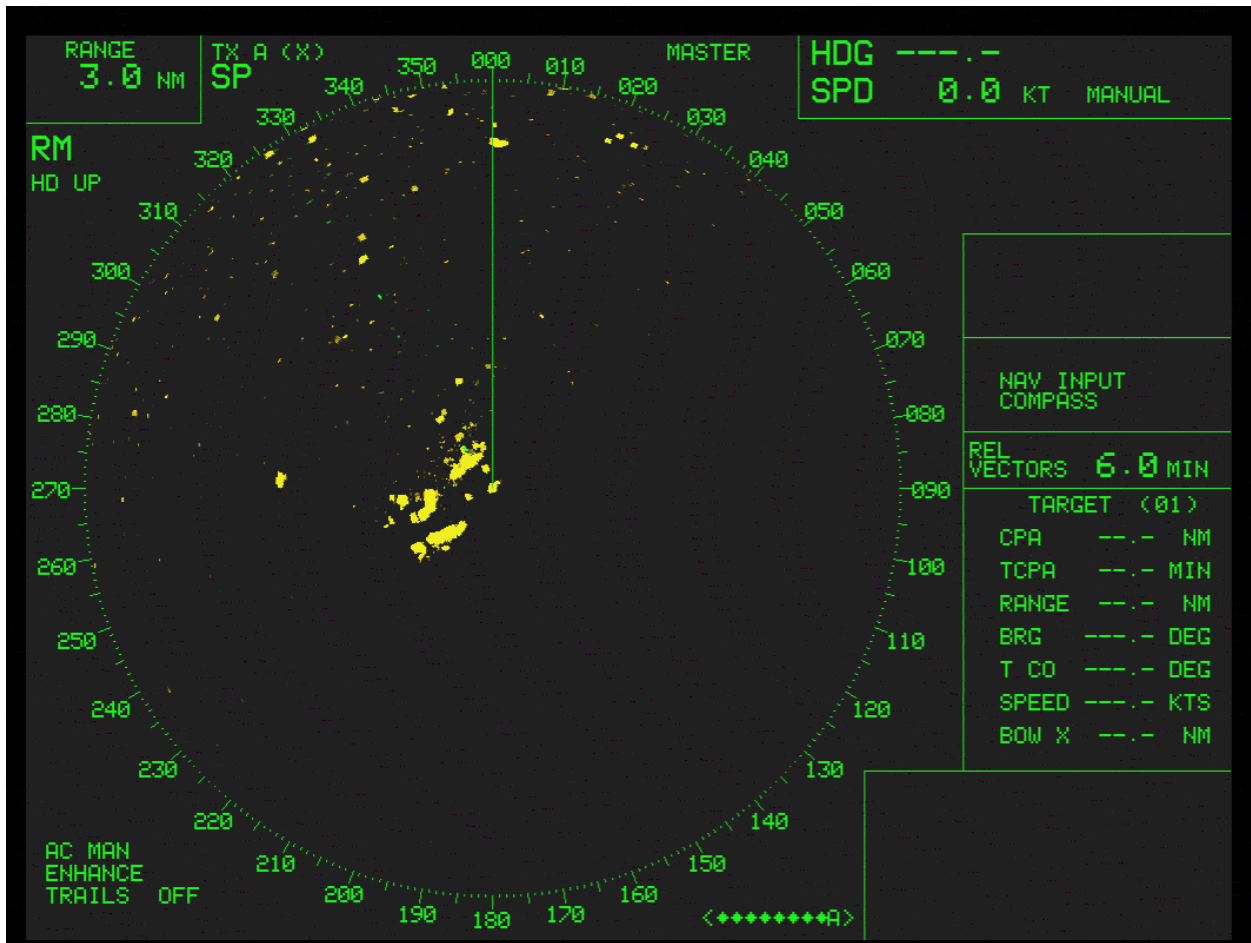
**Figure 63 Marine Radar Display Video - Gain 2, SEA 6**

Figure 63 shows the effect of increasing the sea clutter control to 6. The clutter response is being suppressed to a more usable level. Note there is a moving boat in the upper left of the cursor. The range displayed is 0.85 nmi at a bearing of 357.5 (the cursor is offset from the target so that the target may be more clearly viewed). The bergs to the north and west are clearly visible in this display.



**Figure 64 Marine Radar Display Video - Gain 3, SEA 7**

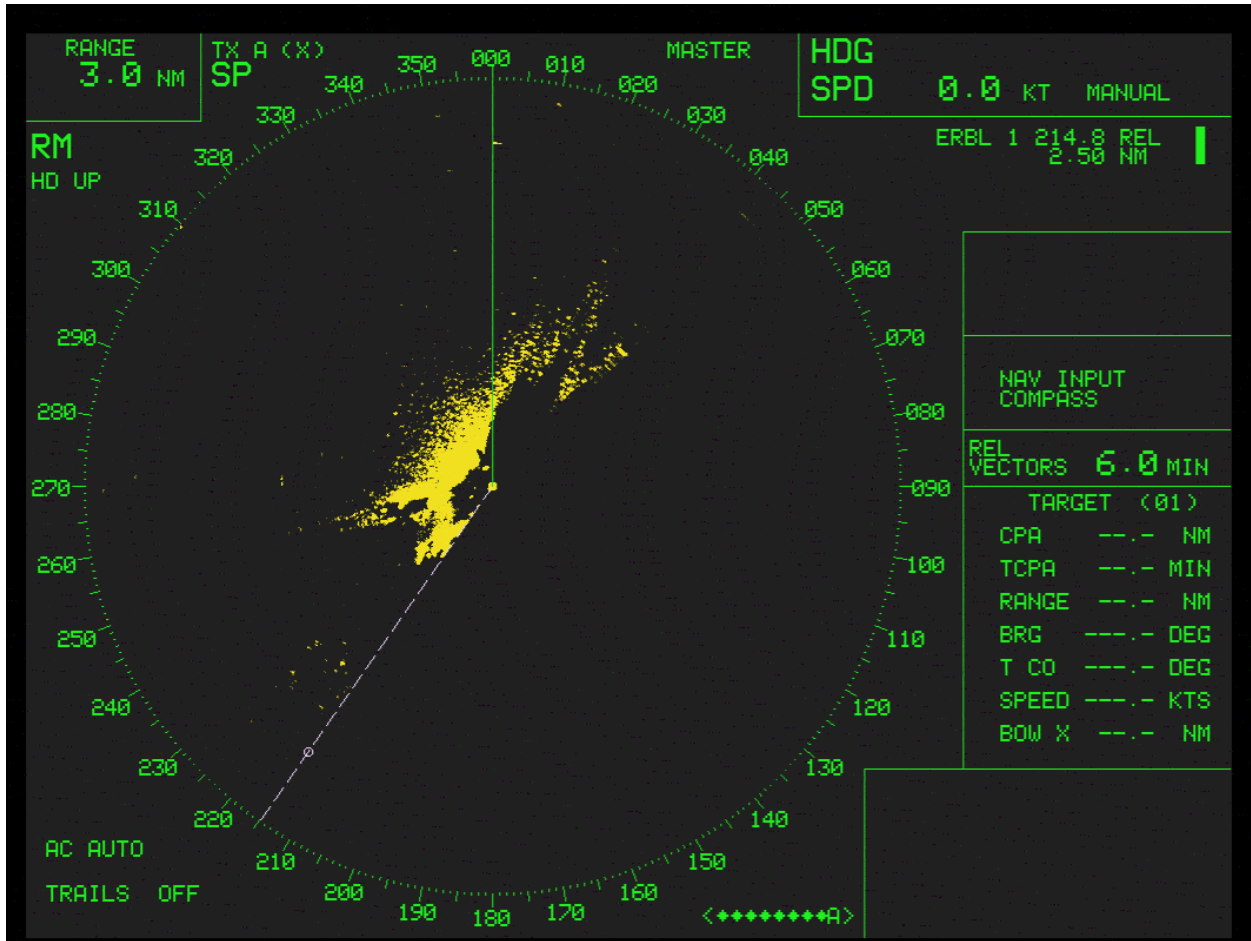
Figure 64 shows the effect of increasing the sea clutter control to 7 and gain to 3. The clutter suppression may be slightly better in this image, but it is close to that of Figure 63.



**Figure 65 Marine Radar Display Video - Gain 3, SEA 7, ENHANCE**

Figure 65 shows the effect of using the ENHANCE function of the display to increase the echo size. This function does not increase detectability but does make targets more obvious on the display.

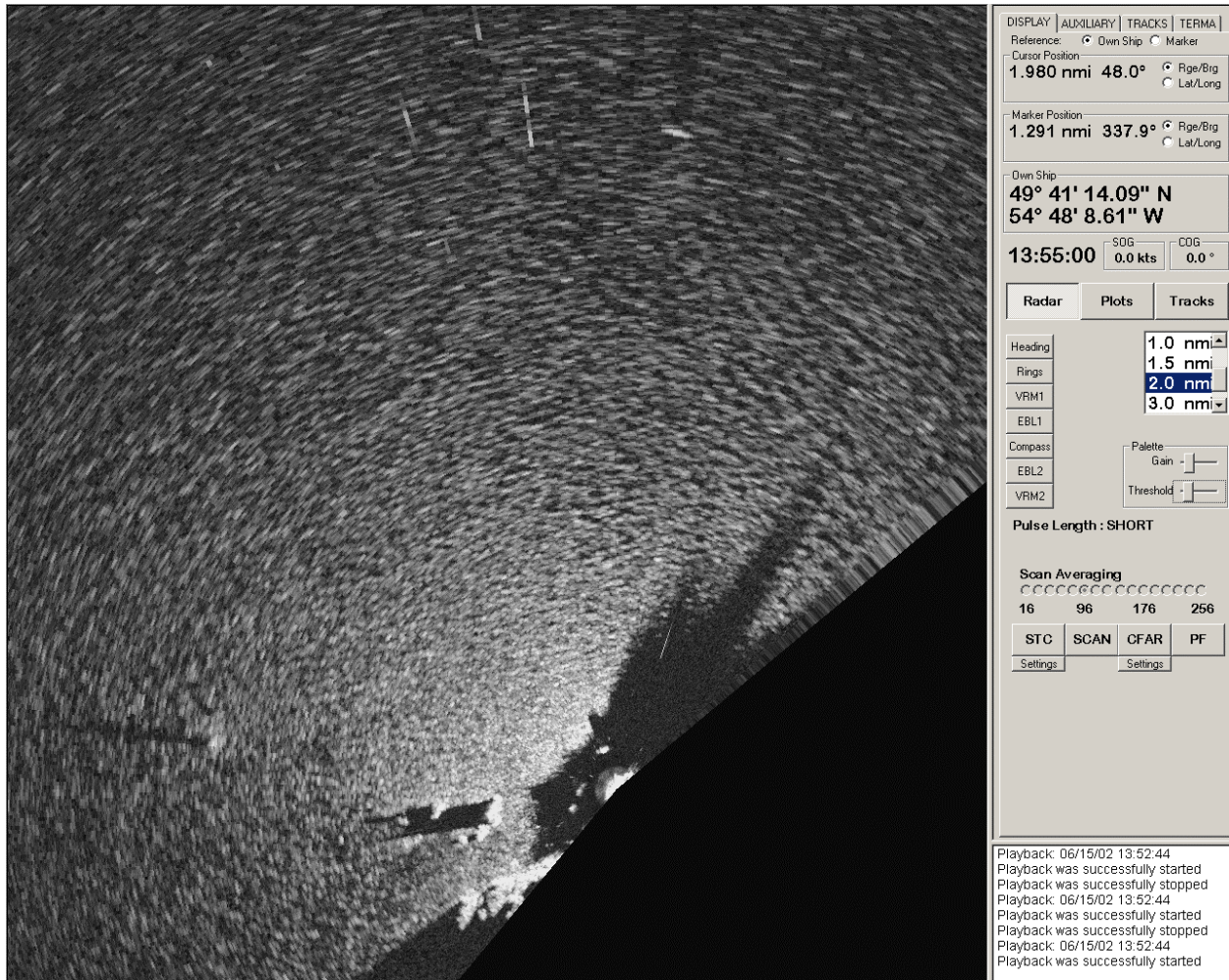




**Figure 66 Marine Radar Display Video - AUTO Clutter, Gain 6**

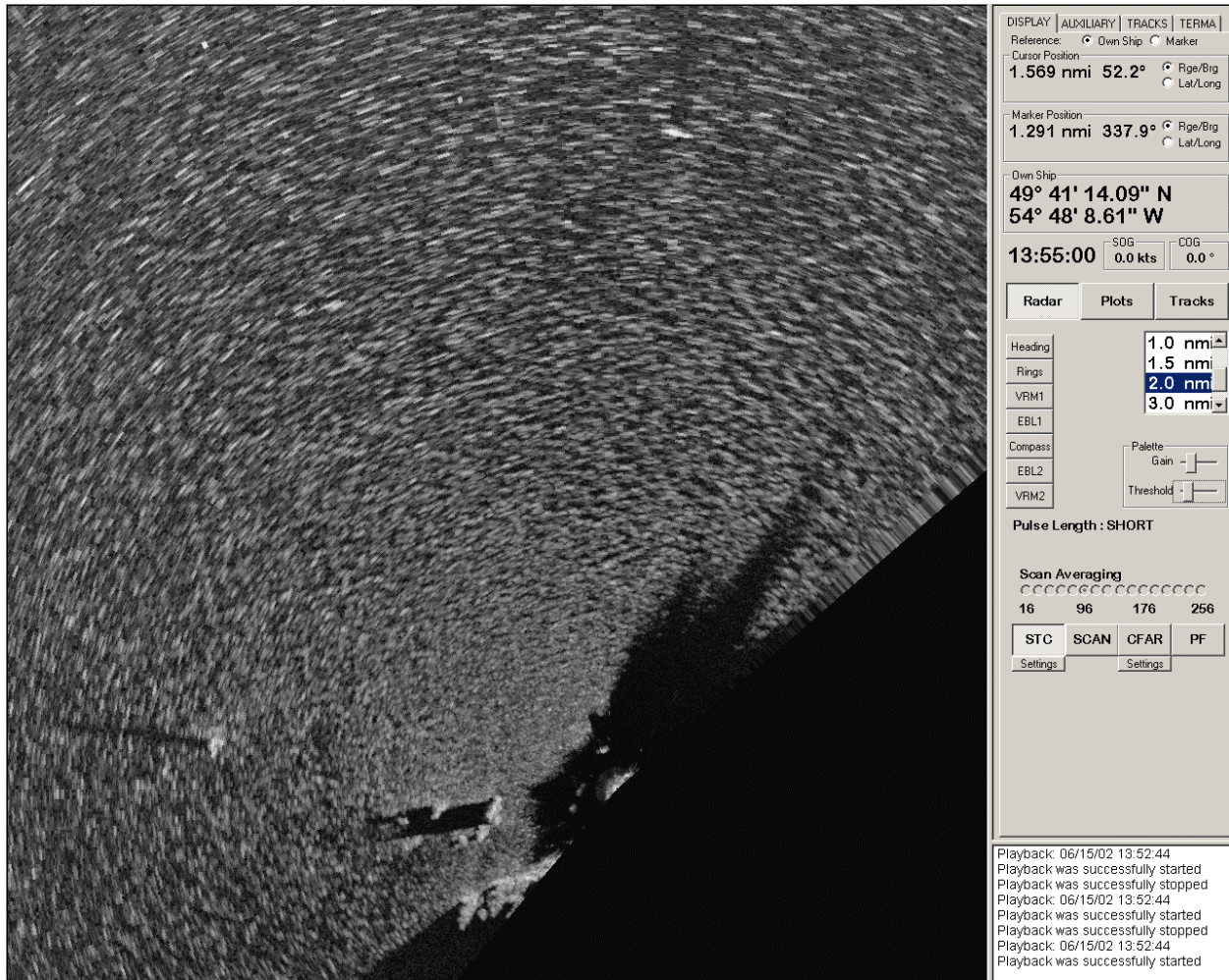
Figure 66 shows the effect of using full AUTO clutter control. In this case, detectability of the medium icebergs is affected and near-range clutter is not suppressed.

For comparative purposes, Figures 67 to 72 present images captured from the Sigma S6 system from the exact same data set.



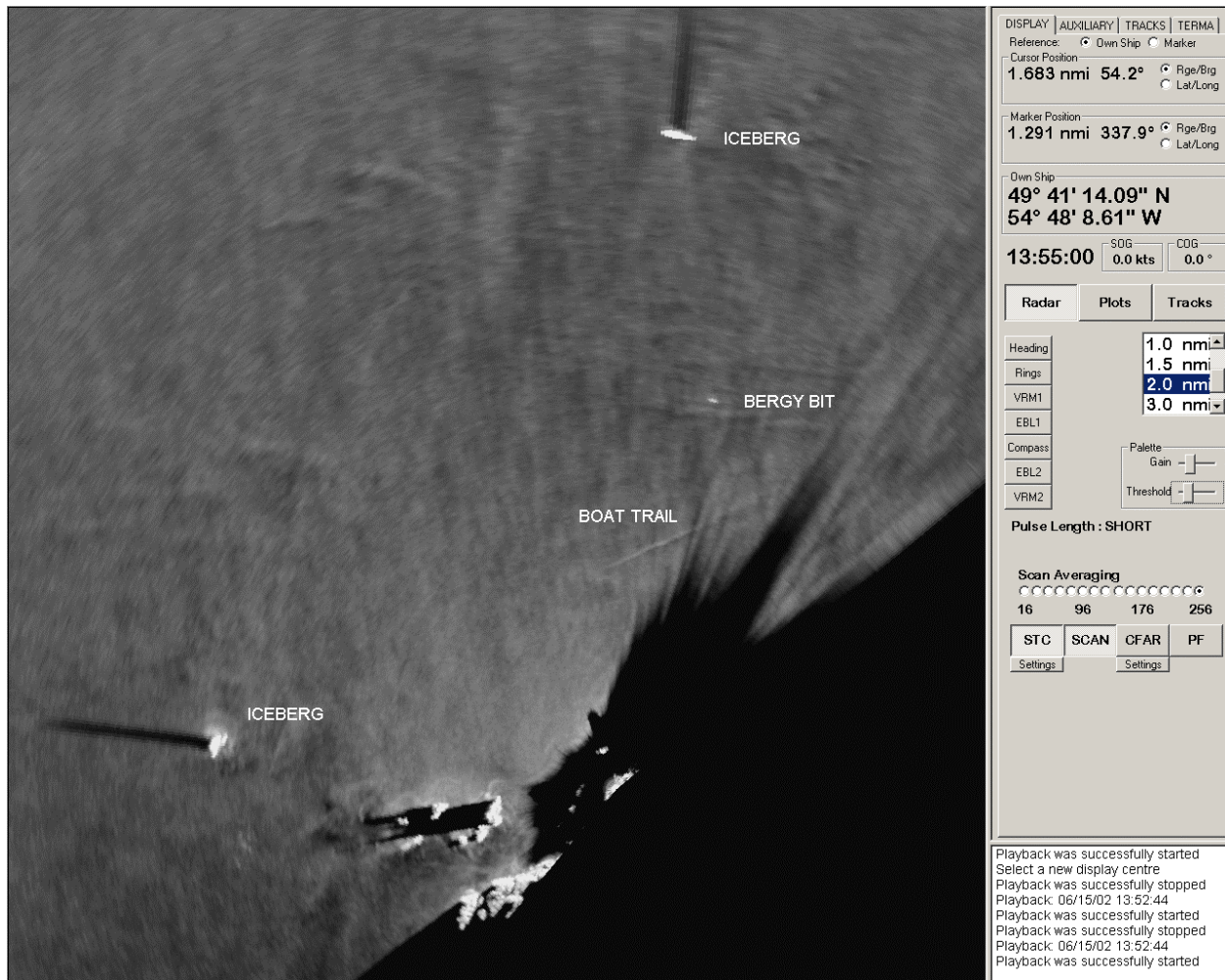
**Figure 67 Sigma S6 Display - RAW Video**

Figure 67 presents the raw video display and would be equivalent to the image from the marine radar display presented in Figure 61, although that image did have some sea clutter processing applied.



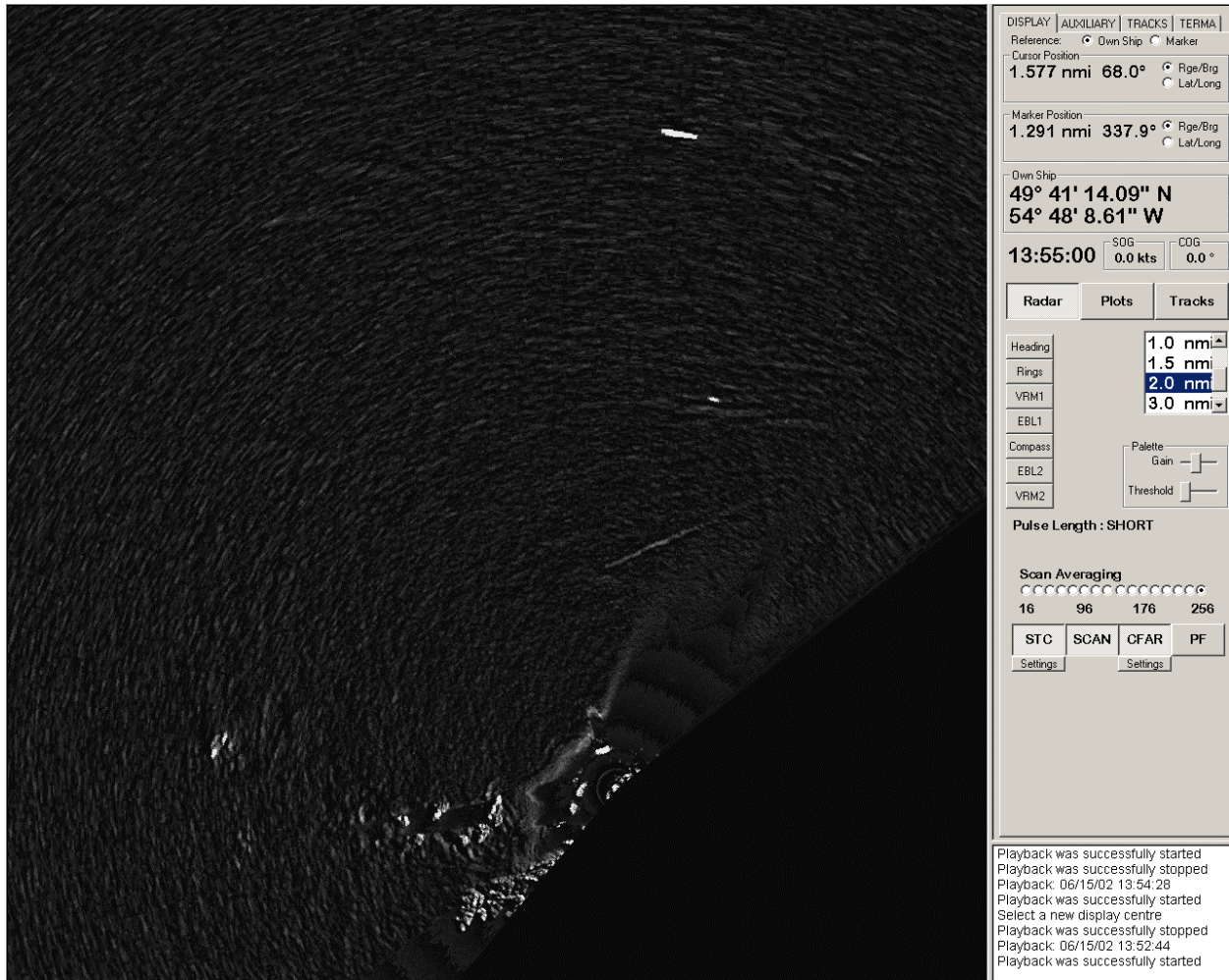
**Figure 68 Sigma S6 Display - STC Applied**

Figure 68 presents the raw video with some STC applied to even out the clutter over the radar display. This would be somewhat equivalent to the marine radar display image in Figure 62; however, in that image a large amount of the clutter has been removed by the gain and sea clutter control. In both images (Figures 67 and 68) it is possible to make out the bergs to the north and to the west.



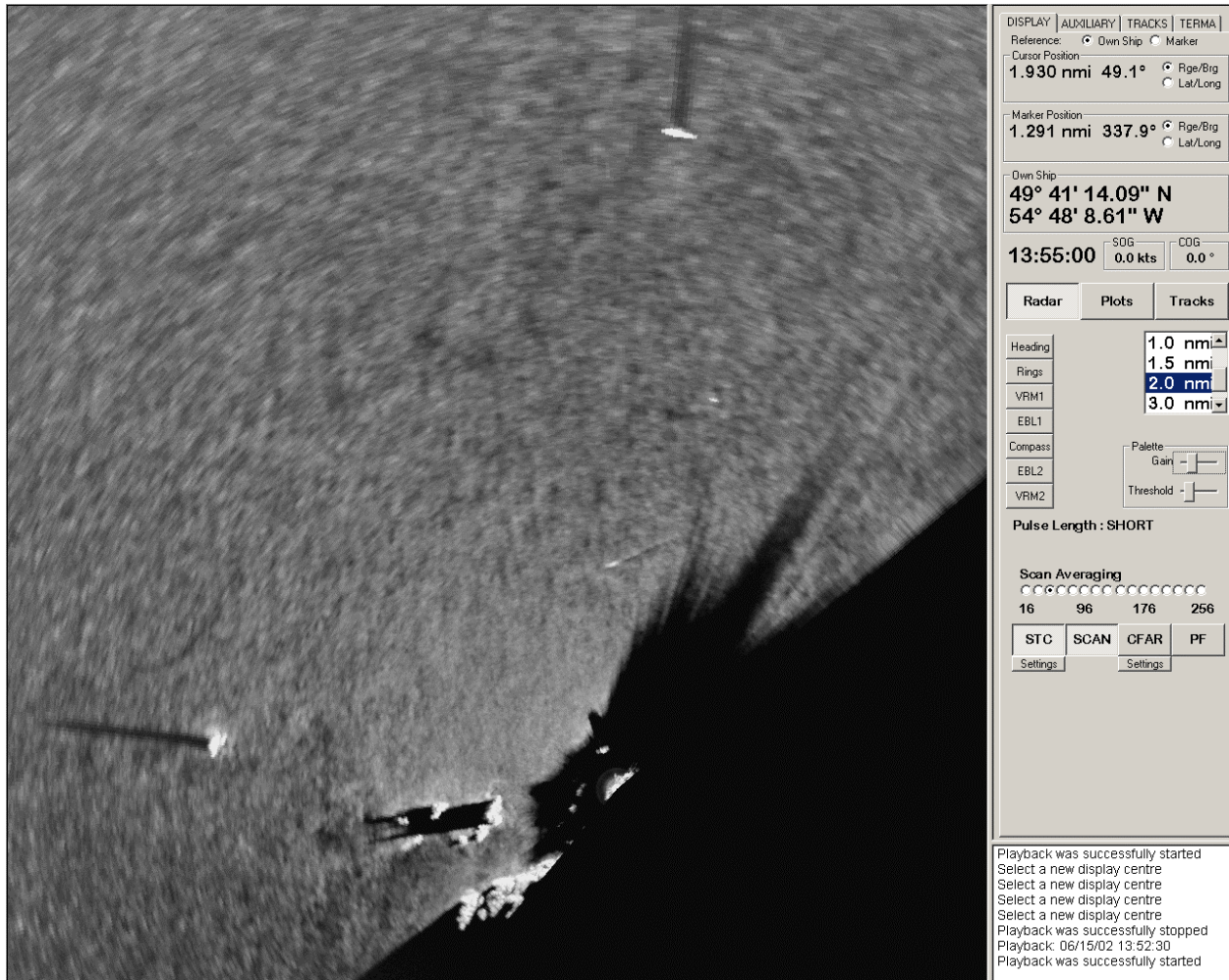
**Figure 69 Sigma S6 Display - STC and 256 Scan Average**

Figure 69 presents the Sigma S6 display with full scan average processing. In this case the icebergs are very clear and much detail is displayed in the ocean surface. There is now also a bergy bit displayed quite clearly to the north of the radar. There is also a feature referred to as BOAT TRAIL. This is the wake left by a boat moving through the field of view during the processing. Figure 63 and Figure 64 show the marine radar display adjusted for best detection. It is just possible to make out the boat in these figures but the bergy bit could not be located.



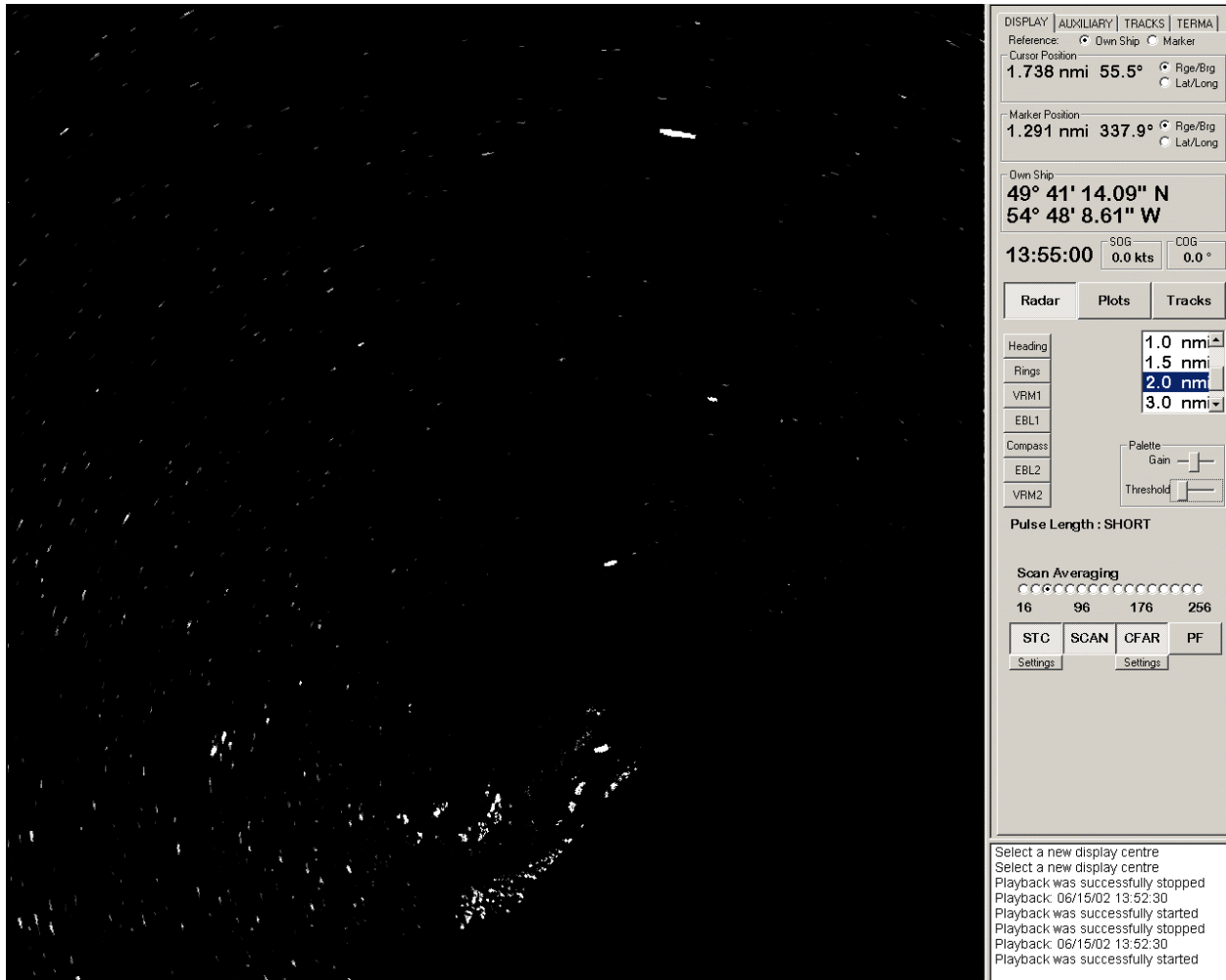
**Figure 70 Sigma S6 Display - STC, CFAR and 256 Scan Average**

Figure 70 shows the effect of applying CFAR to the image in Figure 69. The bergy bit is clearly defined and the boat trail or wake is somewhat enhanced. In this mode the display is optimally adjusted for iceberg detection, and as a result, the fast-moving boat is processed out of the image. Often times it is not necessary to apply maximum processing to achieve good detection performance. Figures 71 and 72 show results for a shorter processing period (fewer scans averaged.)



**Figure 71 Sigma S6 Display - STC and 48 Scan Average**

Figure 71 presents the same data with only 48 scans averaged. In this case both the bergy bit and moving boat are clearly visible. Figure 72 shows the same image with CFAR applied.



**Figure 72 Sigma S6 Display - STC, CFAR and 48 Scan Average**

Figure 72 shows that it is possible to use a setting that can show targets moving at different speeds. However, it is also clear from this figure that the trade-off is increased clutter, as was noted in section 6.5.

## **8 CONCLUSIONS**

This section summarizes the results of the analysis. The conclusions are broken down into sections reflecting the phases of the project and conclusions associated with each.

### **8.1 DETECTION**

#### **8.1.1 Iceberg Detection**

A number of very small bergy bit and growler iceberg targets were analyzed in the heaviest sea conditions encountered. It was found that, using scan average processing, all documented pieces of ice could be detected when processed using 256 scan averaging. These pieces of ice were detected with a high probability in the range of 1 to 2.5 nmi. The seas were in excess of 3 m significant wave height.

These conditions were the maximum that occurred during the field program, so it was not possible to test how well the processing would perform in higher sea conditions.

Also, while there were numerous small pieces of ice at longer ranges on that day visibility was too poor for aerial surveillance and shore-based identification. These icebergs were detected at ranges as great as 5 nmi during these conditions. Given the relative size of the observed radar echoes, it is expected that they would be bergy bit-sized icebergs, indicating that the system should be capable of detecting bergy bit-sized icebergs in excess of 4 nmi.

Overall, it is concluded that the existing scan-to-scan averaging process provides very good target detection, but processing of 256 scans is a practical limit in current computer systems due to the large amount of memory required for the processing. The IIR digital filter approach to scan processing offers the benefits of scan average processing while permitting improved performance with lesser computer storage requirements.



### **8.1.2 Antenna Speed Effects**

The benefit of a faster antenna speed was clearly demonstrated. Trials were conducted that simulated slower antenna speeds from the high-speed data. Two conclusions were reached:

1. Higher values of scans-to-process will most likely correspond to better target detection. With a current practical limit of conventional scan averaging at 256 scans, the digital filter approach (filtered scan processing) is required to achieve improved performance over the current scan average processor.
2. Faster antenna speed means less processing time needed for desired Pfa and Pd values. As many of the targets of interest are moving, the improvement in detection will be limited by the number of scans that can be processed before the target moves out of a particular radar resolution cell.

These two conclusions indicate that, for future improvements to radar performance on slow-moving targets such as drifting icebergs, it will be necessary to implement a higher speed radar antenna (or equivalent) and filtered scan processing

## **8.2 DIGITAL FILTER PROCESSING**

It has been shown that an IIR digital filter can be implemented that may be used for Filtered Scan Processing and that this filter can provide a significant improvement in target detection performance on stationary or very slow-moving targets. Further, it has been found that filter bandwidth (for a given antenna speed) is the controlling parameter in filter performance and that filter order has little influence. This means that there is no benefit in using IIR filters with order greater than two for scan-to-scan processing.

The flexibility offered by IIR filters means that it is possible to construct a filter that can effectively process 512 or 1024 scans of data. It is not feasible to do this with scan average processing without developing a hybrid filter approach.

Tests with weighted FIR filters demonstrated that these filters would be much too large for implementation on current PCs, and real-time operation would likely not be possible.

### **8.2.1 Target Motion**

Target motion effects were investigated and it was determined that these must be considered carefully when choosing operating parameters of a system that has only one filter running at a time. On moving bergy bit targets, degradation in detection performance was starting to be noted visually when using the 0.0017 Hz digital IIR filter. This effect may be mitigated by running a number of filters simultaneously looking for targets moving at differing speeds. This would require a new innovative processing architecture.

### **8.3 DISPLAY COMPARISONS**

A new technique was used to compare the results of radar signal processing to what is expected to be viewed on a standard marine radar display. The technique involves the playback of digital radar data in an analogue form into a marine radar display. The results of the comparison clearly show that standard marine radar displays are not capable of detecting bergy bit-sized targets in heavy seas.

## **9 RECOMMENDATIONS**

Filtered scan processing shows significant potential for improving the detection of small iceberg targets in heavy sea clutter. The following recommendations outline new initiatives that will investigate technology and processing techniques to take advantage of this type of filtering.

### **High Speed Antenna**

It has been shown that the 120 rpm antenna provides for improved detection over a normal scanning radar by acquiring the radar data in a shorter time interval. The improvement is expected to continue as the antenna speed increases and the sea clutter remains uncorrelated from scan to scan. The maximum speed that may be effectively used is limited by the correlation characteristics of the sea clutter and the technical limitations of the increased antenna speed. The experimental radar used for the 120 rpm work had a pulse rate of 3000 Hz, providing about 4 pulses per radar beamwidth. Increasing the antenna speed to 240 rpm would require a corresponding increase in pulse rate to 6000 Hz in order to maintain the same number of pulses per beamwidth.

It is recommended that an investigation be undertaken to ascertain the maximum effective antenna speed that may be achieved and the way in which detection performance is influenced as the sea clutter becomes more correlated from scan to scan. This investigation will require construction of a radar system capable of operating at effective antenna speeds of up to 500 rpm with a pulse repetition frequency in the range of 12 KHz.

### **Filtered Scan Processor**

Coupled with this effort, it is recommended that a new implementation be considered for the filtered scan processor to permit real-time detection and tracking of small targets at

these high antenna speeds. The new implementation should investigate the benefits/tradeoffs of various cascaded combinations of FIR/IIR filters, utilizing low order IIR filters as a front end and various tandem FIR filters as post processors.